New Phosphorescence Based Probes and Techniques for the Analysis of Cellular Oxygen and Respiration.

A thesis submitted to the National University of Ireland, Cork

In fulfilment of the requirements for the degree of

Doctor of Philosophy by

Alina Kondrashina

School of Biochemistry and Cell Biology

National University of Ireland, Cork

2014

Head of School: Prof. David Sheehan

Supervisor: Prof. Dmitri Papkovsky

Declaration

This thesis has not been submitted in whole or part to this or any other university for any degree, and is, unless stated, the original work of the author.

Alina Kondrashina

December 2014

To my family

Abstract

Real time monitoring of oxygenation and respiration is on the cutting edge of bioanalysis, including studies of cell metabolism, bioenergetics, mitochondrial function and drug toxicity. This thesis presents the development and evaluation of new luminescent probes and techniques for intracellular O_2 sensing and imaging.

Oxygen consumption rate (OCR) monitoring techniques in microtiter plate and quartz cuvettes suffer from low sensitivity and end-point measurements. A new OCR platform based on the commercial microfluidic perfusion channel μ-slides compatible with extra- and intracellular O_2 sensitive probes was developed. The design of semi-closed channels allows cell treatments, multiplexing with other assays (extracellular acidification, immunofluorescence) and two-fold higher sensitivity to compare with microtiter plate. The μ-slide platform was evaluated with MEF, PC12 and HCT116 cells in different measurement conditions, media compositions and upon metabolic stimulations, such as mitochondrial uncoupling and inhibition, depletion of extracellular Ca^{2+} and inhibition of histone deacetylation. Comparison of different cell respiration techniques is important for their standardization, benchmarking and correlation of O_2 reporter parameters obtained in independent experiments. Here three common platforms were compared: hermetically sealed quartz cuvettes for absolute OCRs, partially sealed with mineral oil 96 well plates (96-WPs) for relative OCRs, and open 96-WPs for local cell oxygenation. Both 96-WP platforms were calibrated against absolute OCR platform with MEF cell line, phosphorescent O_2 probe MitoXpress-Intra and time-resolved fluorescence reader. A constant factor 5.35 was determined for our system to convert relative OCRs into absolute values. Oxygenation signals were also related to absolute OCR values and the calibration obtained allowed tracing of cell respiration over time in a high throughput format with the possibility of cell stimulation and of changing measurement conditions.

Successful intracellular oxygen sensing requires both advanced platforms and O_2 sensitive probes. The development and evaluation of a new multimodal intracellular O_2 probe was described. Phosphorescent reporter dye PtTFPP with emission at 650 nm and fluorescent FRET (Foerster resonance energy transfer) donor and two-photon antennae PFO were embedded in cationic hydrogel nanoparticles RL-100 by water precipitation.

This probe, called MM2, is easy to fabricate and possess high brightness, photo- and chemical stability, low toxicity, efficient cell staining and high-resolution intracellular O_2 imaging. Analytical performance and applications of the MM2 probe were demonstrated in physiological experiments with 2D and 3D mammalian cell cultures in intensity, ratiometric intensity and phosphorescence lifetime-based modalities with fluorescence readers and FLIM (fluorescence lifetime imaging microscopy) microscopes. Extended range of O_2 sensitive probes was designed and studied in order to optimize their spectral characteristics and intracellular targeting. Anionic PMMA-MA polymer was used for preparation of a MM2 probe analogue called PA2. This probe has low cytotoxicity, high brightness, short loading time, efficient staining of different mammalian cell lines and can be used with 2D and 3D cell models in different detection modalities. PMMA-MA polymer was also used for preparation of longwave multimodal probes based on the sensing and reference pairs of PtTFPP and coumarin (MM1x) or PtTPTBPF and azaBodipy (MMirx). This polymer provides reliable encapsulation of small molecules such as coumarin and equal distribution of dyes for efficient FRET. Having sizes below 100 nm, these probes utilize mixed endocytic energy- and temperature-dependent mechanisms of cell entry. Excitation optima at 470 nm for MM1x and 620 nm for MMirx probes allow mild irradiation of cell samples and deep light penetration. Molecular probe approach was also evaluated on conjugates of PtTFPP dye with glucose and galactose residues. Pt-Glc and Pt-Gal probes demonstrated short loading time (1-6 hours) with a wide range of mammalian cell lines, low working concentrations and toxicity.

These results show that the newly developed O_2 probes and techniques provide useful tool for high sensitive monitoring and imaging of intracellular O_2 in different detection modalities and measurement formats. The presented improvements allow studies of cell metabolism, bioenergetics, adaptation to hypoxia and different (patho)physiological conditions.

List of abbreviations

2D – two-dimensional

3D – three-dimensional

96-WP – 96-well plate

AntA – antimycin A

Arg - arginine

ATP – adenosine triphosphate

BA – sodium butyrate

Baf – bafilomycin A1

BSA- bovine serum albumin

CCD – charged coupled device

CMA – concanamycin A

cps – counts per second

CPZ – chlorpromazine

CTX – cholera toxin, subunit B

DIC – differential interference contrast

DMEM – Dulbecco's modified eagle medium

DMF - N,N-dimethylformamide

DMSO - dimethyl sulfoxide

EC- extracellular

ECA – extracellular acidification

EGTA – ethylene glycol-bis(2-aminoethylether)-*N*,*N*,*N*′,*N*′-tetraacetic acid

EIPA - 5-(N-ethyl-N-isopropyl)amiloride

ER - endoplasmic reticulum

ETC – electron transport chain

FBS – fetal bovine serum

FCCP – carbonyl cyanide-4-(trifluoromethoxy) phenylhydrazone

FLIM – fluorescence lifetime imaging microscopy

FRET – Foerster resonance energy transfer

HIF – hypoxia inducible factor

HS – horse serum

IC- intracellular

icO_2 - intracellular O_2

Ksv – Stern-Volmer constant

LED – light emitting diode

MβCD - methyl-β-cyclodextrin

NP – nanoparticle

OCR – oxygen consumption rate

OM – oligomycin

PBS - phosphate buffered saline

PdCP – tetracarboxylic palladium (II)-coproporphyrin I

PDL – poly-D-lysine

PEBBLE – probes encapsulated by biological localized embedding

PEG – polyethylene glycol

PLIM - phosphorescence lifetime imaging microscopy

PMMA-MA- poly(methyl methacrylate-co-methacrylic acid

PFO - poly(9,9-diheptylfluorene-alt-9,9-di-p-tolyl-9H-fluorene)

PtCP – tetracarboxylic platinum (II)-coproporphyrin I

PtTFPP -Pt(II)-tetrakis(pentafluorophenyl)porphine

PtTBTBPF - platinum(II)-*meso*-tetra(4-fluorophenyl)tetrabenzoporphyrin

ROI – region of interest

ROS - reactive oxygen species

RT- room temperature

TBST – Tris-buffered saline, Tween 20

TCSPC – time-correlated single photon counting

TR-F - time-resolved fluorescence

Val – valinomycin.

Table of Contents

Chapter 1. Literature review.

Probes and techniques for optical oxygen sensing in biological systems

Molecular oxygen (O_2) is important part of the atmosphere (21 kPa at sea level) and is involved in numerous physical, chemical, biological and ecological processes on Earth. Living systems are highly associated with O_2 production and consumption upon metabolic processes. Aerobic organisms require O_2 to maintain live and reproduce. This metabolite is involved in the oxidative phosphorylation (OxPhos) process in mitochondria, being crucial substance for energy production [1]. A large group of enzymes uses O_2 as a required electron acceptor to convert substrate into final product of reaction with high rate for biological processes. Under physiological conditions O_2 concentrations in different tissues vary in a narrow range (normoxia), depending on the environment, metabolic activity and development stage (proliferation, differentiation, apoptosis). However, normoxia in more complex organisms depends on the specific localization: the highest O_2 concentration is in the respiratory system, decreasing towards other tissues (3-10 kPa or 30-100 μM) [2]. *In vitro* experiments with live tissues and organs often require hypoxia chambers - to model *in vivo* normoxia, maintain physiologically low oxygen level and prevent oxidative damage due to its excess (hyperoxia). Similarly, in terms of the whole body, O_2 concentration over 50 kPa is toxic for mammalians, causing convulsion and lung disorders after long exposure. Therefore, artificial lung ventilation, space and diving suites with high O_2 concentration in gas mixtures should be used under careful control [3].

Living at high altitude or in deep waters, intensive physical activity and hibernation cause insufficient O_2 concentration or hypoxic conditions. Such systems are popular for studying of hypoxia signaling, energy and reactive oxygen species (ROS) production, and require accurate measurement of O_2 concentration [4]. Moreover, pathological states, such as ischemia, stroke, cellular toxicity and cancer, are often followed by local anoxia or deep hypoxia. Monitoring of O_2 in live systems over time can report about these states if performed with sufficient sensitivity [5]. All these processes make detection of molecular oxygen of high bioanalytical and clinical interest, especially in physiological liquids, single cells, 2D and 3D cell cultures, live tissues and whole organisms.

O_2 in biological systems can be measured in a number of different ways depending on the sample, conditions and their changes, required sensitivity, throughput and prospective application (for laboratory, industrial, clinical use). The most popular measurement parameters are:

1) Concentration of O_2 (oxygenation) – for studying of tissue homeostasis, hypoxia, signaling, pathological states;
2) Oxygen consumption rate (OCR) – for the assessment of cell respiration, metabolic activity, responses to metabolic stimulations;
3) O_2 gradients – for studying tissue physiology and pathology, cell culture and single cell heterogeneity, stem cell niches;
4) Secondary parameters related to O_2 concentration, such as hemoglobin saturation, ROS production, NADH redox state, hypoxia stains – for monitoring of patient conditions in neurophysiology and sport medicine [6].

Different bioanalytical applications and objects put specific requirements on O_2 sensing, where low toxicity and invasiveness are essential for most of them to avoid related artifacts. Quantitative techniques often require high throughput, flexibility and broad applicability, when for single cell analysis high sensitivity is more important. Therefore, a variety of O_2 sensitive materials, techniques and platforms have been developed to perform these bioanalytical tasks.

1.1 O_2 monitoring techniques

O_2 detection has been actively developing over last decades and nowadays there is a variety of physical, chemical and biochemical techniques. Often the best method is a compromise on sensitivity, availability and convenience of existing tools. In this chapter an overview of the main techniques currently applied for biological O_2 detection is given.

1.1.1 Traditional methods of O_2 detection in solution

One of the first methods of O_2 detection in water samples was Winkler titration, which is based on the oxidation of $Mn(OH)_2$ by dissolved oxygen into brown precipitate MnO_2. This product can further convert iodide ion into iodine for titration with a thiosulfate solution [7] or be directly titrated by EDTA [8]. Determination of dissolved O_2 by gas chromatography, is still popular for industrial purposes where high accuracy is required, however it has limited use for solutions and sophisticated, high cost equipment [9].

The Clark type electrode substituted the cumbersome chemical and physical methods for measurement of dissolved O_2. This method employs Pt electrode polarized against Ag/AgCl electrode (potential difference about +0.7 V) in KCl solution, which is separated from the sample by the Teflon membrane [10]. O_2 from the sample penetrates this membrane and gets electrochemically reduced at the cathode, producing current proportional to the O_2 concentration. Due to the relative simplicity, low cost and wide availability of the electrodes [11], this technique for a long time was a "golden standard" for the monitoring of dissolved O_2 in complex biological samples, such as blood, urine, and for OCR measurements in suspensions of cells, yeast and bacteria cultures, isolated mitochondria and small organisms [12-14]. Clark type electrode principal drawbacks are O_2 consumption by the system ($O_2+2H^++2e^-=H_2O_2$), the need of sealed, thermostated and stirred cuvette to minimize the development of local O_2 gradients and additional calculation to consider unwanted O_2 consumption [15, 16]. However, miniaturization of Clark type electrodes and adaptation for transcutaneous monitoring made this method less invasive and suitable for clinical use [17].

Together with other types of Pt electrodes [18] there is also a group of bulk, thin film and nanoparticle golden electrodes [19-21]. Their implantable modifications demonstrate high sensitivity and convenience for multiple use as well as for contentious monitoring in medical applications, however, the problems of biocompatibility and protein adsorption on the sensitive surface still has to be addressed [22, 23].

1.1.2 Instrumental methods

1.1.2.1 Oximetry

Studies of tissue metabolism and respiration, monitoring of patients vital parameters require methods for rapid and convenient determination of the circulating blood O_2 saturation [24]. A simple method was proposed for such measurements, employing incandescent light bulb, selenium barrier level photocell and two color filters [25]. Sensing through green filter was expected to be independent of blood saturation, providing measurements of total hemoglobin, when absorbance of red light depends on it and corresponds to the deoxygenated hemoglobin. Later it was substituted by a related method of blood oxygenation monitoring, which is still very popular for monitoring of intensive care patients, pilots and sportspeople - pulse oximetry [26]. It uses similar principle with monitoring of the light absorption by oxygenated hemoglobin at 940 nm and by deoxygenated hemoglobin at 660 nm. However, here the problem of measurements dependence on the amount of present arterial blood (pulse) is solved. Subtracting of the minimum transmitted light from the maximal at both wavelengths allows correcting the readings for the effects of venous blood, skin, bone, muscle, fat, and other tissues [27]. Collecting of transmission spectra requires thin parts of the body (fingertip, earlobe), when reflection spectra can be monitored at any relevant region [28].

1.1.2.2 Electron Paramagnetic Resonance

Electron Paramagnetic Resonance (EPR) technique uses intrinsic physical properties of the O_2 molecule. It is based on the variation of the linewidth of paramagnetic spin probe or direct quantification of paramagnetic O_2 molecule (with lower sensitivity) at different O_2 concentrations [29]. This technique shows particular accuracy and sensitivity in O_2 monitoring due to the uniform distribution of the spin probe in the sample and no substrate consumption [30]. However, EPR requires sealed setup, where additions of stimulants and changing of ambient oxygen upon measurement are not possible [31]. Moreover, significant distortion of the results can be caused by air bubble in the cuvette. Recently, Electron Paramagnetic Resonance Imaging (EPRI) is successfully used for non-invasive and quantitative 3D mapping of tissue, organ and tumor oxygenation [32].

1.1.2.3 Imaging techniques.

Recently, sophisticated imaging techniques, such as functional magnetic resonance imaging (fMRI), positron emission tomography (PET), Optical Imaging (OI) of intrinsic signals, have found their application for hemodynamic studies [33-35]. This group of methods is based on the determination of the oxyhemoglobin/deoxyhemoglobin ratio as a parameter of blood or tissue oxygenation, which corresponds to brain activity [36, 37]. To generate a three dimensional image of tissue, organ or the whole body oxygenation strong radiowaves, emitted gamma rays and optical properties of live sample in specific reflection are used. Non-invasive O_2 sensing techniques also include Near Infrared Spectroscopy (NIRS) that uses excitation wavelengths between 800 and 2500 nm for the building of the reflection or transmission spectra. The time resolved NIRS method provides deep light penetration, however low molar absorptivity in the NIR range limits its sensitivity [38].

Altogether, imaging techniques for indirect O_2 monitoring are valuable medical tools for non-invasive (or minimally invasive) estimation and continuous monitoring of patient conditions in neurology, neurophysiology, cognitive neuroscience and sport medicine, however, in research laboratories their use is limited.

1.1.3 Optical O_2 sensing

Optical methods of O_2 sensing represent a large group, quickly developing due to a number of important advantages. First of all, many optical methods are minimally or non-invasive and not associated with O_2 consumption upon measurement. Progress in development of powerful lasers, LEDs, detectors and integrated optics led to increased number of measurement formats [39]. Moreover, the high potential for miniaturization, flexibility in samples, platforms and detection modes, intravascular and intracellular studies make optical sensing of O_2 an important bioanalytical tool.

The physical and chemical properties of O_2 molecule make its direct quantification by optical methods challenging. Therefore, a variety of indicators are used to obtain a

corresponding to the O_2 concentration signal. Such indicators can be endogenous, which are already contained in the biological sample (hemoglobin, NADH, FAD, mioglobin), or exogenous dyes, conjugates, particles, probes, sensors, introduced to the area of interest [40]. To produce a characteristic signal, the indicator should enter a physical, chemical, enzymatic, biological or photophysical process, where O_2 is involved according to known mechanism and can then be quantified [41].

Table 1. Common techniques of O_2 monitoring.

Method	**Principle**	**Measurement parameters**	**Samples**	**Advantages**	**Limitations**
Winkler titration	Chemical	[O_2]	Aqueous solutions	Direct measurement, simple equipment	Long, cumbersome, not accurate
Pt, Au electrodes	Electrochemical	[O_2], OCR	Aqueous solutions; physiological liquids; cell, yeast, bacteria, isolated mitochondria suspensions	Widely available, direct, quantitative, suitable for clinical applications	Consumes O_2, sealed setup, limited applicability
Oxymetry	Luminescence absorption	Hemoglobin/ deoxyhemog-lobin ratio	Circulating blood	Suitable for clinical applications, non-invasive	Semi -quantitative, indirect method
fMRI, PET, NIRS	Radio wave/ gamma rays/ 800-2500 nm irradiation	Hemoglobin/ deoxyhemog-lobin ratio	Live tissue, circulating blood	Suitable for clinical applications, non-invasive, 3D imaging	Qualitative, indirect method
EPR	Measurement of linewidth of paramagnetic resonance probe	[O_2], OCR	Aqueous solutions; physiological liquids; cell, yeast, bacteria, isolated	Direct, quantitative, high sensitive	Sealed setup, expensive equipment

	or O_2		mitochondria suspensions		
Lumines-cence quenching	Quenching of the reporting dye luminescence	[O_2], OCR, 2D and 3D oxygenation imaging, O_2 gradients	Gas mixtures, aqueous solutions; physiological liquids; cell, yeast, bacteria, isolated mitochondria suspensions, 2D and 3D live objects, tissues, organs, whole organisms	Direct, quantitative, high sensitive, high flexibility in samples, modalities and platforms	Mostly exogenous probes, possible toxicity

1.2 Quenched luminescence O_2 sensing.

This direct sensing method utilizes luminescent indicators sensitive to O_2 concentration. It is based on the process of dynamic quenching of excited state luminophore molecules by O_2, whereby monitored luminescent signal can be related to O_2 concentration. Luminescence quenching sensing is the basis of a large and diverse group of methods, which address many tasks of cellular O_2 sensing (Table 1).

1.2.1 Principles of luminescence.

Luminescence is a phenomenon of light emission from electronically excited molecules, which are produced by chemical reaction, electrochemical process, crystallization, mechanical stress, absorption of light or heat [42]. According to the mechanism of photon emission, photoluminescence can be in form of fluorescence and phosphorescence. Fluorescence is spin-allowed and fast process with average lifetime of about 10 ns (10^{-8} s). Fluorescence measurements are popular due to the large variety of dyes with different structural and photophysical properties. Phosphorescence is a process of photon emission from the triplet excited state, where electron on the excited orbital has the same spin as the one on the ground state. In this case returning of the electron to the ground state is forbidden and this process requires longer time (10^{-6} – 10 s). Phosphorescence should not

be mixed with delayed fluorescence, where electron spontaneously moves from triplet state back to the singlet, and photon emission is identical to fluorescence with phosphorescence-like lifetime.

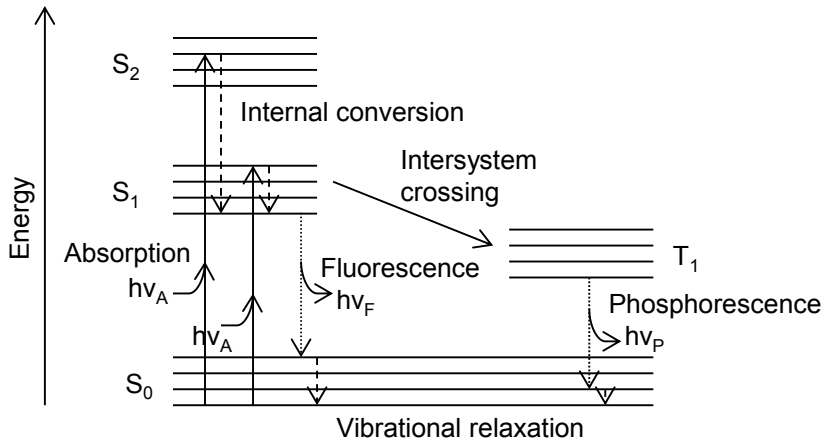

Figure 1.1 A simplified Jablonski diagram.

The processes, which occur in the system between excitation and emission, are described by Jablonski diagram (Fig.1.1), where singlet and triplet states are depicted as S and T respectively. On this scheme absorption and emission by fluorescence or phosphorescence are radiative transitions, and vibrational relaxation, internal conversion and intersystem crossing – non-radiative, which are fast and do not influence the lifetime of the luminophore. The energy loss between excitation and emission, known as a Stokes' shift, can be explained by these non-radiative processes, solvent effects and energy transfer.

1.2.2 Luminescence quenching by O_2.

Quenching is a decrease of luminescence intensity caused by formation of non-fluorescent complexes, energy transfer or molecular rearrangements. Static quenching is due to formation of non-fluorescent complex between fluorophore and quencher. Collisional quenching is a process of energy loss due to the contact of excited luminorophore molecule with the quencher, followed by return to the ground state without photon emission and chemical changes [43]:

$$M^* + Q = M + Q.$$

For both dynamic and static quenching the contact between molecules is essential, so temperature and pressure in the system having strong influence on the process. Common molecular quenchers are aromatic and aliphatic amines, halogens and halogenated compounds, heavy atoms (Cu^{2+}, Cd^{2+}, Ag^{+}, Cs^{+}) and pyrimidines. O_2 has been shown as a collisional quencher of the long-lived excited triplet states of luminophores (long-decay phosphorescence indicators) [42].

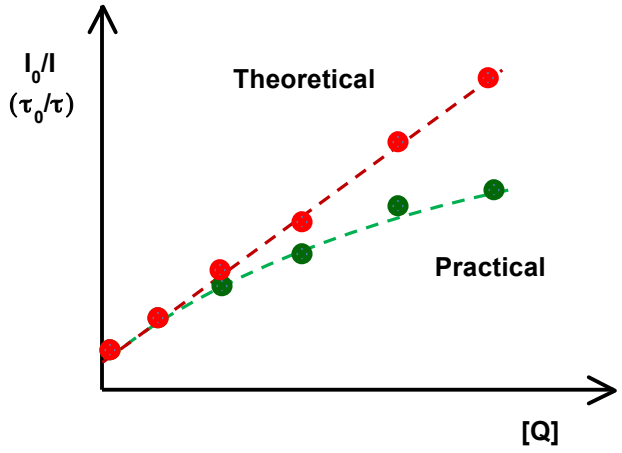

Figure 1.2 Examples of theoretical and practical Stern-Volmer plots.

The process of quenching by O_2 is described by the Stern-Volmer equation:

$$\frac{F_0}{F} = \frac{\tau_0}{\tau} = 1 + k_q \tau_0 [Q], \qquad \text{(Eq.1.1)}$$

where F and F_0 are intensities of luminescence; τ and τ_0 are luminescence lifetimes with and without quencher respectively; k_q is a bimolecular quenching constant, and [Q] is a quencher concentration (O_2 in our case). Luminescence lifetime is an average time, which

luminophore spends in the excited state. This is an intrinsic feature of the luminescent material, independent on the indicator concentration and way of measurement, but influenced by microenvironment. It can cause curved downwards Stern-Volmer plot in condensed phases (Figure 1.2). Increasing O_2 concentration reduces both luminescence lifetime and intensity [44]: $[O_2] = f(1/\tau, 1/I)$.

1.3 Detection modalities.

O_2 sensing is based on the measurement of indicator luminescence signal and relating it to O_2 concentration. Three main detection modalities are: intensity measurements at a single wavelength, ratiometric intensity measurement with a reference, O_2 insensitive dye and lifetime-based measurement [45].

1.3.1 Intensity mode

Intensity measurements represent the most simple and straightforward way of quenched photoluminescence O_2 monitoring. Sensitive material with known calibration $I = f([O_2])$ upon contact with the sample reversibly changes its intensity depending on the O_2 concentration. To read the signal, sensitive material is excited at optimal wavelength and emission at a single wavelength is collected (Fig. 1.3 A). Luminescence intensity can be measured in the desired range of O_2 concentrations with simple equipment and various probes. However, intensity signals are influenced by the concentration and photobleaching of the reporter dye, measurement geometry and sample optical properties, which makes measurements mostly qualitative rather than quantitative. Furthermore, instability of the light source and detector can lead to considerable signal variability, affecting calibrations. All these reasons stimulated interest in development of alternative O_2 detection modalities, which minimize or overcome these drawbacks.

Time-Resolved Fluorescence (TR-F) intensity measurements significantly improve sensitivity of the method and the signal to noise ratio (Fig. 1.3 C). It is based on the measurement of luminescence intensity at certain time after short-pulse excitation of the

sensitive material in contact with the sample of interest [41]. Phosphorescence decay is long and described by the exponential equation:

$$I_t = I_0 e^{-t/\tau}, \qquad \text{(Eq.1.2)}$$

Excitation pulse is followed by appropriate delay time to exclude interfering influence of the short-lived light scattering and autofluorescence and then intensity signal is collected. Such approach is specifically applicable for long lived fluorescence (or phosphorescence) and despite losing a fraction of luminophore emission, allows large improvement of signal-to-noise ratio.

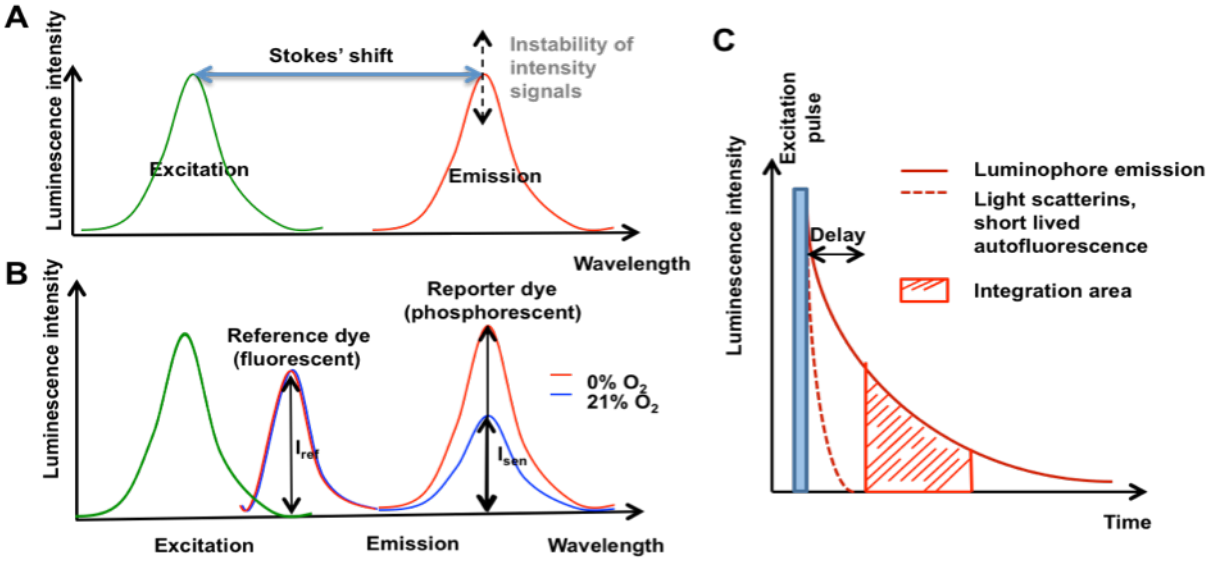

Figure 1.3 Intensity based detection modalities. A. Intensity measurement at a single wavelength. Phosphorescence spectra with large Stokes' shift. B. Ratiometric intensity measurement. Excitation and emission spectra of oxygen sensitive (phosphorescent) and reference (fluorescent) dyes at 0 and 21% O_2. C. Principle of time-resolved fluorescence (TR-F) intensity measurements.

1.3.2 Ratiometric intensity mode

Ratiometric intensity mode was introduced to overcome some limitations of intensity measurements related to instability of signals and O_2 calibrations. It involves parallel intensity measurements in two spectral channels of O_2 indicator and reference O_2 non-

sensitive dye (Fig.1.3 B). The ratio signal of the O_2 sensor and reference intensities corresponds to the O_2 concentration: $I_{sen}/I_{ref} = f([O_2])$.

In order to perform such measurements, optimal reference should be found for each sensor dye. A combination of phosphorescent O_2 sensing material and fluorescent reference is a popular solution. Phosphorescence emission has a large shift towards longer wavelength and provides well-resolved spectral window for collection of fluorescent reporter signal. Combination of two dyes allows exclusion of errors related to concentration effects, light source (or detector) fluctuations and even photobleaching in case of similar light degradation mechanism for both dyes. The optimal situation is observed when signals of O_2 sensitive and reference dyes can be monitored at the same time point. This can be realized for dyes excited at one wavelength with simultaneous collection of emission intensities in two channels. However, even in the case of sequential measurements in ratiometric modality, stable linear calibration can be obtained on different detection platforms. High signal-to-noise ratio for each signal improves the sensitivity of ratiometric method and allows for bioanalytical applications with complex samples [46].

1.3.3 Lifetime based O_2 sensing

In contrast to intensity, luminescence lifetime is the intrinsic feature of the substance and independent of concentration. Moreover, luminescence lifetime is less sensitive to photobleaching, measurement geometry and instrumental instabilities, which makes this modality preferable for accurate quantitative measurements [47]. Lifetime based methods can be classified into (1) phase modulation and (2) time-domain techniques. Excitation in phase-fluorimetry is performed by a periodically modulated light, and phase shift (ϕ) of the luminescent signal is measured and used for lifetime calculation (Figure 1.4 A):

$$\tau = \frac{\tan(\phi)}{2\pi\nu}, \qquad \text{(Eq.1.3)}$$

where ν is modulation frequency of excitation. In complex biological samples calibration instability of phase measurements can be due to the autofluorescence and light scattering.

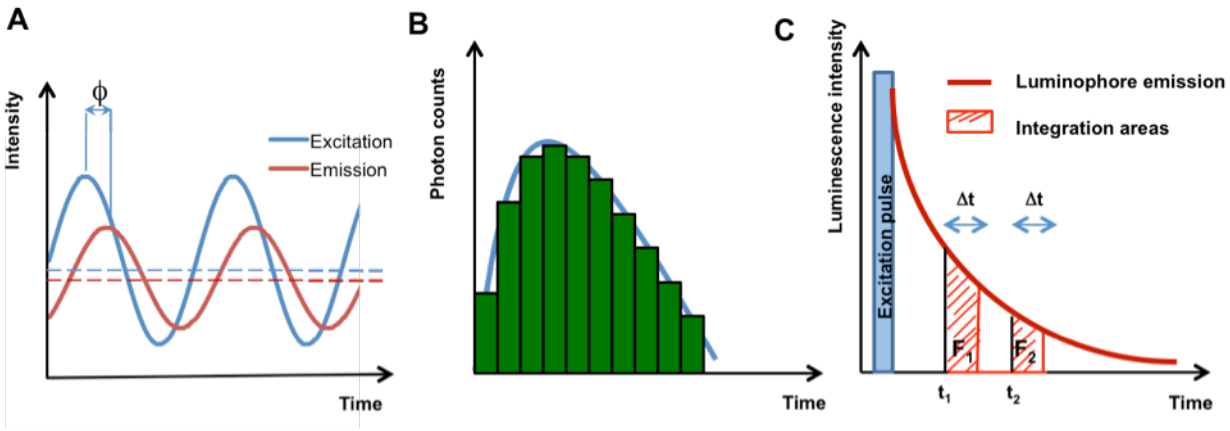

Figure 1.4. Lifetime based detection. A. Principle of phase modulation O_2 detection. B. Principle of TCSPC detection. C. Schematic presentation of the RLD method.

The time domain technique requires excitation of the luminophore by short (shorter than its lifetime) pulses for accurate lifetime measurements. This is rather difficult to realize with short lived fluorophores, but well suited for phosphorescent dyes. Direct measurement of the decay can be performed by shifting of the detector gate time after excitation and generating emission decay curve with a time gated detector (Fig.1.4 B). The time correlated single photon counting (TCSPC) method is based on the detection of arrival time for individual photons and reconstructing the histogram of decay.

A simplified version of direct luminescence decay measurement by TR-F is Rapid Lifetime Determination (RLD) (Fig.1.4 C), whereby two emission intensity signals (F_1, F_2) are taken with different delay times (t_1 and t_2) and fixed gate time [48]. Calculation of the luminescence lifetime by RLD is performed according to the equation:

$$\tau = \frac{(t_2 - t_1)}{\ln(F_1 / F_2)}, \qquad \text{(Eq.1.4)}$$

Measured lifetime values are used for the calculation of O_2 concentration by applying a calibration equation, specific for a given sensor material. To obtain this equation, a series of measurements of the luminescence signal under stable conditions (temperature, pressure, probe concentration) are performed and plotted versus different known O_2 concentrations.

Instrumentation for luminescence lifetime measurements is generally more sophisticated than for intensity measurements, but not uncommon. TR-F mode overcomes problems with sample autofluorescence, scattering and is widely used for O_2 detection in complex biological samples. Many modern instruments often have build-in TR-F detection mode for use with phosphorescent probes, which have lifetime in microsecond range, however they cannot detect short lifetimes (nanoseconds - <10 μs).

1.4 O_2 sensitive materials

O_2 sensors are materials which in combination with appropriate detection system provide measurement of O_2 concentration (or related parameter) in samples of interest. An O_2 sensor consists of a luminescent *dye*, which can be efficiently quenched by O_2, generating signals corresponding to its concentration. To provide optimal quenching properties and to protect from the unwanted interfering quenching, the dye is often placed in a specific environment, called *quenching media*. Depending on the chemical structure, manufacturing process and application area, this sensor material can be in the form of *solid-state* sensors or *soluble probes* (molecule conjugates, supramolecular probes and particles).

1.4.1 Oxygen sensitive dyes

Since the reversible quenching of luminescence by O_2 was first observed by Kautsky in 1939 [49], the pool of O_2 sensitive indicators was significantly enlarged. The choice of the dye is mainly justified by the desired spectral characteristics, brightness, chemical and photo-stability, luminescence lifetime range and possibility for chemical modification or

immobilization. Live tissue O_2 imaging requires deep light penetration and mild irradiation energies, which can be performed with red and infra-red (IR) indicators, excitable above 600 nm, or with multi-photon lasers. On the other hand, most of standard optics and detection systems used in laboratory applications are designed for visible range indicators, emitting at 550-700 nm. Brightness and photostability of the dye directly influence sensitivity and accuracy and should be considered for each measurement task. In lifetime-based modality phosphorescence dyes with relatively short lifetimes are preferable for the fast data acquisition and high-throughput measurements, while dyes with long lifetime are irreplaceable for high sensitive measurements of low O_2 concentrations in the range of 0-5 kPa. Existing O_2 sensitive dyes can be classified by their structure in several groups: polycyclic aromatics, transition metal polypyridyl complexes, cyclometallated complexes and metalloporphyrins [50]. Their spectral characteristics, stability, sensitivity to O_2 and possible bioanalytical applications vary significantly.

Polycyclic aromatic hydrocarbons represent an old group of fluorescent dyes suitable for O_2 measurement. One member of this group – pyrene – for a long time was an important part of solid-state O_2 sensors due to adequate sensitivity and wide availability [51]. However, its instability in polymeric matrices led to the development of functional derivatives with lipophilic chains and branched architecture. Perylene dibutyrate was used for *in vivo* O_2 measurement as a part of an optical fiber device [52]. Intracellular O_2 sensing can be performed with 1-pyrenebutyric acid (Fig. 1.5 A), which was delivered into isolated rat liver cells by passive loading [53]. This group of indicators has a number of important drawbacks, such as, moderate brightness, short fluorescence lifetimes (<200 ns), low solubility in polymeric matrices and short excitation wavelength (300-390 nm), which causes background fluorescence. This limited the use of indicators even in simple solid-state sensors and led to their fast substitution.

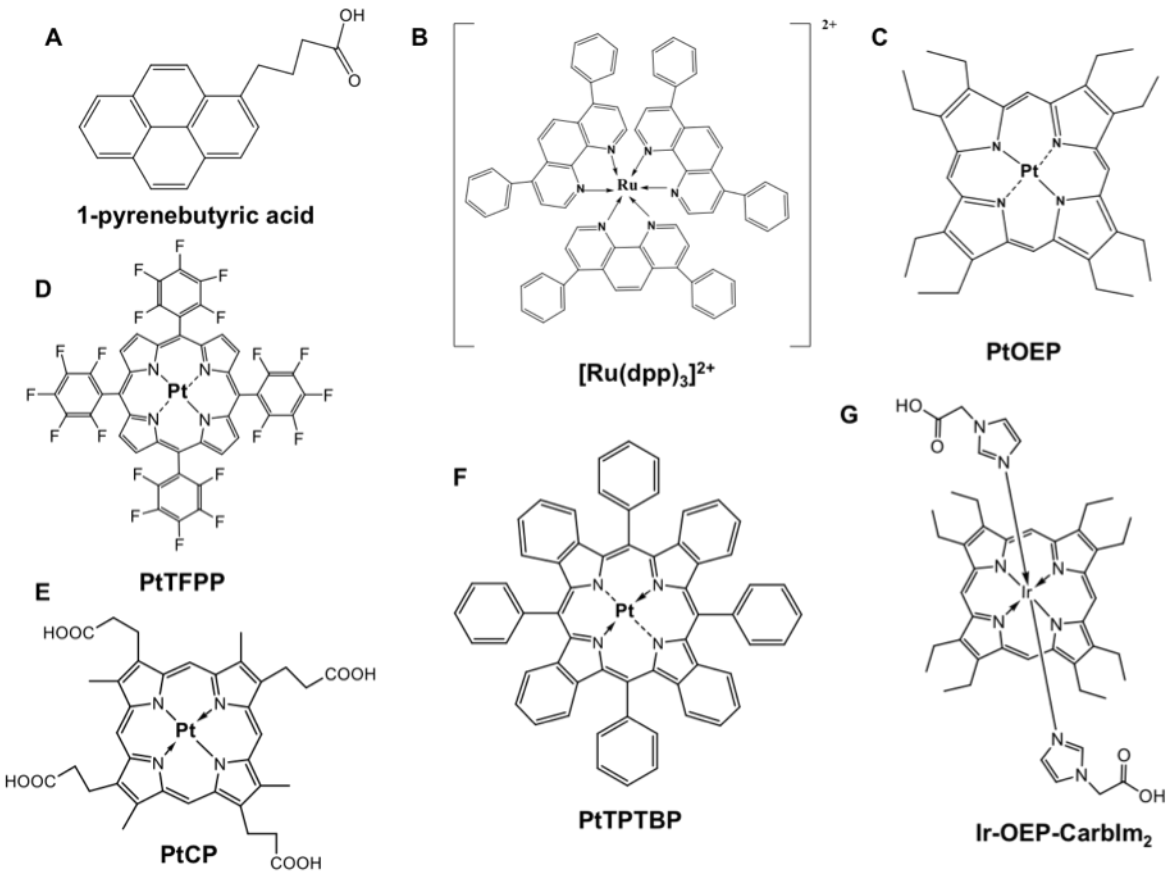

Figure 1.5. Structures of some popular O_2 sensitive dyes.

Within the group of *transition metal polypyridyle complexes* mostly Ru(II), Os(II) and Re(I) containing compounds were used for O_2 sensing. These dyes are photostable, have excitation and emission bands in the visible region and large Stokes' shift. Ru(II) complexes, and especially tris(4,7-diphenyl-1,10-phenanthroline) ruthenium(II) $[Ru(dpp)_3]^{2+}$ (Fig. 1.5 B), are popular indicators due to their longer lifetimes (up to 6.4 μs), moderate brightness and simple preparation methodology [51]. However, blue excitation, high temperature dependence of emission, insufficient sensitivity and wide luminescence spectra, which require filters and preclude multiplexing with other fluorescence dyes, caused development of alternative Os(II) complexes. Having similar structure, Os(II) complexes have higher photostability and excitation in more convenient red spectral range. Within this group, $[Os(phen)_3]^{2+}$ and $[Os(dpp)_3]^{2+}$ were most frequently used in solid-state O_2 sensors [54]. Brightness and luminescence lifetime of such indicators are lower than for Ru(II) complexes. Re(I) complexes such as

$[Re(dpp)(CO)_3CNR]^+$, having optimal excitation below 400 nm, moderate brightness and long lifetime around 40 μs, were used in some O_2 sensors [55].

Another group of indicators, which was actively developing recently, includes *cyclometallated complexes* of Ir(III) and Pt(II). Examples of this series are [Ir(ppy)3], $Ir(C_S)_2$(acac), C^N3Pt(acac) and their derivatives [56, 57]. They have emission in the range from green to near-IR with large Stokes' shift and moderate photostability, however their low molecular absorption and short luminescent lifetimes about 10 μs require improvement.

The most common and diverse group of indicators for O_2 sensing includes *phosphorescent Pt(II), Pd(II) and Ir(III) porphyrins* and related structures. They became popular due to their long lifetimes (up to milliseconds), large Stokes' shift and spectral characteristics, which can be changed by simple chemical modification. Platinum and palladium tetrakis(4-carboxyphenyl)porphyrin PtTCPP and PdTCPP were initially used in O_2 probes, but have moderate brightness and photostability [58]. Octaethylporphyrins PtOEP, PdOEP are still popular indicators having phosphorescence lifetimes of 91 and 990 μs respectively and high brightness. Photodegradation and hydrophobicity of such indicators resulted in their use mostly in solid-state form after immobilization on polystyrene, ethyl cellulose and other matrices [59]. Stability problem was solved by introducing of Pt(II) and Pd(II) porphyrin ketones (PtOEPK, PdOEPK) with optimal absorption bands shifted to 600 nm, however such modification led to the decrease of lifetime and brightness [60]. Platinum tetrakis(pentafuorophenyl)porphyrin (PtTFPP), tetracaboxylic Pt(II) coproporphyrin I (PtCP) and their Pd(II) analogues superseded the previously discussed indicators [61]. Pt(II) complexes of this group have phosphorescence lifetime in the convenient range of 20-80 μs and spectral bands in the visible area, which ensures sensitive monitoring with laboratory detection systems. PtCP does not possess the high photostablity characteristic of PtTFPP, however their solubility and ease of chemical modification proved valuable for tuning of the dye to different applications and detection platforms [62]. PdTFPP and PdCP dyes having lifetime about 1 ms are more applicable for the measurement of trace O_2 amounts. To measure O_2 concentrations in 3D cell models and tissues, red and IR probes for deep light penetration

are required. Highly-photostable porphyrin lactones (PtTFPPL, PdTFPPL) and benzoporhyrins (PtTPTBP, PdTPTBP) form a group of near-IR indicators (excitation over 600nm) for such tasks [63]. Benzoporphyrins show high brightness upon excitation of both Soret and Q-band. Nowadays these indicators are actively used for intracellular sensing and *in vivo* imaging after appropriate modifications [64]. Metalloporphyrins with new architecture were synthesized with Ir(III) central atom from Ir-OEP-CO-Cl precursor [65]. Chemical modifications of axial ligands of this complex allow changing of indicator solubility, brightness, lifetime and photophysical characteristics. Functional groups for intracellular delivery of O_2 sensor were also introduced to the Ir(III) complex [66].

1.4.2 Quenching media

Supporting material (i.e. microenvironment or quenching media) for luminescent reporter dye is an important part of O_2 sensor. It directly surrounds the dye, affects many of its properties, providing optimal environment for sensing [67]. For water-soluble dyes, quenching media is represented by the sample itself, i.e. aqueous solution of particular pH, salt and serum concentration. The main requirements for solid-state quenching media (usually polymeric materials or coatings) are: 1) physical strength and sufficient adhesion to the surface of support; 2) sufficient solubility and efficient encapsulation of the reporter dye; 3) optimal O_2 permeability; 4) appropriate optical properties; 5) keeping or improving of photophysical properties of the dye and reducing the unwanted interactions with surrounding media.

High solubility of the reporter dye in the quenching media is important for its homogeneous distribution within sensor material and for the uniform microenvironment for all dye molecules. Many polymeric materials produce non-linear, curved downwards, Stern-Volmer plots and influence sensor performance. This can be explained by a mechanistic model, where microheterogenity of the luminescence material leads to the formation of two sites with different quenching rates. This model can be described with the basic equation:

$$\frac{F_0}{F} = \frac{\tau_0}{\tau} = 1 \Big/ \left(\frac{f_{01}}{1 + K_{sv1}[Q]} + \frac{f_{02}}{1 + K_{sv2}[Q]}\right), \qquad \text{(Eq.1.5)}$$

Where f_{01} and f_{02} are fractions of the total emission of each component without quencher, K_{sv1} and K_{sv2} are associated Stern-Volmer constants, and [Q] is a quencher concentration [68]. The non-linear Stern-Volmer equation allows better fitting of experimental data and calculation of O_2 concentration.

Solubility of dyes in polymeric material can be improved by including long aliphatic groups in their structure. Gas permeability of the quenching media controls the process of O_2 diffusion to the encapsulated reporter dye, response time and sensitivity of the sensor. Encapsulation can also change the photophysical properties of the dyes. Thus, Ru(II) complexes possess stronger luminescence and longer decay times in solid matrices than in a soluble form, due to decrease of interfering interactions. Some combinations of the dye and quenching media can cause significant shift of the maximal luminescence wavelength [67].

Immobilization of a sensitive dye on solid support can be performed physically by adsorption or encapsulation, or chemically by covalent binding. Chemical linking is preferred for reusable sensors due to long shelf-life, however the procedure is often time-consuming and can change the properties of the dye. Physical methods are simple and fast, though sensors with adsorbed dye are rather unstable due to insufficient attachment. Encapsulation ensures homogenous distribution of the dye with minimized leaching, which made it more popular over the last few decades [69].

The media used for indicator immobilization are organic (polyethylene, poly(methylmethacrylate), poly(vinylchloride), fluoropolymers [70, 71], cellulose derivatives [72]), inorganic (sol-gels [73], silicone polymers) and hybrid silicon-oxide matrix with organic fragments (ORMOSIL) materials [74]. Photostability of encapsulated dyes is generally increased compared to soluble forms. The best results were observed for sol-gel and fluorinated materials [75, 76]. Organic polymers show high O_2 permeability and oxidative stability, whereas for inorganic polymers simple preparation, efficient encapsulation and biocompartibility is more characteristic. The use of organic polymers

is limited by their toxicity upon preparation and probe leaching. Hybrid polymers can be less fragile than inorganic matrices and form a promising group of quenching media [69].

1.5 Phosphorescent O_2 sensors

1.5.1 Solid state sensors

The large variety of measurement tasks, from gas analysis in packaging to live tissue imaging, necessitates the development of optical O_2 sensors in a number of different formats.

Solid-state sensors represent one of the first and most diverse groups of materials for O_2 measurement. They utilize the simple idea of reporter dye immobilization on a solid support. This technique allows applying a large amount of sensitive dye to a small surface area and providing high sensitive point measurement without contamination of the sample. Solid sensors protect the dye from quenching interference of the media and achieve optimal photophysical properties, so they can be used even in intensity mode with high accuracy. This solid-state approach is employed in fiber optic sensors, integrated systems and in sensitive coatings (films, paints).

The most developed group of solid state sensors includes O_2 sensitive *coatings, paints and films* (Fig.1.6 B). Reporter dye in an appropriate polymeric matric is typically forming a thin film coating on the surface of a solid support, such as microwell, biochip, customized cell, cuvette, microscopy dish or fluidic chamber (Fig.1.6 C) [77, 78]. Sample is placed in one of these assay vessels, in direct contact with the sensor, while the luminescence detection system is usually located outside, providing contactless measurement.

In contrast to microsensors, *fiber optic O_2 sensors* (Fig. 1.6 A) enable the same spatial resolution around 50 μm are easy to prepare, have stable calibration in the range of 0-100% O_2 and can be manufactured with different reporter dyes and polymeric matrices depending on the measurement task [79]. The size of sensor tip influences its invasiveness, response time, sensitivity and physical stability [80]. Fiber-optic

microsensors with a tip size below 10 μm are fragile and used mostly in small volume aqueous samples, whereas for complex biological systems a size 30-200 μm is preferred [81]. A number of fiber optic O_2 or multi-analyte sensors can be built on one detection platform. An example of such *integrated system* with O_2 and pH sensors coupled to the fiber-optic waveguides is the XF24 Extracellular Flux Analyzer (Seahorse Bioscience, Billerica, MA) [82]. It enables parallel measurements of OCR and extracellular acidification (ECA) by adherent cells in customized microtiter plates with sealed microchambers. Another type of integrated optical sensing is represented by 96-WP with sensitive and reference fluorophores in the bottom for monitoring of dissolved oxygen concentration during microbial cultivation [83].

Solid state O_2 sensors are simple to use, they do not contaminate sample under investigation and provide accurate measurement of extracellular O_2. However, they do not have sufficient flexibility and compatibility for O_2 sensing in complex biological samples, monitoring of gradients, intracellular measurements and O_2 imaging.

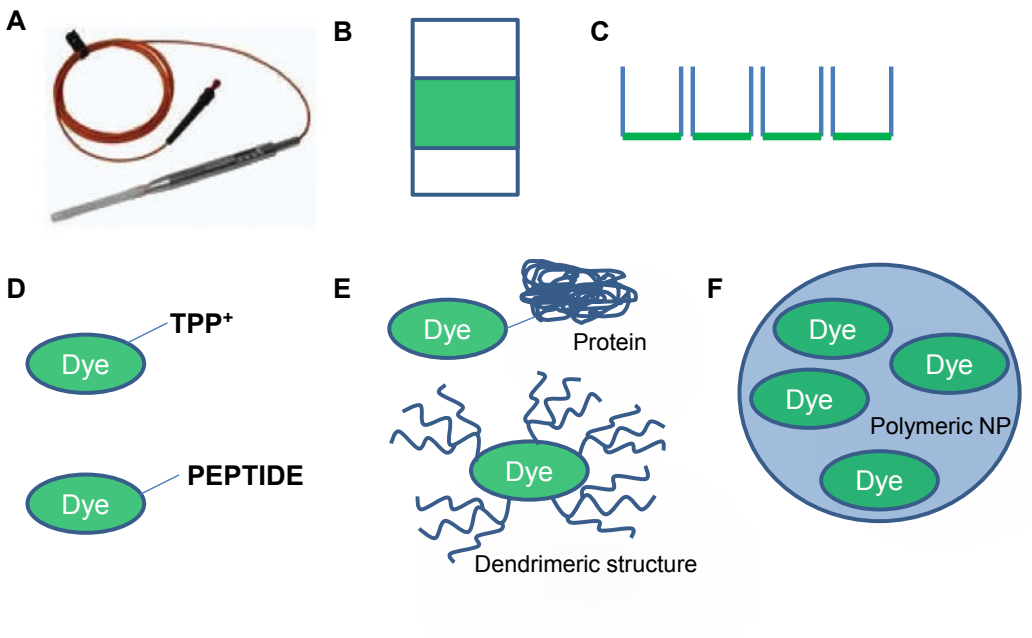

Figure 1.6 Schematic representation of the main solid-state O_2 sensors: A) fiber optic, B) thin film, C) coating of the wells; and soluble O_2 probes: D) small molecule, E) supramolecular, F) nanoparticle-based.

1.5.2 Soluble O_2 probes

Soluble probes in comparison with solid state sensors provide significant freedom in application to different samples, platforms and measurement tasks. They can be distributed across the measured sample, providing possibilities for monitoring of O_2 gradients and live imaging. The soluble probe format can be used in complex biological models, such as cell cultures, tissues and even whole organisms without additional preparations. Nevertheless, they also have some drawbacks, mostly associated with contamination of the sample if used in high concentrations, self-quenching in solution and matrix effects, moderate photostability and possible toxic effects on biological objects. These problems are now under intense investigation and are no longer limiting the use of such probes. The existing O_2 probes, based on their cell penetration properties, can be categorized into extra-, peri- and intracellular, and by their structure - into small molecule conjugates, supramolecular structures and nanoparticle based probes.

1.5.2.1 Small molecule probes are represented by hydrophilic free dyes such as PtTCPP, PtCP and Ru(II) complexes, and their derivatives modified with functional groups (Fig. 1.7 D) [84]. Water solubility of free dyes can be achieved by means of carboxylic and sulfonate groups in their structure, however they often possess significant non-specific adsorption and interaction with proteins and biopolymers. The chemical modification of indicator dyes has several aims: 1) to increase their solubility in aqueous samples and to avoid the step of pre-dissolving in organic solvents, which can cause cytotoxicity, 2) to increase cell permeability, 3) to target them to specific sub-cellular compartments. Probe solubility is often required in combination with intracellular delivery and in vivo imaging tasks. Low solubility in these assays can cause distortion of the luminescence spectra, aggregation in aqueous solution or upon contact with physiological liquids, unstable calibration and measurement artifacts.

1.5.2.2 Supramolecular probes. Binding of distinct functional moieties to the dye is an effective approach to improve their O_2 sensitive properties and cell permeability. For example, conjugation with proteins and polymeric carriers can prevent cell penetration or binding to surfaces, improve probe stability in solution and O_2 calibration (Fig. 1.7 E). MitoXpress probe, comprising BSA conjugate of a PtCP dye, is used for respirometry

analysis with cell, bacteria, yeast cultures, isolated mitochondria and even 3D cell models. Simple in preparation, it shows high brightness, stable calibration and optimal O_2 sensitivity for different measurement tasks [85].

Dendrimeric (or core-shell) structures are efficient for development of O_2 probes with improved characteristics. They typically contain reporter dye modified by brunched dendrimeric groups to protect it from interference by media components and self-quenching. Such, probes based on Pt(II) porphyrine and benzoporphyrin with poly(glutamate) dendrimeric shell, introduced by the Vinogradov group [86], are highly soluble in physiological liquids, and provide oxygen sensing in red and near-IR range, suitable for monitoring of oxygenation in vasculature of live animals. Additional hydrophilic polyethylene glycol (PEG) chains in the exterior layer improve solubility, stability in aqueous solutions and biocompatibility [87]. Multi-component dendrimeric structures enable tuning of the probe. For example, π-extension of the porphyrin macrocycle changes spectral characteristics, whereas hydrophobic dendrimers in the structure influence O_2 diffusion and dye shielding [88, 89]. Dendrimeric structures with protected dye possess large size (typically around 500-800 nm) and are mostly used for extracellular sensing.

1.5.3 Micro- and nanoparticle based probes

Particle-based probes combine advantages of both solid state sensors and soluble probes [90]. Polymeric shell protects sensor dye from interferences, self-quenching and photodegradation, and stabilizes oxygen calibration, whereas particle format allows minimal invasiveness, flexibility in the sample and platform choices. Variability of sizes and constructions of the probes can satisfy many bioanalytical tasks [91]. Nanoparticle (NP) O_2 probes can be prepared by impregnation of pre-formed polymeric beads, inclusion of indicator during emulsion polymerization or by precipitation method. The last method is attractive due to a simple and controlled procedure, uniform distribution of the dye in polymeric matrix with efficient retention and minimal leakage [92]. Hydrophobic dyes with optimal photophysical properties, but otherwise high toxicity and

low solubility in water, can be used in NP probes [93]. Thus, PtTFPP dye possessing high photostability and brightness became popular for different NP probes [94]. Probes produced by biologically localized embedding (PEBBLEs) were developed for a number of metabolic substrates. For O_2 sensing one of the first probes of this type contains reporter dye entrapped in polyacrylamide shell in an inverse microemulsion with final size about 20 nm [95]. Polymeric materials for PEBBLEs formation, such as polyacrylamide and polystyrene show high biocompatibility [96]. PEBBLEs were actively applied for intracellular sensing, employing different delivery techniques, such as pica-injections, electroporation, gene gun and liposomal transfer [97]. Recently, cell permeability was proven for some polymeric NPs with average size of 35 nm [94].

The possibility of measurement of cellular O_2 concentration in ratiometric mode is desirable, due to simple setup and moderate accuracy. This can be achieved by combining the reporter dye with a luminescent reference moiety in one NP entity. A ratiometric probe was developed by embedding of O_2 sensitive $[Ru(dpp)_3]^{2+}$ and reference Oregon Green 488-dextran dyes in sol-get matrix, followed by NP stabilization by PEGylation [98]. This probe has a relatively wide size range (50-300 nm) and a heterogeneous distribution of dyes across particles, however it can be used for intracellular applications after active delivery. A technique to decrease the size of NPs and increase brightness by excluding ballast polymeric shell from the structure was also developed [99]. Copolymer of Pt(II) porphyrin and 9,9-dioctylfluorene was prepared which allowed adjustment of intensity of both reporter and reference signals in the detection system by varying the amount of monomers. This copolymer is excitable at one wavelength (380 nm) with spectrally resolvable emission maxima at 416 and 650 nm for reference and reporter dyes respectively. Side chains of copolymer can be used for further chemical modification with microcariers (for example PEG) to form NPs.

1.5.4 Cell-permeable O_2 probes.

Measurement of cellular respiration and oxygenation is important for metabolic and bioenergetic studies. Information about the cellular O_2 concentrations can be obtained by

direct sensing in intracellular locations or by measurement of O_2 in the extracellular space (Figure 1.7). In the first case, information about O_2 gradients, cell culture heterogeneity and dynamic changes of oxygenation can be obtained with high sensitivity. However, extracellular sensing is also valuable for fast screening tests with minimal sample preparation and invasiveness. Both methods have found application niches.

For *extracellular* O_2 sensing brightness and minimal non-specific adsorption of the probe are of the highest importance. The use of free O_2 sensitive dyes and small molecule probes is limited in extracellular sensing due to the random penetration of some cells, adsorption on the cell or vessel surface and formation of aggregates. Soluble and stable in solution, supramolecular probes possessing bigger size are preferable. Different types of PEGylated dendrimers and conjugates with cargo-proteins are effectively used for extracellular sensing. They show applicability in tissue oxygenation monitoring and metabolic studies with mammalian cells [88, 100]. Core-shell structure with encapsulated PtTPTBP reporter, and covalently attached to the surface TFPP dye, was introduced for simultaneous measurement of extracellular O_2 and pH [101].

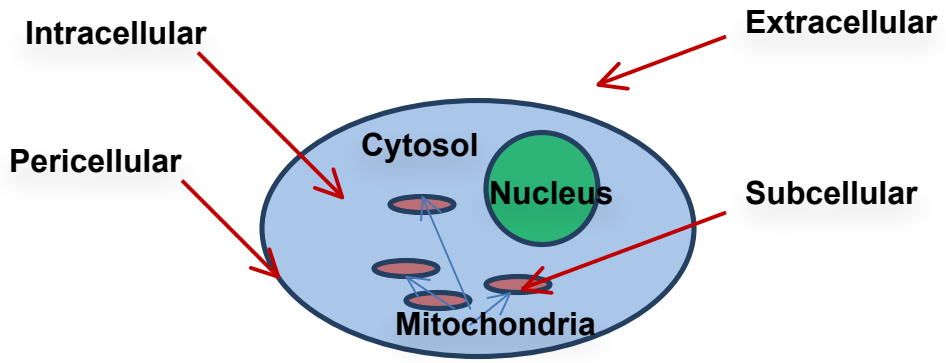

Figure 1.7 Measurement of cellular O_2 at different locations.

Measurement of *intracellular* O_2 is becoming popular nowadays due to the fast development of new prospective cell permeable probes. By "intracellular O_2 probes" we mean soluble compounds and NPs, which can penetrate cells by passive means.

One group of intracellular O_2 probes is formed by macromolecular conjugates. The concept of cell penetrating peptides (CPP) conjugated to a luminescent dye to provide intracellular or subcellular targeting, is actively developing over the last decade [102]. For delivery of metalloporphyrins, trans-activator of transcription (TAT)-derived peptides were used. The PtCP dye was conjugated to the TAT peptides and their oligoarginine derivatives [103]. The probes obtained in this way possess efficient delivery to all studied cell lines (HCT116, PC12, HeLa, SH-SY5Y) by direct translocation and endocytosis. Although showing non-specific adsorption to the surfaces, they were used in physiological studies for monitoring of dynamic changes in O_2 concentrations [104]. Ir(III) complexes were conjugated with arginine- and proline-rich peptides bearing histidine residues [66]. Reporter probe can also be targeted to specific compartment of the cell. Delivery to mitochondria with positively charged residues of rhodamine, triphenylphosphonium (TPP) and mitochondria targeting peptides (MPPs) has been demonstrated for detection of ROS [105]. However a probe for direct measurement of mitochondrial O_2 concentration is still not available.

Peri-cellular O_2 probes combine conjugates of dyes with residues facilitating binding to cell membrane. Surface targeting groups are mostly represented by peptides, so these probes can be included in supramolecular category. One such peri-cellular probe, which consists of PtCP dye conjugated with ER9Q protein, efficiently binds to the surface of PC12 cells [106].

Nanoparticle based probes for intracellular O_2 sensing are under active development. Polymeric NPs caring Ru(II) O_2 sensitive dyes and combination of Pt(II)-porphyrin and reference dyes have been introduced for ratiometric sensing of intracellular O_2 in mammalian cells [107, 108]. Such probes provide diffuse intracellular staining after long incubation (24-72 hours), they show significant cytotoxicity or require facilitated delivery techniques (e.g. electroporation, gene gun). Success in intracellular NP delivery was achieved with positively charged RL100 polymeric NP, caring PtTFPP dye [94], which provide fast (6-16 hours) and bright intracellular staining with minimal toxicity. Such probes have become popular for physiological studies, however some specificity in cell loading has been observed.

1.6 Measurement of cellular O_2 and physiological applications.

Cellular O_2 concentration and consumption rate can be used as an indicator of cell viability, development state, pathological conditions and toxic effects. An adequately chosen measurement technique provides informative picture about the sample without cumbersome calculations. Often, measurement task requires prolonged monitoring of the sample in changing conditions, upon metabolic treatments and with parallel measurement of other parameters. A number of techniques have been developed, where O_2 concentration, its fluctuations or cell respiration is monitored. A TR-F plate reader can perform monitoring of these parameters with cell population, while single cell analysis, 2D and 3D O_2 imaging require microscopy techniques.

1.6.1 OCR measurement formats and platforms.

Cellular respiration or OCR is a useful indicator of cell viability, bioenergetics, mitochondrial function, effects of internal and external stimuli, drug toxicity and changes in cell metabolism [109, 110]. Average OCR can be measured with extracellular probe placed to the sample, solid-state sensor incorporated into the assay vessel or intracellular probe. They all are interchangeable and provide similar information, however require different setups and measurement procedures. Measurement of absolute OCR values requires sealed setup to eliminate O_2 back-diffusion interference. To avoid formation of gradients inside the vessel, which can distort measurements of absolute OCR, continuous stirring is often provided. Designed for such measurements gas-impermeable (glass, quartz) cuvettes and chambers can be equipped with a port for solid-state sensor placing or addition of stimulants [111].

For high throughput analysis, such as toxicity or metabolic screening, measurement of the absolute OCR values is not necessary [5]. Comparison of relative OCR values, which contain the same source of errors, is informative for assessment of cell samples with different metabolic treatments, culturing conditions or media composition. The vessel for

such relative readings does not require gas-impermeable material and complete sealing. A plastic microplate platform with the partial sealing of the sample (cell suspension or adherent cells covered with media) by the layer of mineral oil on the top is introduced [111]. It forms the diffusion barrier and promotes gradients formation inside the assay vessel [112]. Measurement of relative OCR was also performed in open plate with solid state Ru(II)-based sensor embedded into the wells bottom [113]. This setup required long monitoring for over 24 hours to see clear difference in respiration levels and was used to study the correlation between cell oxygenation and OCR.

Mitochondria consume most of the cellular oxygen (about 90%) for energy production by oxidative phosphorylation. Respiration activity informs about mitochondrial dysfunction, toxicological or adaptation effects, changes in bioenergetics [109]. Mitochondria can be isolated from cells without losing vital properties and used for OCR measurement. Initially Clark-type electrodes were used for such assays, however recently quenched luminescence methods became more popular [114, 115]. Mitochondrial respiration was monitored with PtCP-based probe MitoXpresss-Xtra (Luxcel Biosciences) in intensity and lifetime-based modalities on a standard luminescent plate reader [116]. In this assay partial sealing with mineral oil in standard 96 and 384-well microtitter plates is used. Solid-state platforms with fiber optic sensors, dipped into assay vessels, were also used for mitochondrial respiration monitoring upon metabolic treatments [117]. The lack of cell context limits the use of mitochondrial respiration techniques in bioanalysis.

Analysis of respiration in intact cells needs to take into account the probe's membrane penetration properties, cell specific metabolism, transport mechanisms and the natural conditions of cells (adherence, forming of aggregates). Respiration of individual mammalian cells is rather low, and large populations of cells in suspension or adhering to surface are required, with special attention to possible O_2 back-diffusion interference. Microtitter plate with partial sealing by mineral oil was used for measurement of mammalian cell respiration. This platform, as in case of mitochondrial respiration monitoring, does not provide absolute OCR values, however give good estimation of treatments effect (comparison with untreated cells) and allows multiplexing with ECA assay [112]. Fully integrated system XF Analyser was developed by Seahorse

Biosciences for adherent cells. Connected to the moving platform solid state sensors come close (200 nm) to the cell layer and form partially sealed microchambers, in which OCR and ECA are measured simultaneously. XF Analyser allows an addition of treatments during the experiment and monitoring of cells under different conditions, what makes it popular for cell bioenergetic and metabolic studies. Such, changes in the oxidative phosphorylation, glycolysis and their contribution to the cellular energy production were assessed [118]. A special algorithm to correct for O_2 back diffusion through plate material is used to calculate absolute OCRs [119]. High interest was shown to single cell respiration analysis. Methods of cell trapment in the microvessels and sealing were developed [77, 120]. They allow study of culture heterogeneity, behavior of cells in changing conditions, however lacks tissue context in physiological cell conditions. Existing methods for absolute OCR monitoring usually have sealed setup, which leads to the end point measurements of each sample.

1.6.2 Monitoring of local cell oxygenation.

Although OCR techniques are popular for screening assays with cell culture in adherent or suspension state, they are not informative about O_2 distribution, local gradients and their dynamics. Direct measurement of O_2 concentration in cell layer at steady-state or microfluidic conditions can address these goals [78]. Solid-state sensors have limited applicability to oxygenation monitoring due to biocompartibility issues of films and coatings and spot measurements with fiber-optic sensors [106]. Soluble probes provide higher flexibility, however, extracellular sensors are distributed around the sample and show only overall picture of oxygenation. The development of intracellular oxygen (icO_2) probes extended the possibilities of reliable and minimally invasive oxygenation monitoring, especially with live respiring cell and tissue samples [121]. These probes can be loaded in cells in their natural state (adherent, suspension) and monitored with available detection systems, such as TR-F plate readers, microscopes. To provide optimal monitoring conditions, cell density, sample geometry, temperature and ambient O_2 concentration should be controlled [46]. A variety of probes (discussed above) were developed and applied towards intracellular sensing. Monitoring of cell culture

oxygenation upon cell growing, attaching and differentiation, study of cell culture heterogeneity and measurement of other parameters related to cell respiration were demonstrated [122]. A new platform for high throughput oxygenation monitoring employs open microtitter plates with adherent or suspension cell loaded with icO_2 probes [123]. Steady-state oxygenation in this setup is a function of cell respiration activity and thereby of OCR. So far, correlation of cellular OCR and oxygenation has not been studied, however this correlation is of great interest.

Consumption of O_2 by mitochondria and its passive diffusion to the sample lead to the formation of O_2 gradients in respiring samples. Monitoring of gradients over cell cultures, tissues and whole organs is possible by "mapping" with O_2 sensing and imaging techniques.

O_2 gradients in microfluidic system are often observed due to small medium volume and limited gas exchange. They can have negative effect due to cells exposure to heterogeneous conditions and local hypoxia, which are difficult to estimate. However, gradients can be generated deliberately to mimic natural conditions, for example in the study of cell migration processes and ROS production [124-126]. In an open assay vessel, formation of vertical O_2 gradients is typical, sometimes with complete hypoxia in the layer of respiring adherent cells. Such situation was modeled for 96-well plate with differentiated PC12 cells at 21, 10 and 5% of ambient O_2 and then used to study cell adaptation and responses to metabolic treatments [121].

"Sub-cellular" O_2 gradients are formed for similar reasons, however their monitoring requires probes with different intracellular localization and/or spectral characteristics. The absence of significant oxygen gradients between the exta- and the intracellular space was reported for Hep3B cells, possibly due to low respiration activity [127]. The difference between O_2 concentration in mitochondria of lung fibroblasts and surrounding media was stated, based on the measurements of delayed fluorescence of endogenious protoporphyrin IX [128]. Cellular gradients were also studied with MEF cells and three different probes with intra-, peri- and extracellular localization [106]. Significant reduction of O_2 concentration in the cellular space compared to the surrounding media was detected on a TR-F plate reader. Different cell densities were used to optimize these

gradients and improve assay sensitivity. Studies of local O_2 gradients become important for 3D tissue models and tissue engineering [129].

1.6.3 Cell metabolism and drug toxicity studies.

Cell metabolism studies require understanding of the specific pathways used in physiological and pathological conditions. Available drugs can target many of them. Cell respiration, being sensitive to small changes in metabolism, can be used as a reporting parameter in the monitoring of cell responses to metabolic stimulations, adaptation to hypoxia conditions and drug toxicity screenings. Therefore, continuous monitoring of cellular respiration and O_2 upon changing conditions is desirable.

OCR assay can clearly detect both uncoupling and inhibition, being more specific than standard cell viability (or non-specific toxicity) measurement by total cellular ATP level [118]. Drug toxicity that influences glycolytic ATP pathways can be analyzed by combined OCR/ECA assay [114]. The platform for this assay was developed based on a combination of extracellular MitoXpress probe and standard 384-well plate [130]. It was validated with 200 common drugs and mammalian cell line HL60 in suspension. Seahorse XF analyzer was also applied for the similar task, however it lacks flexibility and requires specific plates and plate readers [131]. OCR can be multiplexed with other assays to reveal complex toxic effects of some drugs [132].

The toxicity of newly developed probes for cellular O_2 measurements is usually tested, because it can significantly distort the result of OCR and oxygenation assays [133]. Cytotoxicity is mostly caused by the quenching media and by supramolecular groups, which can influence metabolic pathways. The *in vivo* toxicity of NPs has been discussed previously in details with regards to size, shape, surface charge, composition and roughness [134].

For cell metabolism studies, sequential treatments and changes of measurement conditions are often required. Optimally, control response is measured in standard conditions, followed by treatment with continuous monitoring. OCR measurement with a

cell population can provide detailed information in such tasks; however sealed setups allow only end-point measurements [112]. Treated samples can be measured only in parallel with control, depending on the sample throughput. This problem was partially solved by a Seahorse XF analyzer, which allows four additions in the course of the experiment [109]. Bioenergetic status of the mammalian cell was assessed with this platform by measurement of normal, maximal and non-mitochondrial respiration. Oxygenation monitoring with icO_2 probes has an open setup, which allows multiple treatments or changes of sample conditions (pH, temperature, ambient O_2) [135]. In these measurements, lower ambient O_2 can be used to improve the method's sensitivity. Local cell oxygenation monitoring was used to study mitochondrial uncoupling by FCCP with mammalian cells depending on the media composition [100].

1.6.4 O_2 imaging formats and applications

Studies of O_2 gradients in cell cultures (2D and 3D) with single cell resolution require dedicated imaging techniques. The development of new imaging O_2 probes and detection systems to address these challenges is receiving much attention. Different types of O_2 sensitive probes (Ru(II), Pt(II) and Pd(II) dyes, small molecule, supramolecular and nanoparticles) were actively delivered inside cells by electroporation, microinjections, gene gun and transfection techniques to provide fluorescence microscopy imaging with improve resolution [98, 136, 137]. However, the invasiveness of such techniques leads to low cell viability, heterogeneity of cell culture and the appearance of imaging artifacts. Furthermore, selective delivery to certain cells and cell compartments is not sufficient to study O_2 gradients in complex biological models. NADH and FAD autofluorescence correlates with intracellular O_2 and can be used for non-invasive imaging, however, short decay times cause low sensitivity [114]. The development of intracellular probes, which can be delivered by passive loading, significantly improved performance of O_2 imaging. Study of culture heterogeneity, natural or obtained gradients and monitoring of O_2 during experiments, become possible with big variety of intensity-based or lifetime-based imaging techniques [94, 138]. Ratiometric-based imaging probes with reference dye and often FRET antenna at the same time found application for simple (intensity mode) and

high sensitive imaging [108, 139, 140]. The delivery of imaging probes to cancer cell lines by conjugation of dyes with tumor-specific peptides demonstrated high selectivity and possible application for tumor hypoxia imaging [141]. Mitochondria targeting of probes for O_2 sensing and imaging is now under active development [142]. Visualization of O_2 probes is possible with a number of imaging techniques depending on their spectral characteristics, brightness and type of cell sample.

In *wide-field microscopy,* the reporter dye in biological sample is excited with mercury lamp, laser or LED, and the emission is collected in a focal plane and the surrounding area [41]. To increase the contrast of the resulting image, the sample can be scanned through pinhole system to reflect all light except the light from the focal plane in *laser-scanning confocal microscopy*. Reconstruction of a 3D image is possible from the collected Z-stacks of the sample. Both wide-field and confocal microscopy can operate in intensity and lifetime modes. Fluorescence (phosphorescence) lifetime imaging microscopy (FLIM, PLIM) can overcome probe photodegradation issues and other drawbacks of the intensity mode [143]. Background signals and autofluorescence can be eliminated by gating out for probes with long luminescence lifetimes in micro- and milliseconds range, such as Pt(II) and Pd(II) porphyrins [144]. For live tissue, organs and thick 3D objects, imaging by *multi-photon microscopy* with deep light penetration (up to 1 mm) shows the best results [145].

Ex vivo models, such as tissue slices and organs, are actively employed for O_2 monitoring in developmental biology and drug testing. They preserve the native communications between cells; however lack active supplies from substrates. In one example, dynamic changes of intracellular O_2 were studied upon different treatments and contractions of skeletal muscle fibers [146]. In isolated salivary glands of blowfly, changes in O_2 consumption as a result of hormone-induced secretory activity were monitored by Pt(II)-based nanoparticles [147]. Accurate and sensitive monitoring of O_2 concentration *in vivo* is highly desirable for clinical and biomedical applications. 3D models, such as spheroids, cell aggregates and artificial organs are actively used for studying *in vivo* processes [148]. They possess natural cell microenvironment, communication and O_2 distribution. Models with cortical neural cells (neurospheres) and ovarian cancer cells

(tumor spheroids) were used to mimic (patho)physiological hypoxia [133, 149]. Their heterogeneous structure allows assessment of cell physiology, drug toxicity and cancer treatment efficiency by O_2 probes delivered spontaneously or upon formation of a sphere. A 3D scaffold seeded with cells is an alternative approach of tumor modeling for future O_2 monitoring [150]. Near-IR luminescent probes are highly desirable and are being actively developed for 3D cell models due to their soft irradiation and deep light penetration. In one specific case, ruthenium complexes were used for selective binding of cellular surface by avidin-biotin interaction and future monitoring of O_2 concentration in formed cell aggregates [151]. *In vivo* O_2 monitoring allows performing experiments in physiological normoxia for each tissue (in the range of 0.5-10% O_2) and avoiding measurement artifacts. A two-photon excitable (optimal at 840 nm) O_2 probe was used for in vivo imaging of bone marrow in an intact mouse skull [152]. Tumor and vascular oxygenation, neuronal activity, microcirculation and responses to sensory stimulation were studied *in vivo* with intravital and intracellular O_2 probes [46]. Unfortunately, many of these studies provide qualitative rather than quantitative information about oxygenation and oxygen consumption.

1.7 Conclusions

O_2 sensing by quenched luminescence technique offer advantages over alternative detection systems, such as non-invasiveness, no O_2 consumption upon measurement, high sensitivity, throughput and flexibility. The existing O_2 probes provide a platform for various applications. Solid state sensors occupy the niche of high-throughput semi-quantitative or quantitative O_2 monitoring, with limited choice of sample and detection platforms. Soluble, especially intracellular probes are under active development, but the existing probes have significant drawbacks. Small conjugates often have moderate brightness and photostability, self-quenching and aggregation in aqueous solution or biological matrices. Dendrimeric probes show improved brightness and photophysical properties due to protection of the dye; however, their complex structure requires time-consuming preparation and limits their use for intracellular applications. Conjugation of dyes with short peptides and proteins can increase probe solubility and add desirable cell

penetration properties or even targeting to a specific cell compartment without significant increase in size. Nanoparticle probes overcome many of these drawbacks: a sensitive dye is reliably protected from interferences by the polymeric bead, while NP size of 10-100 nm allows intracellular sensing. Depending on the composition, NPs can provide different storage stability, aggregation, cell penetration and toxicity. Current intracellular O_2 sensing techniques are far from optimal. Typically, existing probes suffer from low and cell specific staining, moderate brightness, photodegradation during long-term imaging and toxic effects. At the same time, big variety of O_2 sensitive indicators provides possibility for imaging in the entire visible and near-IR spectral range as well as multiplexing with other assays, using a number of spectrally resolvable dyes. The problem of incorporating these dyes in optimal sensing structures has to be solved. Multi-modal oxygen sensitive materials are of high interest, as they can be utilized on different detection platforms. Growing variety of measurement techniques also requires benchmarking of different probes and conditions, which can be performed with multi-modal probes.

The many measurement tasks discussed above give an idea about wide range of possible application of cellular and imaging O_2 probes in bioanalysis. Measurement of important parameters of O_2 sensing, such as cell respiration (OCR), oxygenation, and O_2 gradients can be performed using a number of different platforms. However, many of them require further optimization to simplify the measurement procedure, and to achieve desirable sensitivity and accuracy. Often such optimization includes all aspects of the platform: from development of the appropriate probes, to adaptation of the assay vessels, detection system and data processing scheme. Assessment of energy budget, study of cell responses to stimulations and drug toxicity screenings require high throughput and a simple procedure allowing additions during the experiment. No optimal platform for such O_2 measurements exists, however many studies to develop one have been attempted. O_2 imaging with single-cell resolution, in 3D cell models, whole organs and organisms is a new and underdeveloped field of research.

Aims and objectives

The main aim of this work was to develop advanced luminescent probes and techniques for intracellular oxygen sensing and imaging. Existing intracellular O_2 probes have significant limitations: low photostability and cell permeability, moderate brightness, short excitation wavelengths, toxic effects, poor compatibility with specific modality and detection systems. To overcome these drawbacks we pursued a number of different experimental approaches in order to develop new O_2 probes:

- Multi-modal probes
- Probes with improved cell permeability
- IR and green shifted probes
- Probes with improved brightness and photostability

It was expected that the development of these new probes would have a number of advantages, including improved sensitivity and accuracy of icO_2 measurements, targeting to an extended range of cell lines, low cytotoxicity, and compatibility with different detection modalities such as intensity, ratiometric intensity and lifetime. To achieve these aims reference and FRET antenna dyes, anionic polymeric NPs, small molecule delivery vectors and different types of IR and green shifted dyes were developed and tested.

We studied the limitations of existing OCR platforms and considered the possibility of overcoming them. The focus was on sensitivity, speed, simplicity, throughput, possibility of treatments and drug additions upon experiment. To improve these characteristics we evaluated new commercially available platforms and data processing strategies with a number of mammalian cell lines, and in different physiological experiments.

Chapter 2. Materials and methods

2.1 Materials

Platinum (II) meso-tetra(pentafluorophenyl)porphine PtPFPP dye and 9,9-diheptylfluorene-2,7-diboronic acid were obtained from Frontier Scientific (Inochem Ltd, Lancashire, UK). Coumarin C545T and 3,5-bis(trifluoromethyl) phenylboronic acid were obtained from Aldrich (Austria); 2,7-dibromo-9,9-di-p-tolyl-9H-fluorene was obtained from Luminescence Technology (Taiwan). Poly(9,9-diheptylfluorene-alt-9,9-di-p-tolyl-9H-fluorene) (PFO) was kindly provided by Prof. Sergey Borisov (Graz University of Technology, Graz, Austria). β-D-thioglucose and thiogalactose were obtained from Carbosynth Ltd (Berkshire, UK). Eudragit RL-100 was obtained from Degussa (Germany); poly(methyl methacrylate-co-methacrylic acid), 9:1 (PMMA-MA) was obtained from Polysciences (Warrington, PA, USA). Tetrakis(triphenylphosphine) palladium (O) = $Pd(PPh_3)_4$ was obtained from ABCR (Germany). The extracellular O_2 probe MitoXpress-Xtra, intracellular probe MitoXpress-Intra and mineral oil were obtained from Luxcel Biosciences (Cork, Ireland).

Synthetic G_2R_8-amide and R_2- amide peptides (purity >90% by HPLC; structures confirmed by mass spectrometry) were obtained from Genscript (Piscataway, NJ, USA). Anti-HIF-1a (H1alpha67, NB100-105) antibodies were obtained from Novus Biologicals (Cambridge, UK) and anti-HIF-2a (AP23352PU-N) from Acris Antibodies (Herford, Germany). B27 supplement, Alexa Fluor 488 - labeled secondary anti-mouse and anti-rabbit antibodies and Pro-Long Gold anti-fade reagent were obtained from Invitrogen (Bio Sciences, Dun Laoghaire, Ireland). Fibroblast and epidermal growth factors (FGF and EGF) were obtained from Millipore (Cork, Ireland). Phosphatase inhibitor cocktail (Nuclear extract kit, cat no. 40010) was obtained from Active Motif (La Hulpe, Belgium). Viability Assay kits CellTiter-GloTM and CellToxTM Green were obtained from Promega (MyByo, Ireland). All other reagents and gravity flow columns Discovery® DSC-18 SPE Tube were obtained from Sigma-Aldrich (Dun Laoghaire, Ireland). Desalting MiniTrap G-25 columns were obtained from GE Healthcare

(Buckinghamshire, UK). Standard cell culture grade 96-well plates and white 96 well plates were obtained from Greiner Bio-One (Frickenhausen, Germany). Other plasticware was obtained from Sarstedt (Wexford, Ireland) and Corning (VWR, Ireland). Glass bottom mini-dishes were obtained from MatTek (Ashland, USA). Glass-bottom multiwell inserts, the channel μ-slide VI0.4 (cat no. 80606) and magnetic slide holder were obtained from Ibidi (Martinsried, Germany). Quartz micro-cuvettes (1 ml volume, 2 mm optical path) with Teflon stoppers were obtained from Kromatek (UK).

2.2 Cell culture

Murine embryonic fibroblasts (MEF), rat pheochromocytoma PC12, human neuroblastoma (SH-SY5Y) and human colon cancer cells, HCT116 (wt) were obtained from ATCC (Manassas, VA, USA). Knock-out HCT116 ($SCO_2^{-/-}$) cells [Matsumoto, Takumi 2009] were kindly provided by Prof. P. M. Hwang (NIH, Bethesda, MD, USA). MEF and SH-SY5Y cells were cultured in DMEM medium supplemented with 10% fetal bovine serum (FBS), PC12 cell - in RPMI-1640 media with 10% horse serum (HS) and 5% FBS, HCT116 cells - in McCoys 5A media supplemented with 10% FBS. 10-20 mM HEPES and penicillin-streptomycin were added to all culture media (all obtained from Sigma). PC12 cell aggregates were grown in RPMI-1640 medium supplemented with 10% HS, 5% FBS, 10 mM HEPES-Na, pH 7.2, and penicillin–streptomycin.

For wide-field microscopy a collagen-poly-D-lysine coated glass bottom minidishes (MatTek) or multiwell inserts (Ibidi) were used. For confocal microscopy - 35 mm Cell+ mini-dishes (Sarstedt) without coating were used. For the measurements on a TR-F reader with adherent cells, collagen IV-coated 96 well plates or μ-slides (Ibidi) without coating (MEF cells), collagen IV-coated (PC12 cells) and poly-D-lysine coated (HCT116 cells) were used. 0.1 mg/ml solutions were used for all types of coatings.

For cell staining kinetics, probe leakage, metabolic stimulations and ATP assays cells were seeded on the corresponding prepared assay vessel and cultured for 48 hours to reach 75-100% confluence. The staining with probes was achieved by incubation at the indicated concentration (2.5 - 25 μg/ml) in regular culture medium for 1-24 hours at 37ºC

and 21 kPa O_2, followed by 2-3 washes and addition of fresh medium. Cell viability was assessed by measuring total cellular ATP with a luminescent CellTiter-GloTM kit, according to the manufacturer's protocol. Metabolic stimulations were performed in 35 mm Cell+ mini-dishes (Sarstedt) or in 96-well plate in respiration medium (Phenol Red free DMEM (Sigma D5030) medium supplemented with 1 mM L-glutamine, 10 mM D-glucose, 1 mM sodium pyruvate, 20 mM HEPES and 10% fetal bovine serum (FBS), pH 7.2) by adding of 10x stock solutions of drugs (1/10 of the volume) to the samples.

2.3 Probe preparation

2.3.1 Nanoparticle probes preparation

Preparation of RL-100 based probes. For the MM1 probe preparation 2.7 mg of C545T, 2 mg of PtTFPP and 200 mg of RL-100 were dissolved in 100 ml of acetone and then the particles were precipitated by fast addition of 700 ml of deionised water over 3–5 seconds under intensive stirring in a 1 L glass beaker. Similarly, for the MM2 probe, 20 mg of PFO, 3 mg of PtTFPP and 200 mg of RL-100 were dissolved in the mixture of tetrahydrofurane (45 ml) and acetone (55 ml) and precipitated with 700 ml of water. NanO2-IR probe was prepared similarly, but using 3 mg of Pt(II) benzoporphyrin dye. For MM-IR probe 2 mg of PtTPTBPF and 2 mg of azaBodipy were used for 200 mg of RL-100 beads (1% w/w of each dye). The organic solvents and most of the water were then removed slowly under reduced pressure over 4-6 hours, to bring probe stock concentration to about 10-15 mg ml^{-1}.

Preparation of PMMA-MA based nanoparticles. For PA1 probe 200 mg of PMMA-MA and 3 mg of PtTFPP were dissolved in 45 ml of tetrahydrofuran and the solution was diluted to 100 ml with acetone. The solution was transferred into a 1 L glass beaker and 600 ml of deionised water were added as described before. Aggregates were removed by centrifugation and the solution was stored at 4^oC. PA2 nanoparticles were prepared similarly, but using 2.4 mg of PtTFPP and 20 mg of PFO. For MM-IRx probe 1 mg of PtTPTBPF (0.5%) and 2 mg of azaBodipy (1%) were used for 200 mg of PMMA-MA beads. For 125 mg of MM1x and MM1xB NPs 1.25 mg of PtTFPP (1%) and 1.5 mg of

corresponding coumarin (~1.2%) were used. Using rotary evaporator, organic phase was removed and NPs were concentrated to 10-15 mg ml^{-1}.

Particle size and charge were determined on a particle size analyzer Zetasizer Nano ZS (Malvern Instruments, Germany). Depending on the polymer, presence of one or two dyes and the speed of addition of water, NP of various sizes and Z-potential were produced.

2.3.2 Small molecule probes preparation and purification

Click modification of PtPFPP was performed according to the modified method [153]. For the conjugation with L-Arg-O-methyl ester or peptides, PtPFPP was first modified at one or four *p*-fluorine atoms with two or ten equivalents of 3-mercaptopropionic acid in DMF in the presence of triethylamine (40–70°C, 3–16 h), followed by RP-HPLC purification. The derivatives of PtPFPP were coupled with the peptides by the carbodiimide method, using EDC, DMSO as the solvent, twofold excess of the peptide per carboxylic group and 16 hours incubation at room temperature, followed by RP-HPLC purification [62]. Purified conjugates were reconstituted in DMSO and stored at 4°C. The structures were confirmed by MALDI-TOF with spectra recorded on a Micro-massTof Spec 2E (reflectron mode at an accelerating voltage of +20 kV). Direct tetra-substitution with hexoses was achieved by incubation of PtPFPP with 5 molar equivalents of unprotected β-D-thioglucose or thiogalactose in DMF in the presence of triethylamine (40°C, 16 h), followed by RP-HPLC or gravity flow purification (gradient of methanol in 0.1% TFA in water). Purified conjugates were dried at 30°C overnight at reduced pressure and stored at -20°C.

2.3.3 Probe characterization

Absorption spectra of the conjugates were measured on a 8453 diode array spectrophotometer (Agilent) in phosphate buffered saline (PBS) containing 0.25% Triton X-100 or 10% fetal bovine serum (FBS) for small molecule probes. Using intensities of

Q-band or Soret band concentration of the corresponding dye was calculated according to the Beer-Lambert law:

$$A = \varepsilon l c, \qquad \text{(Eq.1.6)}$$

where A is absorption, l is a path length and ε is a molar extinction coefficient. The following coefficients were used: ε_{390}=257000 for PtTFPP, ε_{440}=212000 and ε_{620}=1.3 for PtTPTBPF. Knowing the concentration of each dye in nanoparticle probes, the concentration of NPs was calculated.

Luminescence spectra of probes were measured on a LS-50B luminescence spectrometer (PerkinElmer) under air-saturated and deoxygenated (5 mg ml^{-1} KH_2PO_4, 5 mg ml^{-1} Na_2SO_3) conditions. Optimal bands were used for spectra collection: 390/650 nm for PtTFPP, 616/760 for PtTPTBPF, 616/665 for azaBodipy, 390/430 for PFO and 470/515 for C545T.

Phosphorescence lifetimes were also measured under air-saturated and deoxygenated conditions on a TR-F reader Victor2 (Perkin Elmer) [66] and Cary Eclipse spectrometer (Varian-Agilent) using phosphorescence decay application and single-exponential fit [62].

Performance of MM2 probe in ratiometric intensity-based icO_2 sensing was studied in MEF cell suspension (25 μg ml^{-1}, 16 h loading) on LS-50B spectrometer (PerkinElmer). Emission spectra of PFO (415 nm) and PtTFPP (650 nm) were collected after equilibration of suspension at different ambient O_2 concentrations in hypoxia chamber. Ratio values between intensities of PtTFPP and PFO signals were used to plot ratiometric calibration for MM2 probe.

2.4 TR-F measurements on plate reader

2.4.1 Monitoring of local cell oxygenation

Cells were grown in microwells of 96-WP until they reached 80–100% confluence, then loaded with intracellular probes in standard growth media: NanO2, MM2, PA1, PA2,

MM1x, MM1xB (5-10 μg ml^{-1}, 6-16 h), MM-IR, MM-IRx (10 μg ml^{-1}, 16 h), Pt-Glc, Pt-Gal, (2.5 μM, 16 h) if not specified. After incubation, cell samples were washed from excess probe 3 times and equilibrated in 200 μl of respiration medium.

For the platform comparison experiments, MEF cells were grown in 75 cm^2 flask until they reached 80-100% confluence, then the NanO2 probe was added at a final concentration of 10 μg ml^{-1} followed by incubation for 16 h at 37°C. Cells were then trypsinised and prepared as cell suspensions in respiration medium (0-1*10^6 cell ml^{-1}, 1-1.5 ml of each) on a heating block (37°C). Cells were seeded in 96-WP at concentrations of 0-300*10^3 cell $well^{-1}$ in 200 μl of respiration medium.

The samples were then monitored on a time-resolved fluorescence reader Victor2 (Perkin-Elmer), D340 excitation and D642 emission filters, counting at two delay times of 30 μs (t_1) and 70 μs (t_2), gate time 100 μs, and integration time 1 s, typically over 20-300 min. Intensity signals for each reading were then converted into phosphorescence lifetime (τ) values as follows:

$$\tau = \frac{(t_2 - t_1)}{\ln(F1/F2)}, \qquad \text{(Eq.1.7)}$$

where F1 and F2 are the TR-F intensity signals at delay times t_1 and t_2. In the experiment with different ambient oxygen concentrations, the plate reader was placed in a hypoxia chamber (Coy Scientific). After equilibration at given atmospheric O_2 concentration for ~20 min the plate with samples was monitored, then the O_2 concentration in the chamber was changed and the procedure repeated. Probe calibration was performed by collecting of luminescence lifetimes for 5-7 different oxygen concentrations, for about 30 min monitoring per each. In cell stimulation experiments, FCCP (carbonyl cyanide 4-(trifl uoromethoxy) phenylhydrazone) and AntA (antimycin A) were added at final concentrations of 0-1 μM and 10 μM (1/10 of the sample volume) respectively. For NanO2 probe, the following calibration function was used $[O_2]$ = 18 576 * exp (– t / 6.8794). For ratiometric detection of MM2 probe on Victor2 microplate reader D642 and F460 emission filters and an F355 excitation filter were used.

2.4.2 OCR measurement in 96-WP

MEF cells were grown in standard growth medium, then 30 000 cells in 200 μl of medium were seeded in wells of 96-WP and grown for two days. For the measurement, the growth medium was replaced with respiration containing 50 nM of MitoXpress-Xtra, then 150 μl of immersion oil were dispensed in each well and the plate was monitored on a time-resolved fluorescence microplate reader Victor2 (Perkin-Elmer), as described above. The lifetime values were converted to O_2 concentration by applying the calibration function: $[O_2] = 4455.46 * \exp(-t / 7.48284)$ and plotted as time profiles. From these O_2 profiles, OCRs were calculated as initial slopes (5–15 min interval) and expressed in μM min^{-1}. Samples without cells and without probe were also measured and their profiles were used to correct these slopes for temperature and O_2 equilibration effects. OCRs were also measured in the presence of 10 μM antimycin A (AntA), 1 μM FCCP, 10 μM oligomycin (OM) or DMSO (mock).

For intracellular OCR measurements on 96-WP 10 μg ml^{-1} of NanO2 probe were added to the growth medium, incubated with cells for 1–16 h at 37°C, and then washed three times. Luminescence lifetimes of cell samples were measured in the respiration medium as described above, followed by calculation of OCR values.

For the comparison of platforms experiments, suspensions of loaded MEF cells were prepared as above (preloaded with NanO2 probe in culture flask) and seeded in 96-WP at concentrations of $0\text{-}80*10^3$ cells $well^{-1}$ in 100μl of media. The samples were covered with mineral oil (150 μl $well^{-1}$) and immediately measured on Victor2 reader under the same settings for 100-180 min. Probe lifetime values were converted to O_2 concentration and OCR values were calculated as described above and expressed in μM min^{-1}.

2.4.3 OCR measurement in quartz micro-cuvettes

Suspensions of MEF cells ($0\text{-}0.5*10^6$ cell ml^{-1}, 1-1.5 ml of each) preloaded with 10 μg ml^{-1} NanO2 probe were quickly transferred into four preheated quartz cuvettes, sealed tightly with stoppers (no headspace) and fixed horizontally on the cuvette holder.

Phosphorescence intensity, lifetime measurements and OCR calculations were performed as above. Prior to the next use cuvettes were washed with chromic mixture, soaked overnight in MQ water and then dried in the oven.

2.4.4 Measurements in channel μ-slides

Cells were grown under standard conditions, trypsinised, washed with respiration medium, counted, seeded in μ-slides at concentration 15 000 – 90 000 cells in 50 μl of medium per channel, placed in a humidified CO_2 incubator and incubated for 1 hour (MEF) or 3 hours (PC12 and HCT116 cells) for attachment. Additional 50 μl of medium were dispensed per channel after 15 min to prevent cell drying and death. After cell attachment, the channels were washed 3 times, filled with 150 μl of respiration medium containing 50 nM of MitoXpress-Xtra and placed on a magnetic holder in Victor2 reader, equilibrated at 37^{o}C. OCR measurements were performed as described above over 2–5 hours with re-perfusion every 40–80 min. For reperfusion the medium in each channel was replaced 3 times with 50 μl of fresh medium, supplemented with probe and appropriate stimulants. To suppress glycolysis, cells were preincubated for 2 hours in glucose-free (Glc -), 10 mM D(+)-galactose respiration medium. Treatment with 1 mM sodium butyrate (BA) was performed with cells grown at 70–80% confluence in a flask, 16 hours prior to seeding.

For IC O_2 measurements MEF cells suspensions stained with NanO2 probe were preloaded in flask as above. Cells were counted and seeded in μ-slides at 90 000 cells in 50 μl of medium per channel, and measured as described above after cell attachment.

2.5 Fluorescence microscopy and FLIM measurements

2.5.1 Cell sample preparation for microscopy

For wide-field microscopy cells were seeded on glass bottom imaging dishes (MatTEK) or glass bottom multiwell inserts (Ibidi) with collagen-poly-D-lysine coating, typically

30000 cells vessel^{-1}. After reaching 70-80% confluence cells were stained with intracellular probes in standard growth medium: NanO2, MM2, PA1, PA2, MM1x, MM1xB (5-10 μg ml^{-1}, 6-16 h), MM-IR, MM-IRx (10 μg ml^{-1}, 16 h), Pt-Glc, Pt-Gal, (2.5 μM, 16 h) if not specified. Cells were then washed three times, placed in fresh media and imaged. For confocal microscopy 35 mm Cell+ mini-dishes (Sarstedt) without coating were used. In probe calibration experiments cells were treated with 10 μg ml^{-1} of AntA 15 min prior the first measurement to block respiration.

2.5.2 Study of the probe cell penetrating properties and localization

Analysis of cell loading kinetics, comparison of relative brightness, photostability of different probes and their localization were conducted on a wide-field inverted microscope Axiovert 200 (Carl Zeiss, Goettingen, Germany) equipped with 40×/1.3 EC Plan Neofluar objective and gated charge-coupled device (CCD) camera, excitation module with 390, 480 and 590 nm LEDs, ImSpector software (LaVision BioTec, Germany) and humidified chamber with temperature/CO_2/O_2 control (Pecon). "PtCP" filter cube (excitation 390/40 nm, emission 655/40 nm) was used for imaging PtTFPP phosphorescence, DAPI filter (Semrock 5060B ZHE) for imaging of PFO fluorescence, FITC filter cube (excitation 472/30 nm, emission 535/50 nm) for coumarin C545T fluorescence, and "Pt-CP-ketone" filter cube (excitation 595/40 nm, emission 780/60 nm) for PtTPTBPF phosphorescence. For assessment of autofluorescence, non-loaded cell samples were measured at each setting combination used.

MM2 probe (co)localization experiments were performed on a laser scanning confocal microscope Olympus FluoView1000 equipped with temperature and CO_2 control. The probe was excited at 405 nm (20–25% laser power) with emission collected at 410–510 nm (PFO) and 600–700 nm (PtTFPP).

Confocal PLIM for other probes was performed on a system based on an upright fluorescent microscope Axio Examiner Z1 (Zeiss UK) equipped with 20x NA:1.0 W-Plan-Apochromat and 40x NA:1.1 LD-C Apochromat W Korr. objectives, heated stage with motorized Z-axis control, DCS-120 confocal scanner (Becker &Hickl), R10467U-40

photon counting detector (Hamamatsu Photonics K.K.) and TCSPC hardware (Becker &Hickl) [133]. Cells stained with PtTFPP-based probes were excited with a 405 nm picosecond diode laser BDL-SMC (Becker &Hickl) and emission was collected at 635-675 nm. DIC images were recorded with D5100 digital camera (Nikon) connected to the microscope.

2.5.3 Calibration of the O_2 probes

Calibration of the icO_2 probes on wide-field FLIM system was performed using pulsed excitation with 390 nm LED (10 m length, 250 ms exposure time and 1 · 2 binning) with resting and non-respiring (treated with 10 μM AntA) cells at 1-20 % of atmospheric O_2. Different O_2 concentrations were achieved by setting of the hypoxia chamber followed by 20 minutes temperature and gas equilibration of the sample. Since the hypoxia chamber is difficult to equilibrate below 0.1 kPa O_2, the zero O_2 calibration point was produced by chemical deoxygenation with 5 mg ml^{-1} KH_2PO_4 and 5 mg ml^{-1} Na_2SO_3. Calibration lifetime values (for AntA-treated samples) were calculated for a number of Regions Of Interest (ROI) with ImSpector software, plotted against O_2 concentrations and fitted in Origin 6.0 software to determine calibration function. For Stern-Volmer plots (τ_0/τ vs. O_2) the non-linear fitting model was used [68].

2.5.4 Analysis of cellular uptake mechanism

The uptake pathways were studied for anionic nanoparticle based PA2 probe with rat primary neurons (kindly provided by Dr. Ujval Kumar) and neuronal-like PC12 cells. To determine the effect of temperature, cells were pre-incubated for 30 min at 4°C (37°C for the control) and exposed to 5 μg ml^{-1} PA2 probe for 2 hours at the same temperature. The effect of ATP depletion was studied after pre-incubation the cells in 10 mM D(+) galactose Glc - respiration media for 45 min, addition of 10 μM oligomycin (OM) for 15 more minutes followed by staining with 10 μg ml^{-1} PA2 in the presence of galactose and OM for 2 h. To study the effect of endocytosis inhibitors cells were treated for 2 hours

with CPZ (50 μM), EIPA (50 μM) or MβCD (5 mM), then stained with a PA2 probe (10 μg ml^{-1}, 3 h) in the presence of inhibitor and analysed. Standard media and temperatures were used for the control samples.

2.6 Other cell-based assays

2.6.1 Extracellular acidification (ECA) assay

PC12 cell samples stained with MitoXpress-Intra probe by standard procedure were pre-incubated for 2 hours under CO_2-free conditions in phenol-red free DMEM, 10 mM HEPES-Na, pH 7.2, at 37°C. Then the medium was replaced with unbuffered DMEM, pH 7.4, containing 1 μg ml^{-1} of pH-Xtra, 1 μM FCCP and 10 μM OM (maximal uncoupling of mitochondria) or DMSO (mock). Then samples were covered with 150 μl of mineral oil. The plate was measured kinetically for 1 hour at 37°C on a Victor2 reader using time-resolved fluorescence (TR-F) mode and 340 ± 50 nm excitation, 615 ± 8.5 nm emission filters. In each measurement point two TR-F signals (F1, F2) were collected at delay times t_1 = 100 μs and t_2 = 300 μs, and phosphorescence lifetimes were calculated as follows: τ [μs] = $(t_2 - t_1)/\ln (F1/F2)$. Lifetime values were then converted into pH according to the calibration function (37°C): pH = $(1893.4 - \tau)/227.54$ [154].

2.6.2 Immunofluorescence experiments

MEF cells were seeded in μ-slides at 15 000–90 000 cells per channel and OCR measurements were performed as described above. After that, the cells were washed with PBS containing phosphatase inhibitors, fixed with 3% paraformaldehyde in PBS for 15 min, incubated with 50 mM NH_4Cl for 15 min, permeabilized with 0.25% Triton-X100, blocked with 5% FBS, incubated with anti-HIF-1α (1 : 500) or anti-HIF-2α (1 : 250) primary antibodies (overnight, 4°C), washed with TBST buffer and then with Alexa Fluor 488 secondary antibodies (1 : 1000, 50 min, room temperature). Then cells were washed with TBST, counterstained with DAPI (0.3 mM, 5 min) and analyzed on a wide-

field fluorescence microscope Axiovert 200 (Carl Zeiss) under 390 nm and 470 nm LED excitation and emission filters for DAPI and FITC, using an EC Plan Neofluar 40 /1.3 oil immersion objective.

2.7 Data assessment and statistics

Mean OCR and oxygenation/lifetime values were calculated from 6 replicates for 96-WP, 2–6 replicates for μ-slides and 2 replicates for quartz cuvettes, with standard deviation expressed in error bars. Cell loading studies were performed on the wide-field microscope in triplicate, averaging intensity values from 6-10 randomly selected ROI normalized to background signals. Fitting of phosphorescence decays was performed either in ImSpector software (wide-field PLIM) or SPCImage software (Becker & Hickl) using single-exponential decay function and pixel binning as appropriate. The resulting 2D matrices with lifetime data were converted to ASCII format and processed on Microsoft Excel to produce O_2 concentration values using calibration function. To ensure consistency, all the experiments were performed in triplicate.

Chapter 3.

Development of O_2 sensing assays in commercial multichannel biochips μ-slide (Ibidi).

3.1 Introduction

Measurement of cellular respiration and OCRs is useful for studies of cell bioenergetics, metabolism, mitochondrial function, drug toxicity and common pathophysiological conditions such as cancer, stroke, diabetes, Alzheimer's and Parkinson's diseases [155]. Sealed macroscopic chambers with built-in Clark-type O_2 electrodes were initially introduced for OCR measurement [10], however such systems suffer from signal drift, low sample throughput, consumption of O_2 themselves and were substituted by optical techniques [156]. Solid-state O_2 sensors measure only extracellular O_2, have cell compatibility issues, often require specialized and expensive instrumentation, and make difficult any modifications of the setup and measurement of additional parameters (multiplexing capabilities). Soluble O_2 probes provide greater flexibility in assay design, can be used with common bioassay platforms (standard 96- and 384-well microtitre plates, mini-dishes, microfluidic systems), and measured on commercial spectrometers or plate readers in intensity or lifetime mode [123]. In addition, phosphorescent O_2 probes can be multiplexed with other photo- and bio-luminescent probes and assays, allowing detailed multi-parametric analysis of bioenergetics and cellular function in a high throughput format (e.g. measurement of extracellular acidification, membrane potential, ROS, total cell viability) [157, 158]. On the other hand, OCR measurements in microplates have reduced sensitivity due to the partial sealing of the sample (with a layer of mineral oil) and significant O_2 back diffusion [112].

Specialized biochips and microfluidic platforms for live cell O_2 sensing and imaging are under active development [159, 160]. A number of such simple and low-cost microchamber devices are now produced commercially [161].

3.2. Measurement setup

In this study we evaluated disposable polystyrene-based multi-channel perfusion biochips in O_2 sensing assays with mammalian cells. In particular, the 6-channel biochips - μ-slides produced by Ibidi GmbH which have a semi-closed design and small internal volume of 30 μl (Fig. 3.1 A), were used in conjunction with adherent MEF cells and phosphorescent Pt-porphyrin based O_2 probes MitoXpress-Xtra and MitoXpress-Intra (Luxcel).

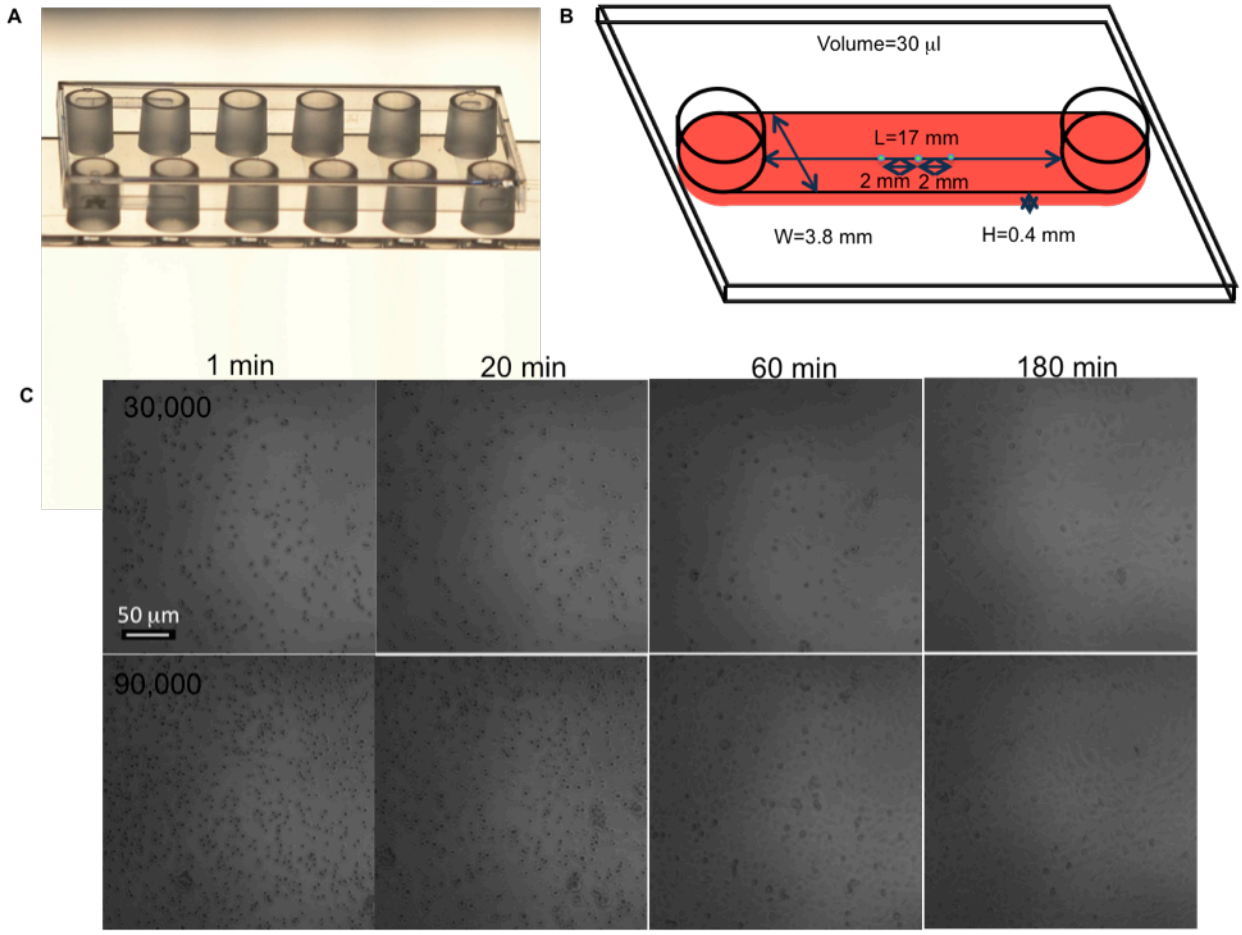

Figure 3.1 A. Photographic image of multi-channel perfusion slide (μ-slide). B. A schematic representation of one channel of μ-slide with merits. C. Kinetics of MEF cells attachment to the surface of μ-slide channel at seeding concentrations 30000 and 90000 cells per channel (37^{O}C, 3 h).

Measurements were performed on standard luminescence plate reader Victor2 with up to 4 μ-slides placed in a holder, in each of the six channels (24 samples altogether). To ensure consistency, readings were taken at three points in the middle part of the channel (shown with green dots on the Figure 3.1 B). Each channel can accommodate up to 90000 of adherent MEF cells (fully confluent monolayer). Special chamber construction and surface of the channels allow simple loading of cell samples with a micropipette, attachment of adherent cells (surface coatings can be applied) or immediate OCR measurements with suspension cells. Such attachment of MEF cells to the surface of non-coated wells was monitored at 30000 and 90000 cells per channel concentrations (Fig. 3.1 C). Brightfield images show sufficient cell attachment already 20 minutes after seeding with flat cell shape after 60 minutes. Semi-closed design of the chamber allows re-perfusion, multiple treatments of cells and multi-parametric analyses in conjunction with other probes. However, oxygenation conditions in such devices, their effects on cells and possible analytical applications have not been investigated in detail. One can anticipate that in sealed samples with respiring cells significant O_2 gradients can develop, depending on the cell number, their respiratory activity, volume of medium and O_2 diffusion rate (i.e. biochip material and geometry) [162]. Incorporation of soluble phosphorescent O_2-sensing probes in such devices enabled us to study these processes and to monitor cell oxygenation and respiration on standard laboratory equipment. The μ-slide platform was compared to the standard microwell plates and evaluated with several different cell types, media and treatments including mitochondrial uncoupling and inhibition, depletion of extracellular Ca^{2+} and inhibition of cellular enzyme histone deacetylase.

3.3 Comparison of OCR measurements in 96-well plate and μ-slides

The established method of OCR measurement in 96-WP includes seeding of cells in the wells, allowing them to adhere (if required), adding the EC probe MitoXpress-Xtra to the medium, covering the samples with mineral oil (O_2 barrier) and monitoring changes in probe phosphorescence intensity or lifetime over time [111]. Typical respiration profiles, produced by resting and stimulated MEF cells (60 000 cells in 200 μl) in a 96-WP, are

shown in Fig. 3.2 A in phosphorescence lifetime scale. The drugs with known mode of action produced the anticipated maximal (ATP synthase inhibition with 10 μM OM and mitochondrial uncoupling with 1 μM FCCP and almost completely inhibited respiration (electron transport inhibition with 10 μM AntA) [109]. Although distinguishable, measured profiles and OCR values show a considerable variation. The need to seal the wells with oil makes repetitive measurements and addition of effectors difficult on this platform.

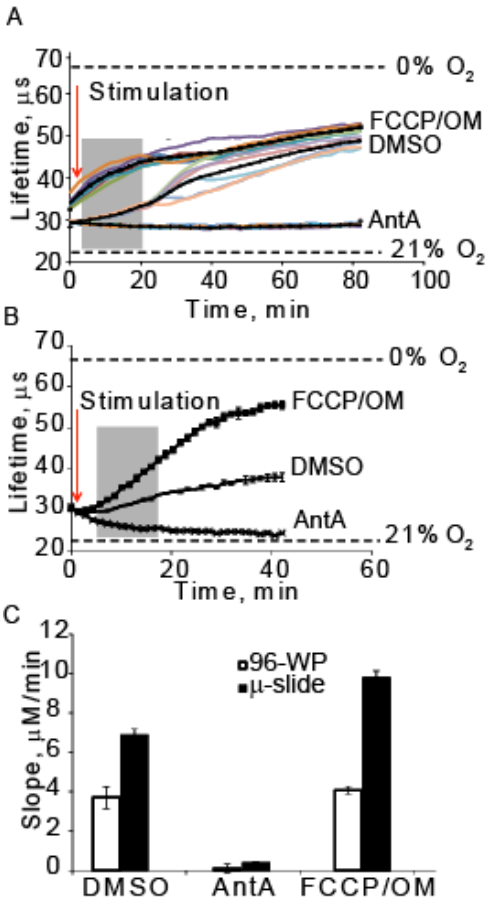

Figure 3.2 Respiration profiles of resting and stimulated (10 μM OM, 1 μM FCCP, 10 μM AntA) MEF cells in A) 96-WP and B) μ-slides, measured with 50 nM of MitoXpress-Xtra. C. OCR signals (expressed as slopes of respiration profiles) of resting and stimulated MEF cells in 96-WP and μ-slides. Mean OCR values are calculated from 6 replicates with standard deviation expressed in error bars.

Similar experiments were performed with μ-slides, using a slide holder (accommodates up to four Ibidi slides) and customized plate map with 1–3 reading points per channel (Fig. 3.2 B). The OCR assay was initiated by flushing the channel with fresh medium (perfusion) containing the EC probe. Respiration profiles show that in the μ-slide the samples are better sealed and less distorted than in 96-WP, resulting in faster and more reproducible OCR measurements. For both platforms, back diffusion of ambient O_2 through plastic body of the assay vessel is still significant and complete deoxygenation of samples is not achieved (lifetime values corresponding to 0 and 21 kPa O_2 are shown with dashed lines). Measurement at three different points in each channel (Fig. 3.1 B) produced consistent results (Fig. 3.2 B), thus proving that spatial O_2 gradients in the microchannels are rather uniform and stable. Importantly, phosphorescence lifetime measurements allow conversion of respiration profiles on an O_2 concentration scale (μM), by applying the O_2 calibration function of the probe (stable, pre-determined or published). Relative OCRs can be accessed from the initial (linear) parts of O_2 profiles for resting or drug-treated cells and expressed in μM min^{-1} units. Fig. 3.2 C shows that with similar cell numbers OCR responses in μ-slides are nearly two-fold higher than in 96-WP (after background correction), when assay time and variation are reduced.

3.4 Optimization of the μ-slide platform for OCR measurement

3.4.1 Effect of cell density and assay vessel material on OCR signals

Sensitivity of OCR platforms depends on the respiratory activity of cells and O_2 back diffusion [123]. Glass is known to have lower gas permeability than plastic and can be used to decrease O_2 back diffusion in measurement platforms.

We found that attachment of glass cover slide to the bottom of the chamber gives only marginal increase in the slope of the respiration profile, however caused significant background signal, which required additional data processing (Fig. 3.3 A). A similar result was observed with glass bottom 96-WP (Fig. 3.3 B). We performed stimulations of MEF cells in μ-slide, plastic and glass-bottom 96-WPs with FCCP/OM, DMSO and

AntA. OCR values calculated from initial slopes (μM min^{-1}) show no significant difference between plastic and glass-bottom plate, while μ-slide maintains its higher sensitivity (Fig. 3.3 C).

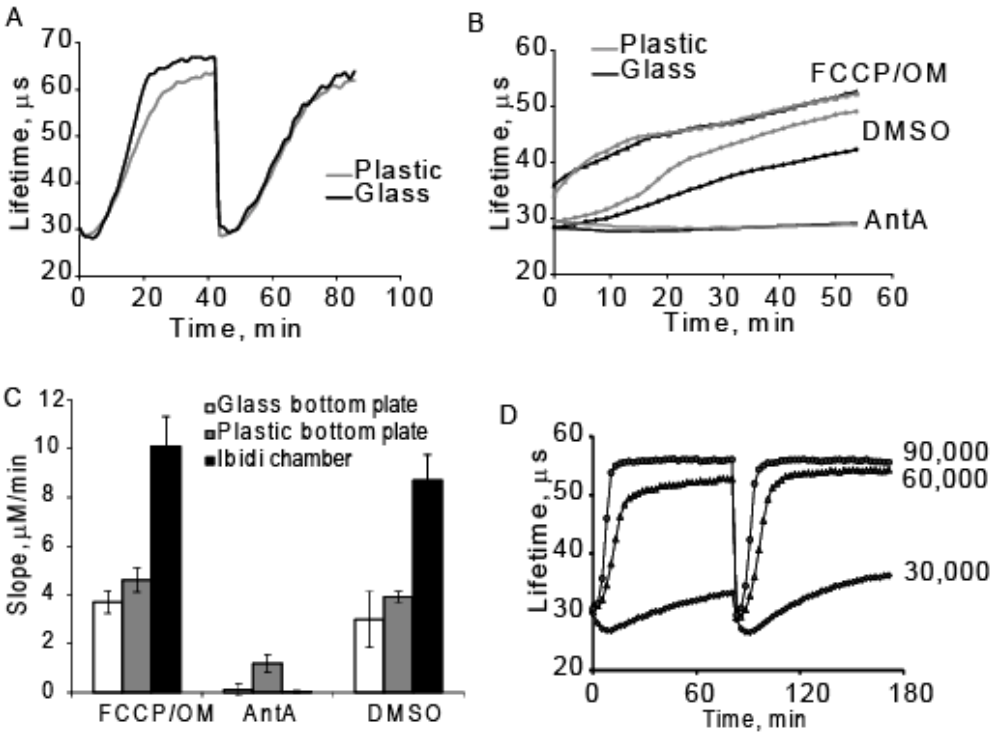

Figure 3.3 Respiration profiles of MEF cells in plastic and glass-bottom A) μ-slide and B) 96-WP, measured with 50 nM of MitoXpress-Xtra. C. OCR values of resting and treated (10 μM OM, 1 μM FCCP, 10 μM AntA) MEF cells in plastic/glass-bottom 96-WP and μ-slide. D. Respiration profiles of MEF cells at different seeding concentrations.

Covering the medium in channel wells with mineral oil also has a small effect on respiration profiles. This step makes re-perfusion experiments awkward and removes the advantage of semi-closed system, so we did not incorporate it into further assays. Temperature is known to have a strong effect on cell respiration, probe response and calibration [50], therefore all O_2 monitoring experiments were performed at 37°C. Cell density is the main parameter which requires optimization. It has great influence on the total O_2 consumption, as can be seen from the Figure 3.3 D. In subsequent experiments we used 90 000 MEF cells per channel, which provides short measurement time (< 30 min) and high sensitivity.

3.4.2 Comparison of IC and EC probes for OCR measurements

Oxygenation in μ-slides can be analysed with EC or IC O_2 probes. We compared phosphorescence intensity signals produced by MitoXpress-Xtra (EC) and MitoXpress-Intra (IC) probes on μ-slide and 96-WP under recommended working dilution [112] or cell loading conditions [106], respectively. Fig. 3.4 A shows that EC probe signals on μ-slides are 1.5-times smaller (to compare with IC probe signals), but still well above the required threshold (25 000 cps [163]) ensuring stable lifetime measurements. The EC probe does not internalize into the cells even after 16 hours incubation, as can be seen from the signal intensity values. 96-WP with IC probe loaded MEF cells (10 μg ml^{-1}, 16h) produces about two-fold higher phosphorescence signals than μ-slide due to the longer optical path, however 1 hour loading in 96-WP is not quite sufficient. It is clear that probe signals can be easily adjusted to the desired levels by optimizing working dilution (EC and IC probes), loading time and cell density (for IC probe).

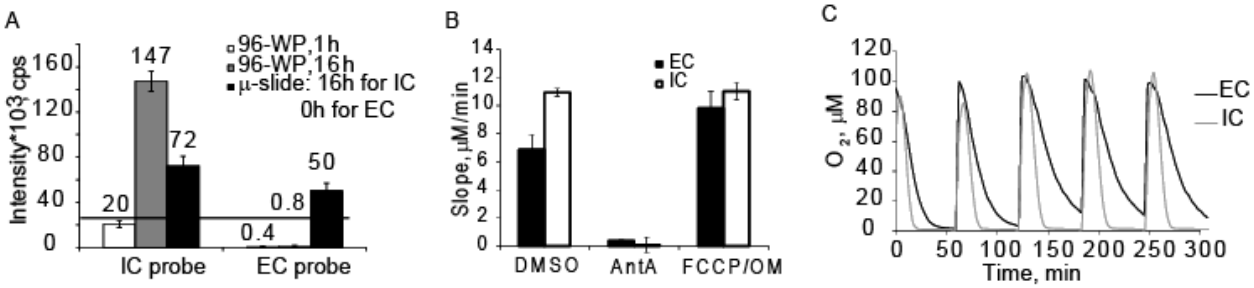

Figure 3.4 A. Phosphorescence intensity signals of IC (MitoXpress-Intra, 50 nM) and EC (MitoXpress-Xtra, 10 μg ml^{-1}) probes on μ-slide and 96-WP. B. OCR values of resting and treated (10 μM OM, 1 μM FCCP, 10 μM AntA) MEF cells with IC and EC probes. C. Respiration profiles of MEF cells upon reperfusions monitored with IC and EC probes. Mean OCR values are calculated from 6 replicates with standard deviation expressed in error bars.

Stimulations of adherent MEF cells with known drugs was performed in μ-slides employing IC probe (preloaded 10 μg ml^{-1}, 16 h) and EC probe (50 nM, added to the media before measurement together with drugs). As can be seen from the Figure 3.4 B, cell responses in form of OCR are higher and more reliable in intracellular space. It can

be explained by closer proximity of the IC probe to mitochondria, where most of the O_2 consumption occurs.

The main advantage of μ-slides over the 96-WP platform is that OCR can be measured repetitively and under different conditions (media, stimulants). Upon reperfusion with fresh medium, phosphorescent signals drop rapidly to air-saturated levels and then respiration profile(s) of adherent cells can be reproduced under static conditions. Figure 3.4 C shows the measurement with five consecutive reperfusions using the IC and EC probes. The slight increase in response over the first 3 cycles (better seen with the EC probe) can be due to the partial washout of cells from the channel and/or cell adaptation to the low O_2 conditions. The IC probe, which senses local intracellular O_2 at the cell monolayer [94], shows greater sensitivity and informs about deeper deoxygenation of the cells that reach complete anoxia (0 μM O_2), while the EC probe informs on average O_2 levels within the channel.

3.5 Application of the μ-slide OCR platform for respiration monitoring

3.5.1 Comparison of respiration activities of different cell types

The key applications of O_2 measurement included studies of cell metabolism, responses to drugs, hypoxia and various stimuli. The assessment of resting cell respiration rates is often required on the preliminary stages of such experiments to estimate possible sensitivity of the method and choose optimal cell line. It can be done by measuring OCR in cell culture, however monitoring should provide reliable information independent on the cell size, shape and adherence. Using the μ-slide platform, we compared respiration rates for the different cell lines: murine embryonic fibroblasts (MEF), rat pheochromocytoma (PC12), human colon cancer cells (HCT116) wild type and $SCO_2^{-/-}$ mutant with inactive cytochrome C oxidase and oxidative phosphorylation [164] (Fig. 3.5).

OCR values are normalized to the number of cells in monolayer due to their different size for each cell line. PC12 cells, which are neuronal-like and have active oxidative

phosphorylation, especially in differentiated stage have the highest OCR [157]. High respiration rate was demonstrated for MEF cells as well, what makes them a popular model for OCR measurements, studies of intracellular and extracellular O_2 gradient [106]. HCT116 $SCO_2^{-/-}$ mutant cells with blocked respiration demonstrated minimal OCR values, as expected (Fig. 3.5).

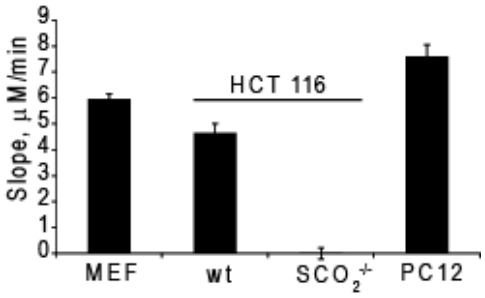

Figure 3.5 Respiration rates for the different cell lines expressed as OCR signals. Mean OCR values are calculated from 6 replicates with standard deviation expressed in error bars.

3.5.2 Effect of media composition

Balance of energy production pathways can vary for different cell types [158], and therefore media composition can affect the results of OCR measurements. We preincubated PC12 cells for 2–3 hours in glucose (Glc +) and galactose (Glc -) containing media and then measured their OCRs in the same conditions. Glc - medium is expected to suppress glycolytic ATP production and increase oxidative phosphorylation consequently, which causes active O_2 consumption and increased respiration rate. Fig. 3.6 A shows significant difference of respiration profiles in these two media (galactose is used in the same concentration to mimic glucose), and this difference remains after cell reperfusion. Uncoupling with 0.5 μM valinomycin (Val) activates respiration in Glc - medium more significant than in Glc + medium, while treatment with 10 μM AntA completely blocks respiration in both cases. Prolonged exposure to both AntA and Val drugs leads to decrease and complete inhibition of cell respiration, which could not be restored after re-perfusion with fresh media (indicative of cell death).

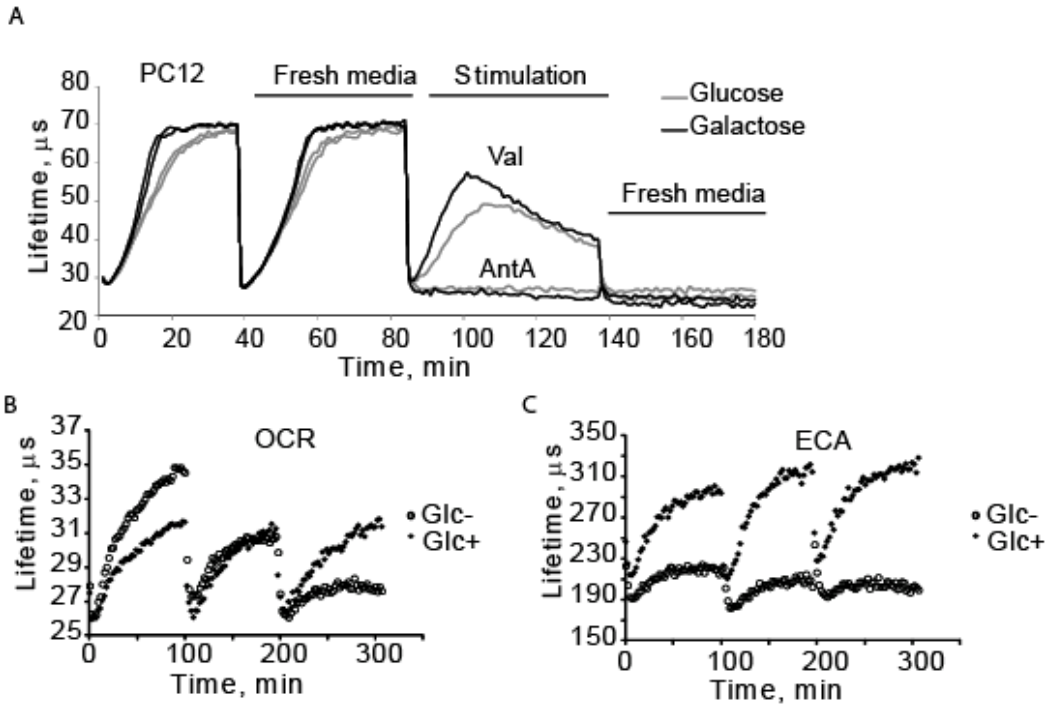

Figure 3.6 A. Respiration profiles of PC12 cells upon resting and stimulations (0.5 μM Val, 10 μM AntA) in Glc + and Glc – media with 2-3 h preincubation. B) OCR and C) ECA monitoring of PC12 cells over 3 reperfusions in Glc + and Glc – media with 3 h preincubation.

The main ATP generating pathways in cells are glycolysis and oxidative phosphorylation. The balance between them (energy budget) can be reliably estimated by parallel measurements of OCR and extracellular acidification (ECA) parameters [165]. μ-slide platform allows parallel use of O_2 and pH sensitive probes and therefore can be employed for such assays. We monitored OCR and ECA of PC12 cells after 3 h preincubation in Glc + or Glc - media over three reperfusions and compared obtained results. As can be seen from the Figure 3.6 B, cell respiration rate remains stable in Glc + media, matching the results of previous reperfusion experiments. At the same time, cell respiration rate in Glc- medium is significantly higher due to the blocked glycolytic pathway and activated oxidative phosphorylation. The gradual decrease of OCR in the later measurements can be explained by the cell adaptation to the low O_2 or death/washout upon reperfusions. As expected, ECA values are significantly lower for Glc - medium, where active glycolysis is not possible (Figure 3.6 C).

3.5.3 Cell responses to metabolic stimulations

Measurement of cell responses to different treatments is important for metabolic studies. Together with used before FCCP, Val (mitochondrial uncouplers) and AntA (inhibitor of respiration), EGTA is often used for cell treatments [109]. EGTA chelates extracellular Ca^{2+}, leading to its reduction in cytosol and mitochondria, minor depolarization of the mitochondrial membrane and significant fast increase in O_2 consumption [166]. Fig. 3.7 A shows the effects of 1 μM FCCP, 0.5 μM Val, 10 μM AntA and 5 mM EGTA treatments in parallel with control reading (DMSO treatment) after collecting of resting HCT116 cells deoxygenation profiles over one hour.

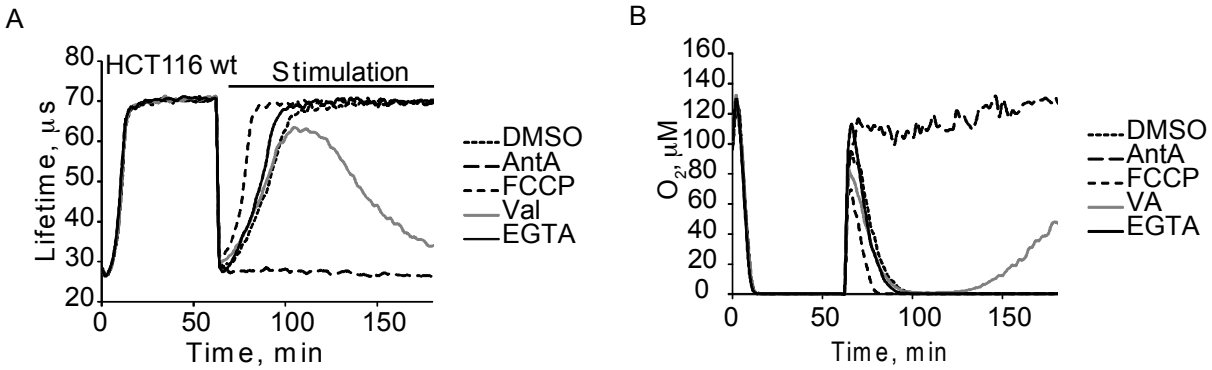

Figure 3.7 Respiration profiles of HCT116wt cells upon resting and stimulations with 1 μM FCCP, 0.5 μM Val, 10 μM AntA and 5 mM EGTA in (A) lifetime and (B) O_2 scales.

The responses measured in μ-slides are consistent with the mechanisms of action and reported data for these drugs [109]. Oxygenation profiles were recalculated from lifetime to O_2 concentration scale according to the calibration function of MitoXpress-Extra probe (Fig. 3.7 B). Due to the high cell density (90 000 cells per channel) and long monitoring time, cell monolayer as well as surrounding media achieved complete anoxia (0 μM O_2) after 15 minutes of monitoring in resting conditions and upon stimulations with uncouplers and EGTA. Maximal O_2 concentration in the well does not exceed 150 μM due to the semi-sealed design and high cell density, what agrees with the results of previous experiments.

3.5.4 Immediate and prolonged respiratory effects of histone deacetylase inhibitor

Histone deacetylases are involved in the regulation of cell metabolism [167]. To illustrate this, we analyzed the immediate and prolonged (16 h) effects of histone deacetylase inhibitor sodium butyrate (BA) [168] on HCT116wt cells. Fig. 3.8 A shows that 1 mM BA increases respiration in a time-dependent manner: small increase when BA was added just before measurement and significant increase after 16 h treatment. The impact of histone deacetylase inhibitor on metabolism can be further shown by treatment of cells with FCCP, which causes additional changes in respiration of HCT116wt cells. Moreover, cells treated with BA for 16 hours shows slight resistance to inhibition with OM (Fig. 3.8 B). The immediate effect of BA can be explained by direct activation of cell respiration, and long-term effect - by changes in gene expression (through histone deacetylation inhibition) and mitochondrial function.

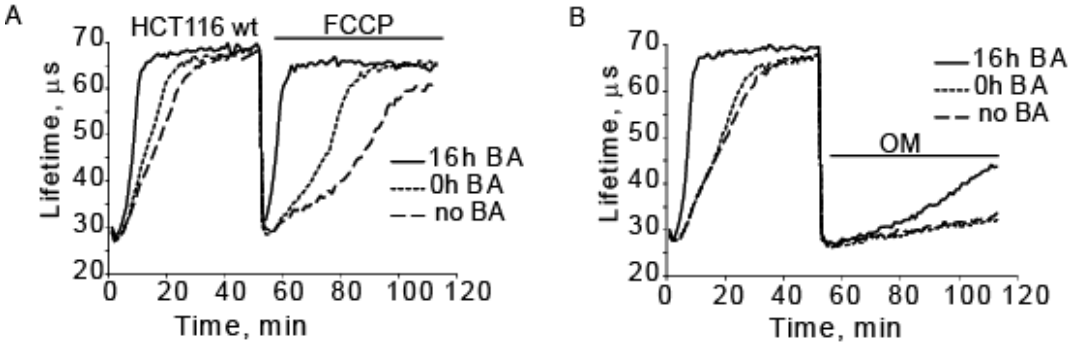

Figure 3.8 Respiration profiles of HCT116wt cells after immediate and prolonged treatment with histone deacetylase inhibitor BA upon resting and stimulations with (A) 1 µM FCCP and (B) 10 µM OM.

3.5.5 Application of µ-slides in multiplexed assays

The above examples demonstrate that µ-slides can be used in conjunction with IC and EC O_2 probes in metabolic studies with various cells. Furthermore, this platform allows parallel analysis of other analytes and parameters using a fluorescence plate reader or

microscope. It has been shown that different respiratory activities of samples may result in various degrees of cellular hypoxia, and this leads to differential activation of hypoxia-inducible transcription factors (HIFs) and cell survival pathways [169]. We seeded HCT116wt cells in μ-slides at high (90 000 cells per channel) and low (15 000 cells per channel) density, monitored their oxygenation for 2 hours (Fig. 3.9 A), then stained with anti-HIF antibodies and analyzed by fluorescence microscopy (Fig. 3.9 B). High cell density leads to fast deoxygenation of the channel (30 μl volume) and deep hypoxia level (<5 μM O_2). The microscopy image shows the increase of the total levels of HIF-α isoforms in hypoxic samples after 100 min incubation at < 5μM O_2 (at high cell density), although the nuclear accumulation of HIF is still insignificant (Fig. 3.9 B, C). These results illustrate that self-deoxygenation of cells in μ-slides may influence their metabolic and physiological state and should be carefully assessed in prolonged microfluidic experiments.

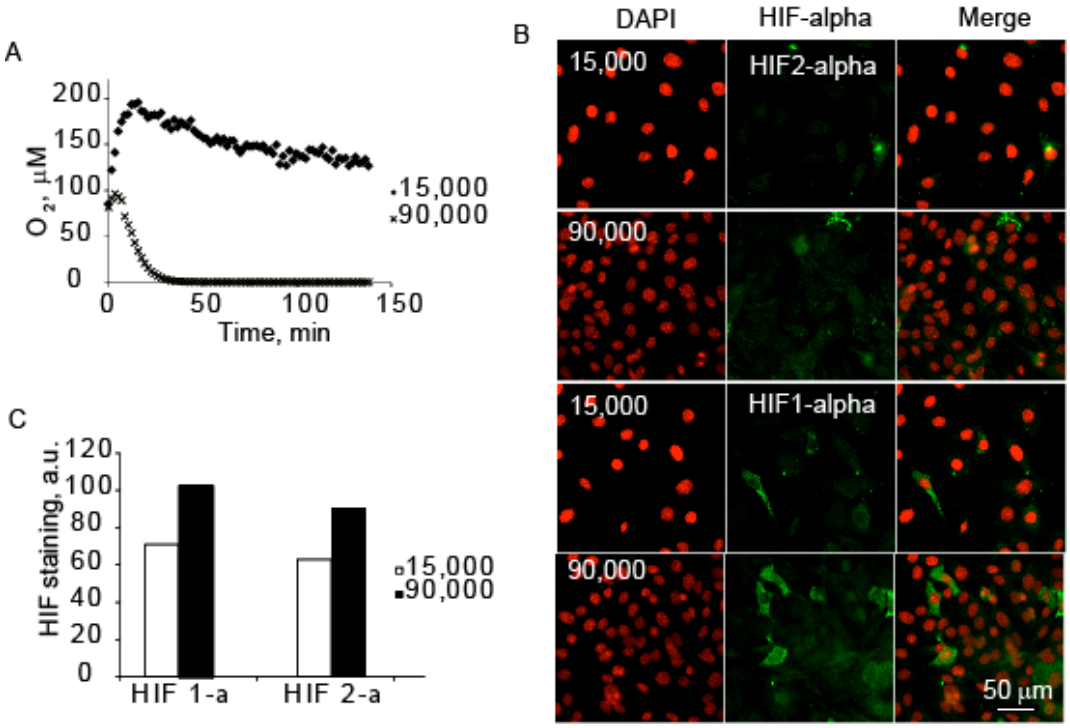

Figure 3.9 A. Respiration profiles of HCT116wt cells at 15000 and 90000 cells per channel seeding concentrations. B. Immunofluorescence images of cells with anti-HIF antibodies staining. C. HIF-1α and HIF-2α staining efficiency at different cell densities.

Performed experiments show that μ-slides are useful for monitoring of cell oxygenation during cell seeding and attachment under static conditions, in hypoxia research and various metabolic studies. In such assays O_2 probe can also be multiplexed with many conventional fluorescence based probes, including the pH sensitive lanthanide probe to measure extracellular acidification [111].

3.6 Conclusions

We have demonstrated that μ-slide devices, originally designed for live cell imaging, can also be used for O_2 measurements with phosphorescent probes on standard plate readers. The sensitivity of OCR measurements on this platform is approximately two-fold higher than in standard 96-WP, allowing more simple, rapid (0.5–1 h measurement time) and reproducible assays. The semi-closed design allows media replacement and re-perfusion, including addition of drugs for metabolic stimulations. The applicability of this platform for OCR was shown with EC and IC O_2 probes, various mammalian cell types, media composition and stimulation modes. Importantly, the O_2 assays retain the original functionalities of μ-slides, and they can be easily multiplexed with other luminescent probes and assays including live cell fluorescence microscopy. Improved reproducibility and reperfusion capabilities eliminate the need for replicated samples and retain a significant sample throughput (up to 24 samples can be measured simultaneously). This makes μ-slides a convenient and versatile platform for O_2 sensing and related cell based assays.

Chapter 4.

Comparison of the three optical platforms for measurement of cellular respiration

4.1 Three main optical platforms for cellular O_2 measurements

Cellular respiration and OCR are popular parameters in screening assays [110]. One technical challenge in performing OCR measurements is to create a system, in which the amount of O_2 consumed by the cells can be quantified reliably and accurately and then related to the cell concentration. Cellular respiration is rather low and hence samples must be sealed from the atmospheric O_2 (present in vast excess) during the measurement to prevent its back diffusion. In OCR assays bulk changes of O_2 dissolved in the medium are usually measured with EC O_2-sensitive probes. Another challenge is to perform OCR assays with large number of samples and cells in their native (adherent) state, using standard laboratory equipment such as plate readers and microtitter plates. However, conventional tissue culture plasticware (polystyrene based) is significantly permeable to O_2 and (with a few exceptions [82, 170]) not designed for air-tight sealing. A simple solution is to work with partially sealed samples (e.g. under a layer of oil, μ-slides), measure relative OCR (with respect to untreated cells), and then try to work out absolute OCRs by means of physical modeling or calibration [119].

Local oxygenation (or self-deoxygenation) of cells, a parameter which is linked to the OCR, can additionally inform on O_2 gradients in respiring samples, hypoxic stress, development of or adaptation to pathophysiological conditions such as ischemia, stroke, and cancer, and on rapid changes in respiration upon metabolic stimulation [121]. In static cultures exposed to atmospheric O_2, local oxygenation of cells is determined by their number and respiration activity, environmental parameters (atmospheric O_2 concentration), measurement conditions (the volume of medium, temperature, viscosity), mass exchange [121]. For cells cultured in standard microtiter plates or other tissue culture vessels, it is possible to keep the main variables constant. Under steady-state conditions O_2 consumption by the cell layer is balanced by O_2 diffusion from the atmosphere. Local oxygenation can be measured by loading the cells with a cell-

penetrating phosphorescent probe such as MitoXpress-Intra (self-loaded by simple addition to the medium and incubation for several hours) [94]. After this, probe signal can be monitored on a TR-F plate reader, which informs on local O_2 levels [171]. This assay normally does not quantify sample OCR directly, but it allows tracing of relative changes in OCR over time, with the possibility of repetitive stimulation of cells with drugs and metabolic substrates and measurements under hypoxic conditions (by setting up different levels of atmospheric O_2 in the plate compartment).

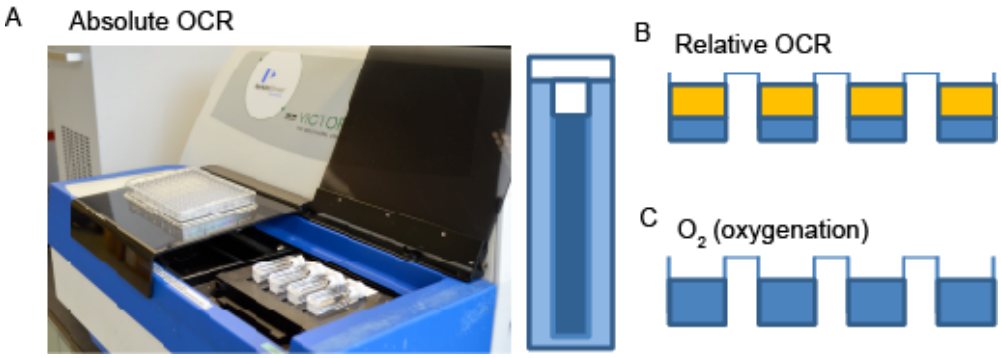

Figure 4.1 A. Victor2 plate reader with polystyrene 96-WP and four quartz cuvettes on the holder. Representation of (A) quartz micro-cuvette with a stopper for absolute OCR measurements, (B) polystyrene 96-WP with mineral oil seal for relative OCR measurements and (C) open polystyrene 96-WP for cell oxygenation monitoring.

An attempt to correlate cellular OCR and local oxygenation in plates with solid-state O_2 sensor material embedded in the bottom of the wells was undertaken previously [113]. However, these results are of limited value due to the measurement of relative OCRs (open plate), very long monitoring time (5 days) and remote location of the sensors (extracellular). Proper calibration of this system was not conducted.

In this study we cross-compared and calibrated three popular platforms currently used for the assessment of cell respiration, which differ in their set-ups, measured parameters, sensitivity and sample throughput. The first platform (Fig.4.1 A) comprised a gas-impermeable quartz micro-cuvette with a stopper (no headspace), which provides measurement of absolute OCRs. It has a low sample throughput (simultaneous

measurement of up to 4 cuvettes on a holder), requires cells in suspension form and relatively large sample volumes (~1 ml). The second platform, which comprised standard polystyrene microplates with mineral oil sealing of samples (Fig.4.1 B), measures relative OCRs. This assay is simple and has high throughput, but lower sensitivity, requires dispensing of oil and makes difficult additions to the sample. Like the first platform, it is essentially an end-point assay. The third platform measures local oxygenation of cells, i.e. icO_2, in an open plate under steady-state conditions (Fig. 4.1 C). This platform allows high sample throughput, fast data collection, simplicity with the possibility of continuous monitoring multiple drug additions. It also provides an indirect assessment of the OCRs for both suspension and adherent cells. Using the first platform, we calibrated the other two and obtained simple algorithms for determination of absolute OCR values from their measured parameters. In all cases, the same batches of MEF cells and O_2 probe (MitoXpress-Intra) were used.

4.2 Comparison of absolute and relative OCR platforms

We measured absolute OCRs in quartz cuvettes with MitoXpress-Intra probe pre-loaded cultures of MEF cells in concentrations $0.1\text{-}0.5*10^6$ cell ml^{-1}. MEF cells are known to possess high respiration activity and good staining with MitoXpress-Intra [94]. Absolute OCR platform provides high sensitivity and speed: for samples with high cell concentration complete deoxygenation was reached in ~30 min (Fig. 4.2 A). Suspensions with smaller cell concentrations give a range of respiration curves, where $0.1*10^6$cell ml^{-1} suspension demonstrates no significant deoxygenation over 60 minutes. For the second OCR platform (96-WP with a layer of mineral oil on the top), diffusion of O_2 through plastic and oil seal is significant, so that probe signals did not reach zero O_2 levels (lifetime value 68 μs) and changes in O_2 were significantly lower (Fig. 4.2 B). Using the initial parts of respiration profiles (highlighted as grey zones) we calculated mean OCRs (in μM min^{-1}) for the samples and related them to cell concentration (Fig. 4.2 C). One can see that both platforms produce the anticipated linear dependence of the OCR vs. cell number in the range $0.1\text{-}0.5*10^6$ cells ml^{-1}. These results imply that the cuvette system is 5.35 times more sensitive than the 96-WP, and that this correction factor can be used to

convert relative OCRs measured in 96-WP into absolute values. It is worth noting that the same strategy can be applied for calibration of other systems measuring relative OCRs. Thus, for plastic microchamber slides (μ-slides, Ibidi), which are 2 times more sensitive than 96-WPs [172], the correction factor for absolute OCRs would be 2.68.

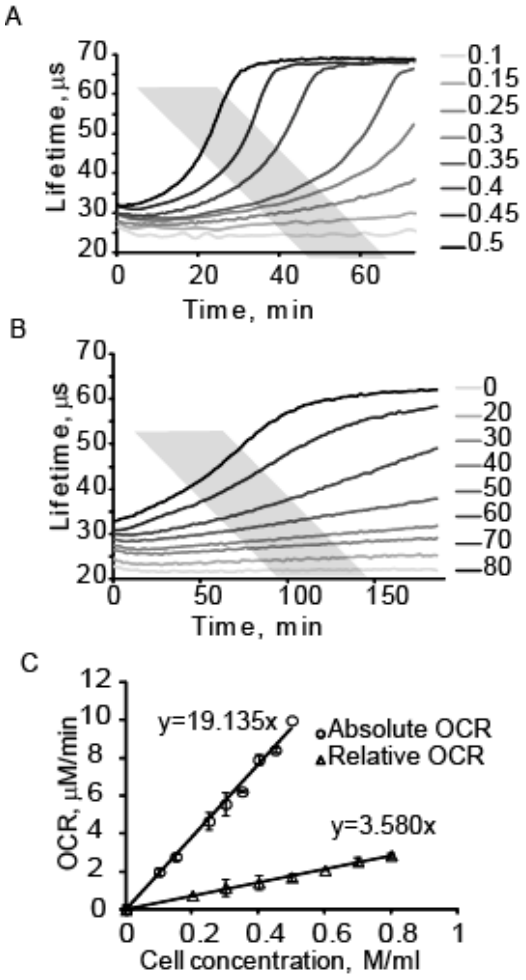

Figure 4.2 OCR measurements with MEF cells A. Profiles of cell respiration in quartz cuvettes (0.1-0.5*10^6 cell ml^{-1}). B. Profiles of cell respiration in 96-WP with mineral oil seal (0-80*10^3 cell $well^{-1}$). C. Correlation of the absolute OCR and relative OCR with cell concentration, which correspond to A and B. Mean values are calculated from 6 replicates for relative OCR and 2 replicates (with 3 repeats) for absolute OCR with standard deviation expressed in error bars.

4.3 Calculation of specific OCRs

Absolute OCR values measured in quartz cuvettes correspond to mean respiration rate of cell population and bulk deoxygenation inside vessel. Average respiration of a single cell in such system can be calculated by dividing the total OCR by the number of cells in suspension. For the range 0.1-1.0*10^6 cells ml^{-1}, specific respiration activity of MEF cell is constant and equal to 18 pM min^{-1} $cell^{-1}$ (or μM min^{-1} $10^6 cell^{-1}$) (Fig. 4.3 A, left axis). It means that in this range of cell concentrations their respiration rate is not affected by oxygenation in the vessel and remains at *in vitro* physiological level. During the measurement cells precipitate forming a thin layer at the bottom of cuvette. In this case, OCR values can also be related to surface area. Figure 4.3 A (right axis) shows that surface OCR values depend linearly on the cell concentration, and proves uniform cell oxygenation in cuvettes and no diffusion limitations.

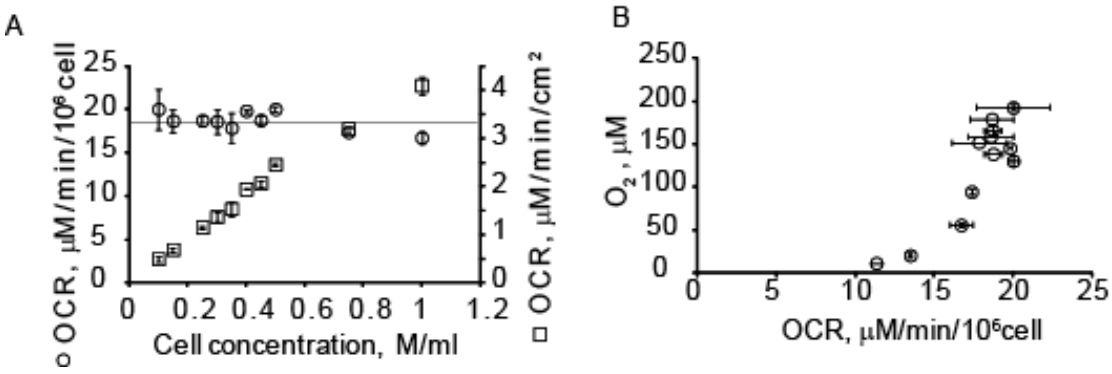

Figure 4.3 A. Absolute OCR per cell (○) and per surface area (□). B. Cell monolayer oxygenation at high cell densities. Mean values are calculated from 2 replicates and 3 repeats with standard deviation expressed in error bars.

The absolute OCR platform has limited use at high cell densities (1.25-1.50*10^6 cells ml^{-1}), since such rapid and deep media deoxygenation in the cuvette (< 20 μM O_2) leads to very fast signal changes, and large errors in OCR determination (Fig. 4.3 B).

4.4 Cell oxygenation in the open plate platform

Using the same cell model, i.e. MEF cells stained with MitoXpress-Intra probe, we measured cell oxygenation in the open 96-WP system. After seeding cells at concentrations 20-250*10^3 cells $well^{-1}$, they were incubated at 37°C for 2 hours to adhere and recover from stress and then measured on TR-F plate reader.

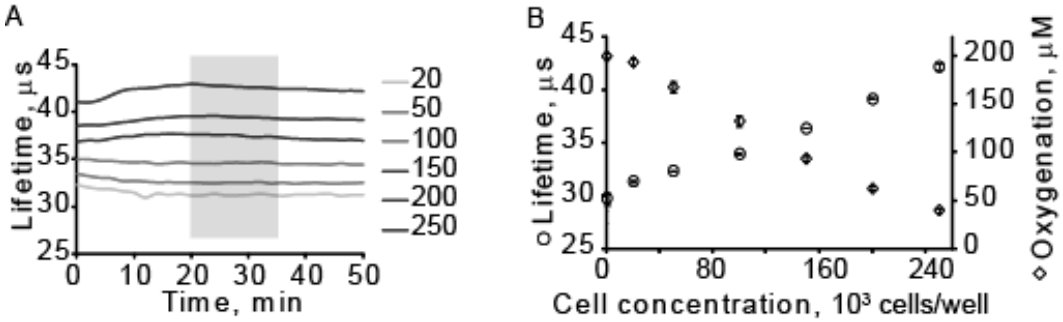

Figure 4.4 Monitoring of MEF cells oxygenation in an open 96-WP. A. Oxygenation profiles of respiring samples containing 20-250*10^3 cells $well^{-1}$. B. Correlation of probe lifetime signal (○) and intracellular O_2 (◊) with cell concentration, 37°C, 21 kPa O_2. Mean values are calculated from 6 replicates with standard deviation expressed in error bars.

Fig. 4.4 A shows that after the initial temperature and gas equilibration (~20 min), the samples produce stable lifetime signals which corresponds to steady state conditions (grey zones). As expected, average cell oxygenation depends on the cell concentration, however deep deoxygenation is not achieved even at the highest cell densities (250*10^3 cells $well^{-1}$, corresponds to 1.25*10^6 cells ml^{-1}). This phenomenon is related to the steady-state conditions of the experiment and balance between O_2 consumption by the cell layer and its diffusion from the atmosphere. Mean lifetime values were determined for the each sample and plotted versus cell concentration (Fig. 4.4 B, left axis). Previously published probe calibration [106] allows calculation of corresponding oxygenation values (right axis), which ranged from 200 to 40 µM O_2 for the different cell numbers.

Ambient O_2 concentration influences O_2 diffusion to cell layer and its steady-state oxygenation. Measurements at lower atmospheric O_2 significantly reduce icO_2 levels

compared to standard conditions. Cell oxygenation was analyzed at 20, 16 and 13% of atmospheric O_2 for loaded with MitoXpress-Intra probe MEF cell in concentrations ranged 0-300*10^3 cells $well^{-1}$ (Fig. 4.5 A).

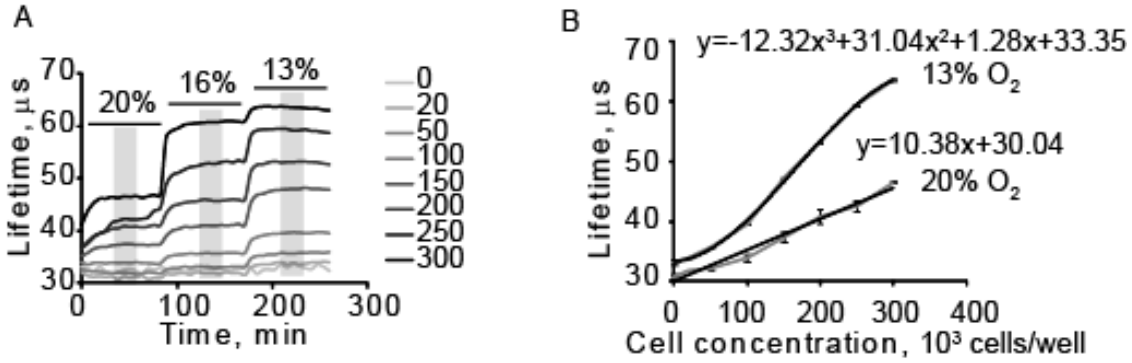

Figure 4.5 A. Oxygenation profiles of MEF cells (0-300*10^3 cells $well^{-1}$) at 20, 16 and 13% of atmospheric O_2. B. Correlation of probe phosphorescence lifetime with cell concentration at 20 and 13% of atmospheric O_2. Mean values are calculated from 6 replicates with standard deviation expressed in error bars.

Measurements were carried out for the same cell sample by changing of ambient O_2 concentration, equilibration of the seeded 96-WP at new conditions for 20-30 minutes and continue measurements for about 80 minutes. Such changing of ambient O_2 concentration forms characteristic "steps" of probe phosphorescent lifetimes. Increasing amount of cells causes deeper steady-state deoxygenation in the sample at each O_2 concentration. Remarkable, that difference between oxygenation levels is increasing at lower O_2 concentration, what can correspond to stable respiration activity of cells upon restricted O_2 diffusion. However, already at 13% O_2 oxygenation levels for 250 and 300*10^3 cells $well^{-1}$ samples are closer due to approaching of complete cell layer deoxygenation. The mean oxygenation was calculated for each sample at three O_2 levels (grey areas) and plotted versus cell concentrations.

The relationships were seen to be close to linear, starting at air-saturated level (209 µM O_2) at low cell numbers and pushing the O_2 level down at high cell concentrations. Thus, at 20% O_2 they ranged from 205 µM O_2 (or 31 µs) for the lowest to 41 µM O_2 (or 42 µs) for the highest cell numbers. As expected, lower atmospheric O_2 leads to the deeper

deoxygenation of cell monolayer: at 13% O_2 probe lifetime achieved the maximal value of 68 μs which corresponds to zero O_2 and leveled off (Fig. 4.5 B). Thus, local oxygenation of cell layer under steady-state conditions in an open microplate is a stable and accurately measured parameter, which shows a linear correlation with cell density.

4.5 Correlation between cell oxygenation and OCR

Using the results of parallel OCR and O_2 measurements (Figs. 4.2 and 4.4), the correlation between measured absolute OCR and lifetime values, corresponding to cell layer oxygenation, can be established (Fig. 4.6 A). At 21 kPa O_2, the initial part (31-39 μs) is described well (R^2 = 0.96) by the following linear function: OCR (μM min^{-1}) = 1.80 * τ (μs) - 52.69, where τ is measured phosphorescence lifetime of MitoXpress-Intra probe. As before, lifetime values can be recalculated to O_2 concentrations by applying of the calibration function for the probe. In O_2 concentration scale the relationship is the following: OCR (μM min^{-1}) = -0.0909 * [O_2] (μM) + 19.4. These correlations between absolute OCR and lifetime or O_2 concentration values are valid for different cell types and respiration activities in the range of approximately 1 – 17 μM min^{-1}. Of course, assay temperature (37°C), sample volume (0.2 ml) and atmospheric O_2 levels should be the same. Higher temperature or cell concentration in the sample as well as lower ambient O_2 concentration would lead to fast changes in respiration responses, affection of steady-state conditions and distortion of presented calibration function.

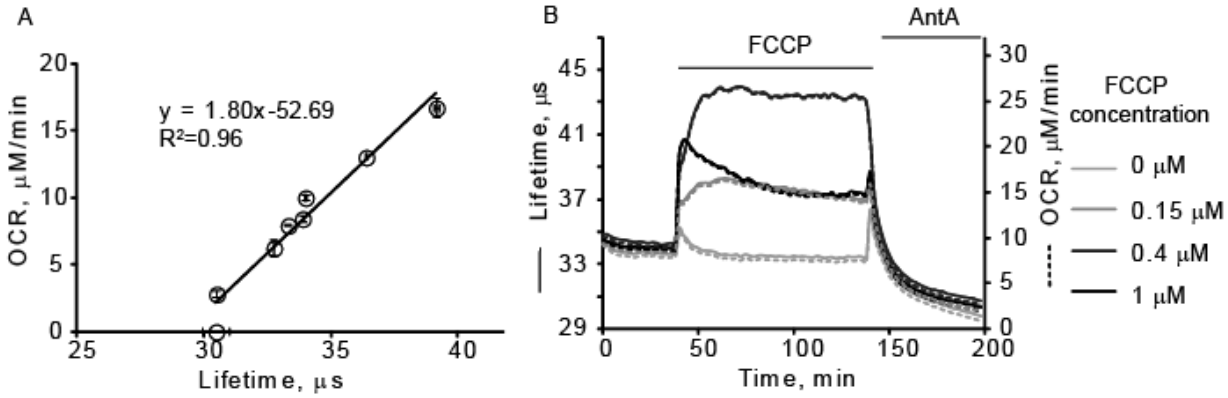

Figure 4.6 A. Correlation of absolute OCR and cell oxygenation, expressed in phosphorescent lifetime of the probe (37^{o}C, 21 kPa O_2). B. Profiles of MEF cells respiration shown in probe lifetime (left axis) and absolute OCR (right axis) scales at rest and upon stimulation with 0.15 - 1 μM of FCCP and 10 μM of AntA (shown by bars).

4.6 Respiratory cell responses to metabolic stimulations

Knowledge of the relationship between O_2 and absolute OCR enables real-time monitoring of cell respiration under changing conditions, such as drug treatment. We demonstrated this by analyzing OCR of MEF cells at rest and upon pharmacological treatment. The effect of FCCP uncoupler is concentration-dependent and such treatment requires careful optimization for different cell lines and assay conditions, to avoid incomplete uncoupling at low doses or non-specific toxicity at high doses. The high throughput of the open-plate platform provides rapid optimization and analysis of dose dependences, either by parallel or sequential addition of drug(s) to the samples with cells. Here we used 0 - 1 μM FCCP concentrations for treatments of MEF cells in 96-WP after collecting respiration signals of resting cells for 40 minutes (Fig. 4.6 B). Blank experiment with addition of matching amount of media demonstrates spike due to the temperature equilibration and the same background signal after stabilization. FCCP at concentrations 0.15 and 0.4 μM causes activation of cell respiration, when 1 μM FCCP appears to be toxic for MEF cells in this assay and leads to decrease of respiration level after initial activation. AntA was applied for all cell samples after monitoring of response to FCCP stimulation and caused expected inhibition of respiration. At different time points, probe lifetime signals or cellular O_2 levels can be converted to absolute OCR values by using of the calibration plot from Figure 4.6 A. Such simple converting allows avoiding additional calculation of cell oxygenation in O_2 scale and possible errors. As can be seen from the graph, due to linearity of correlation plot the shape of cell responses to metabolic stimulations is the same in lifetime and OCR axis and corresponds to particular value at each point (left and right axis).

4.7 Conclusions

In summary, we compared the three optical platforms for cellular O_2 measurements: hermetically sealed micro-cuvettes for absolute OCRs (μM min^{-1}), the partially sealed 96-WP with samples under oil for relative OCRs and open 96-WP for steady state oxygenation of cells (μM). They all appeared to have their merits and limitations. The last two screening platforms are gaining wider use in research labs, but not always on a fully quantitative basis. Local oxygenation measured in an open 96-WP with an intracellular O_2 probe is a simple method which provides high throughput, fast data collection, real-time monitoring over prolonged periods with the possibility of repeating addition of drugs or cell treatments.

Using MEF cell line, phosphorescent O_2 probe MitoXpress-Intra and time-resolved fluorescence reader, we show that relative OCRs produced by the 96-WP platform can be converted into absolute values, which are more relevant indicators of cell metabolism and bioenergetics, by applying a constant factor (5.35 for our system). Measured absolute OCRs for MEF cells were also used to relate signal readings of the open plate platform (probe phosphorescence lifetime, μs) to respiration activity of the cell layer: OCR (μM min^{-1}) = 1.80 * τ (μs) – 52.69, for the O_2 range 200-40 μM (lifetime 31-39 μs), 37^{o}C and 21kPa atmospheric O_2. With such calibration, the open plate system can be used to trace absolute OCR over time, in a simple, high throughput format, with cell stimulation and drug additions, what is difficult to implement with other OCR measurement systems.

Chapter 5.

Cationic nanoparticle-based probe for sensing and imaging of (intra)cellular O_2 in multiple detection modalities

5.1 The concept of multimodal icO_2 probe

Optical probes allow non-invasive quantification and imaging of cellular O_2 [69] using phosphorescence intensity, ratiometric and lifetime measurement modes [173]. The intensity based platforms are widely available, they are rather simple and suitable for qualitative and semi-quantitative O_2 measurements, but hard to standardize and use for accurate readout of O_2 concentration. Ratiometric intensity measurements at two different wavelengths allow for more stable calibration, since O_2 concentration is calculated from the ratio of the O_2 sensitive and reference luminescent signals [108]. However, this ratio can also be influenced by the sample and detection system, e.g., detector noise and blank signals, different photobleaching rates, scattering and autofluorescence in the two spectral channels. Phosphorescence lifetime-based detection is by far regarded as most reliable and stable modality for O_2 sensing and imaging [86, 174], however such systems operating in the microsecond time domain are still rare, unlike the nanosecond FLIM (fluorescence/phosphorescence lifetime imaging microscopy). With respect to the optical setup, wide-field fluorescence microscopy, which allows 2D imaging, has been extended by the laser-scanning confocal and two-photon systems providing 3D and 4D (with time lapse) O_2 imaging capabilities (also in FLIM mode), deep penetration in live tissue, and reduced photodamage to the probe and biological objects [175]. For benchmarking and comparison of different techniques, a probe compatible with all listed modalities, one- and multiphoton excitation is highly desirable. In this chapter one such probe called MM2 is presented, which combines the advantages and overcomes the limitations of existing O_2 probes, allows sensing and imaging of intracellular O_2 in multiple detection modalities.

5.2 Probe design and characterization

Positive charge is known to increase cell penetrating properties of molecules and particles by interaction with negatively charged cell membrane [176]. A number of positively charged conjugates for icO_2 sensing, produced by binding of arginine-rich short peptides to reporter dyes are known [62]. Positively charged polymers that can form core-shell structures were also suggested for intracellular targeting of sensing materials [177]. One of such polymers, Eudragit RL-100, originally developed for preparation of biocompatible coatings and drug delivery systems, also found application in optochemical sensors [178]. A nanoparticle O_2 probe, based on this polymer with embedded PtTFPP dye was developed in our lab [94]. This probe (commercialized under the name MitoImage^{TM}-NanO2) shows high brightness and photostability, high cell-penetration ability with fast (6-16 h) and efficient staining of various mammalian cells, good performance in O_2 sensing and FLIM without significant cyto- and phototoxicity. However, NanO2 probe does not allow for ratiometric or multiphoton imaging of O_2 and cannot be regarded as a universal tool.

We designed new multimodal icO_2 probes (MM series) based on the NanO2 parent structure. The approach included integration of three complementary functionalities in one nanoparticle structure: i) an O_2 -sensitive phosphorescent reporter dye, PtTFPP; ii) an O_2 -insensitive reference fluorophore acting as one- and two-photon light harvesting antennae and FRET donor for PtTFPP; iii) nanoparticle-forming cationic polymer RL-100, which serves as delivery vector, encapsulation and quenching matrix for the dyes. The main challenge was to find a suitable fluorophore that combines the desired photophysical properties, compatible with the fabrication method (encapsulation by precipitation with water) [92], does not perturb the stability, and has the O_2 - quenching properties of the parent nanoparticle structure. To achieve this, two different probe formulations, one containing coumarin C545T and another poly(9,9-dioctylfluorene) (PFO) dyes were produced, termed MM1 and MM2, respectively (Fig. 5.1 A). Spectral characteristics of these probes measured in the air-saturated phosphate buffer are shown in Figure 5.1 B, in comparison with parent probe NanO2 which contains only PtTFPP dye. MM1 probe is excitable at 450–490 nm, emits fluorescence at 510–540 nm and

phosphorescence at 630–700 nm. The shape of the excitation spectrum (detection at 650 nm) reflects efficient FRET between C545T and PtTFPP in the nanoparticles, thus making MM1 a promising candidate for the ratiometric intensity (520/650 nm) and lifetime based (650 nm) detection of icO_2.

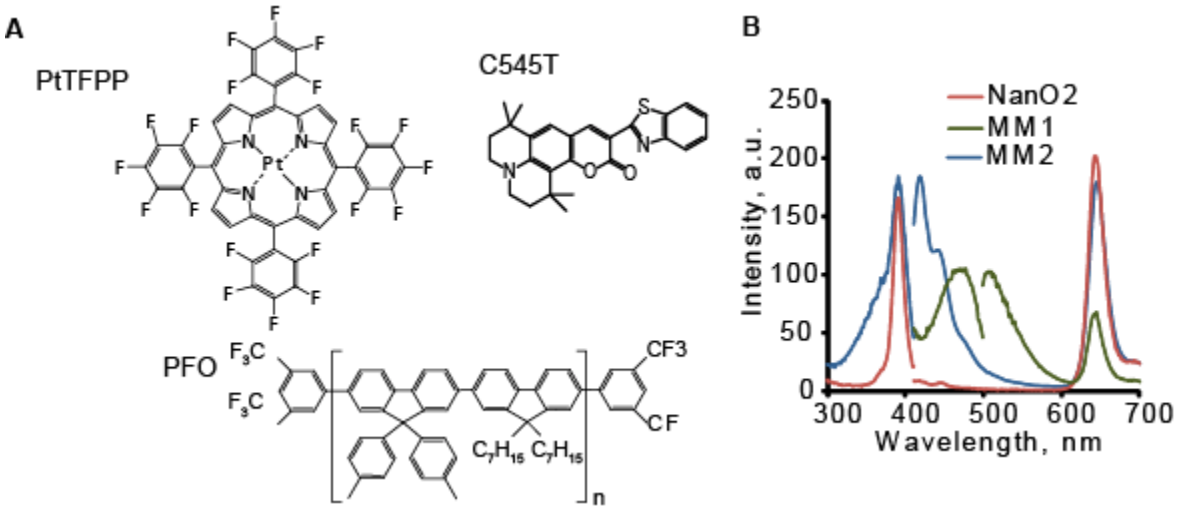

Figure 5.1 A. Chemical structures of the phosphorescent PtTFPP reporter and fluorescent reference and antennae dyes C545T and PFO. B. Excitation and emission spectra of NanO2, MM1 and MM2 probes at 21 kPa O_2.

To verify this, we exposed adherent MEF cells to MM1 (10 μg ml^{-1}, 16 h) and observed effective intracellular accumulation, similar to the NanO2 (Figure 5.2 A). However, microscopy analysis revealed, that luminescent signals of the two dyes have rather different, nonmatching localization patterns, with more diffused fluorescence of C545T in the cytoplasm (see merged image). From this we concluded that upon cell loading and internalization of MM1, C545T dye leaks from the nanoparticles. Such operational instability makes MM1 unsuitable for quantitative sensing of icO_2 due to the drift of its photophysical properties and O_2 calibration. Interestingly, without cells the 1 mg ml^{-1} stock of MM1 remains stable over several months of storage at 4°C. No changes in the excitation spectrum were observed, which would indicate dye leakage from the nanoparticles and degradation of the FRET system.

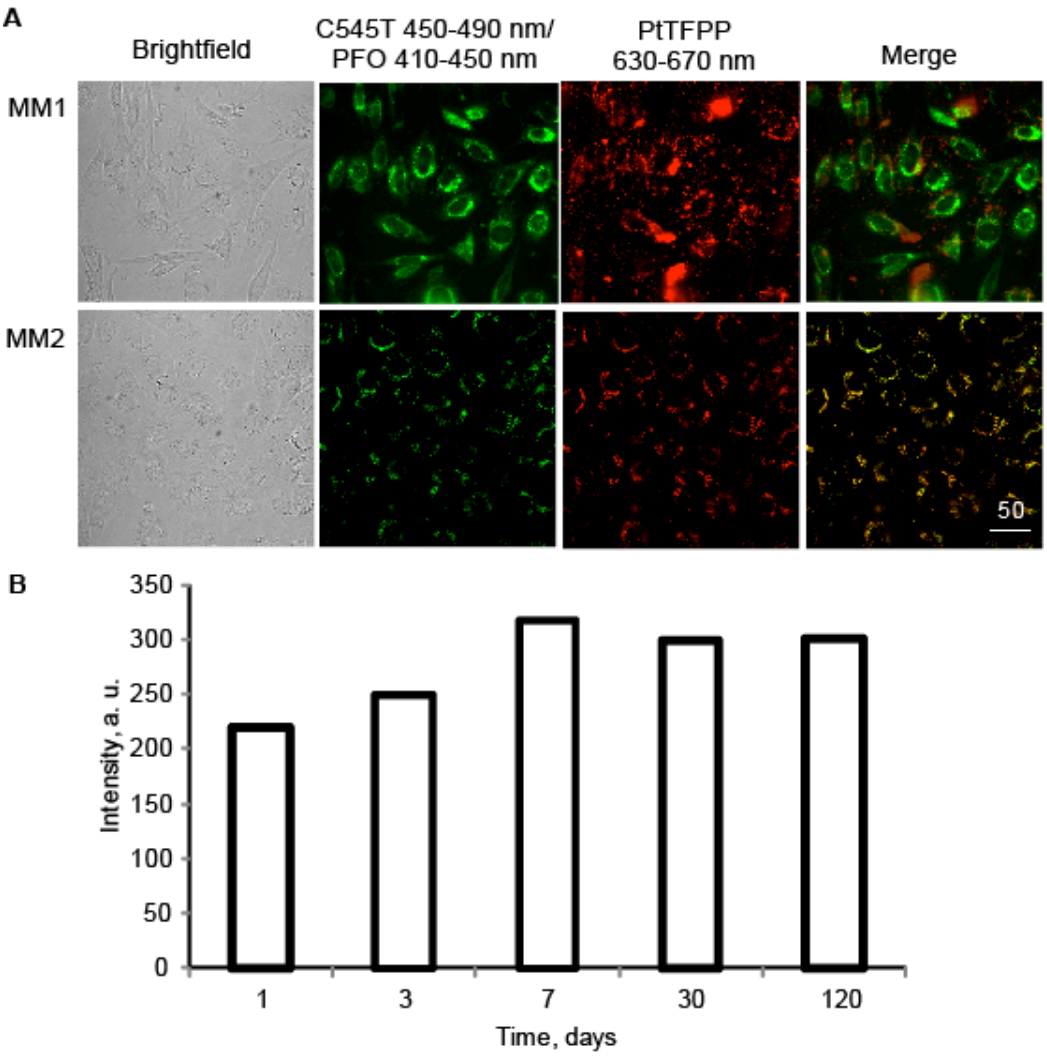

Figure 5.2 A. Staining properties of MM1 and MM2 probes (10 μg ml^{-1}, 16 h) with MEF cells: C545T and PFO fluorescent signals in green channel and PtTFPP phosphorescent signal in red channel. B. Storage stability of MM2 probe by phosphorescence intensity signals (stock 1 mg ml^{-1}, 4°C). Scale bar in μm.

To overcome the drawbacks of MM1, another oxygen probe MM2 was assessed similarly. It was expected, that hydrophobic polymeric fluorophore PFO would be efficiently retained by RL-100 nanoparticles without leakage. The obtained nanosensors with PFO (known as excellent two-photon antennae and ratiometric partner for PtTFPP [99, 179]), produced characteristic spectrum with excitation maxima at 390–405 nm, fluorescence band of PFO at 410-450 nm and phosphorescence band of PtTFPP at 650 nm (Figure 5.1 B). To achieve maximal brightness, FRET efficiency and spectral

visibility, the concentrations and ratios of the two dyes in the nanoparticles were optimized. PtTFPP content of 1.5% w/w produced efficient FRET and strong red phosphorescence when exciting the antenna. For PFO donor 10% w/w concentration provided efficient absorption without aggregation, and strong residual fluorescence that can be used as a reference in ratiometric sensing. Further experiments were performed with this composition of MM2 probe (for comparison, MM1 optimum was 1.33% w/w of C545T and 1% w/w of PtTFPP). The absorption spectrum of MM2 probe is similar to those of NanO2 probe and PtTFPP dye, showing stability of the dye inside polymer without aggregation. Wide-field fluorescence microscopy of MEF cells loaded with MM2 revealed stable co-localization of PFO and PtTFPP emissions (Figure 5.2 A), thus proving that no dye leakage occurs. MM2 stock 1 mg ml^{-1} was stable for at least 6 month of storage at 4°C, as can be judged from the excitation spectra and phosphorescence intensity signals (Figure 5.2 B). As determined from the light-scattering experiments, MM2 beads had an average size of about 70 nm (40 nm for MM1) and homogeneous distribution (PDI=0.103). This size is larger than for the NanO2 (35 nm), but still well below the 100 nm threshold, which is regarded safe for the cells [180]. Zeta potential for MM2 particles was +32 mV, which is lower than for the undoped RL-100 beads (+58 mV) (Synthesis, spectral and size (charge) characterization of MM1 and MM2 probes were performed by Prof. S. Borisov, Graz University of Technology).

5.3 Cell penetrating properties, brightness and toxicity assessment

First of all, the kinetic of mammalian cell loading with MM2 probe was studied. MEF cells were seeded in 96-WP at concentration 30,000 cells $well^{-1}$, grown for 24 hours to achieve 70-80% confluence and stained with 10 μg ml^{-1} of the probe for 0-16 hours. Intracellular accumulation of MM2 in MEF cells after 6-16 hours incubation was found to be similar to that of NanO2 with efficient staining of the cytosol (Figure 5.3). This proves that cell loading with NPs is mostly determined by the polymeric material (RL-100) rather than by encapsulated sensitive material. The probe did not change cell morphology for the time of monitoring, as can be seen from the brightfield images. Control samples (without loading) demonstrated absence of autofluorescence and

background signals at used excitation (390 nm), so all measured phosphorescence signals belong to the MM2 probe. Bright signals from PtTFPP and PFO permitted O_2 detection and imaging in different modalities.

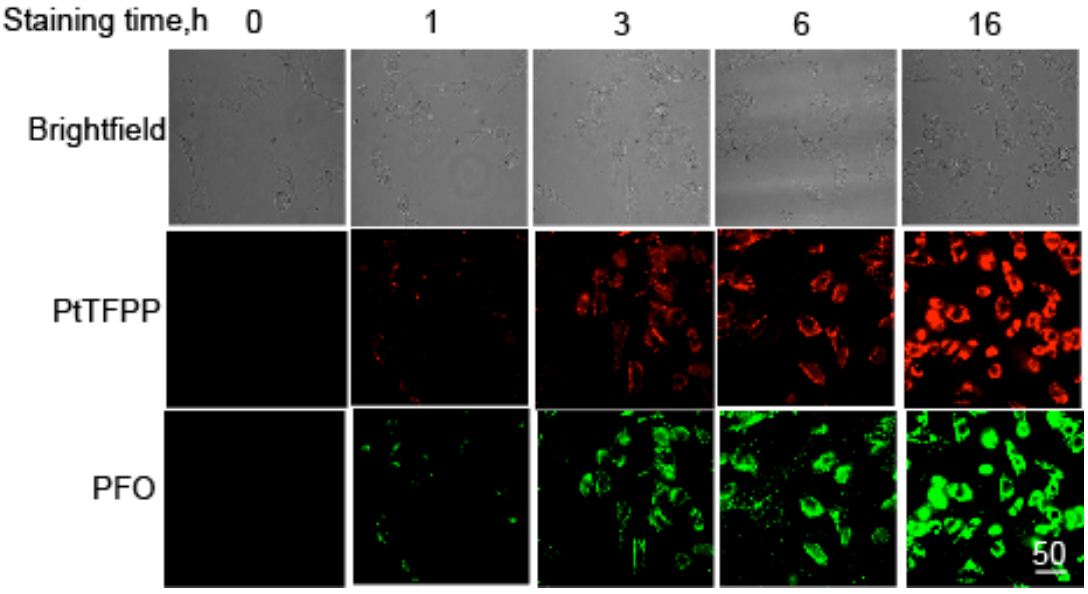

Figure 5.3 Staining kinetics of MM2 probe with MEF cells (10 μg ml^{-1} 0-16 h) shown in PtTFPP and PFO luminescence signals. Scale bar in μm.

Brightness of MM2 and NanO2 was compared by parallel loading of MEF cell monolayers with 0-30 μg ml^{-1} of probes for 16 hours (Figure 5.4 A). According to the plate reader Victor2 detector characteristics, TR-F intensity signals should exceed 30,000 cps for reliable and accurate O_2 measurements in lifetime mode. Thereby, 2 μg ml^{-1} concentration of MM2 is already sufficient. When used with the same measurement settings and concentration as NanO2, phosphorescent signals of MM2 probe were about 4 times higher due to the antennae effect of PFO. Enhanced intensity of signals allowed shorter loading times or lower working concentrations for MM2. To estimate toxic effects of the probe on mammalian cells, luminescence-based ATP assay was used. With loading concentrations up to 30 μg ml^{-1} and exposure times 16 hours no significant influence on cell viability was detected (Figure 5.4 B). Slightly higher cell viability over NanO2 probe can be explained by the differences in particle size and cell penetration pathways.

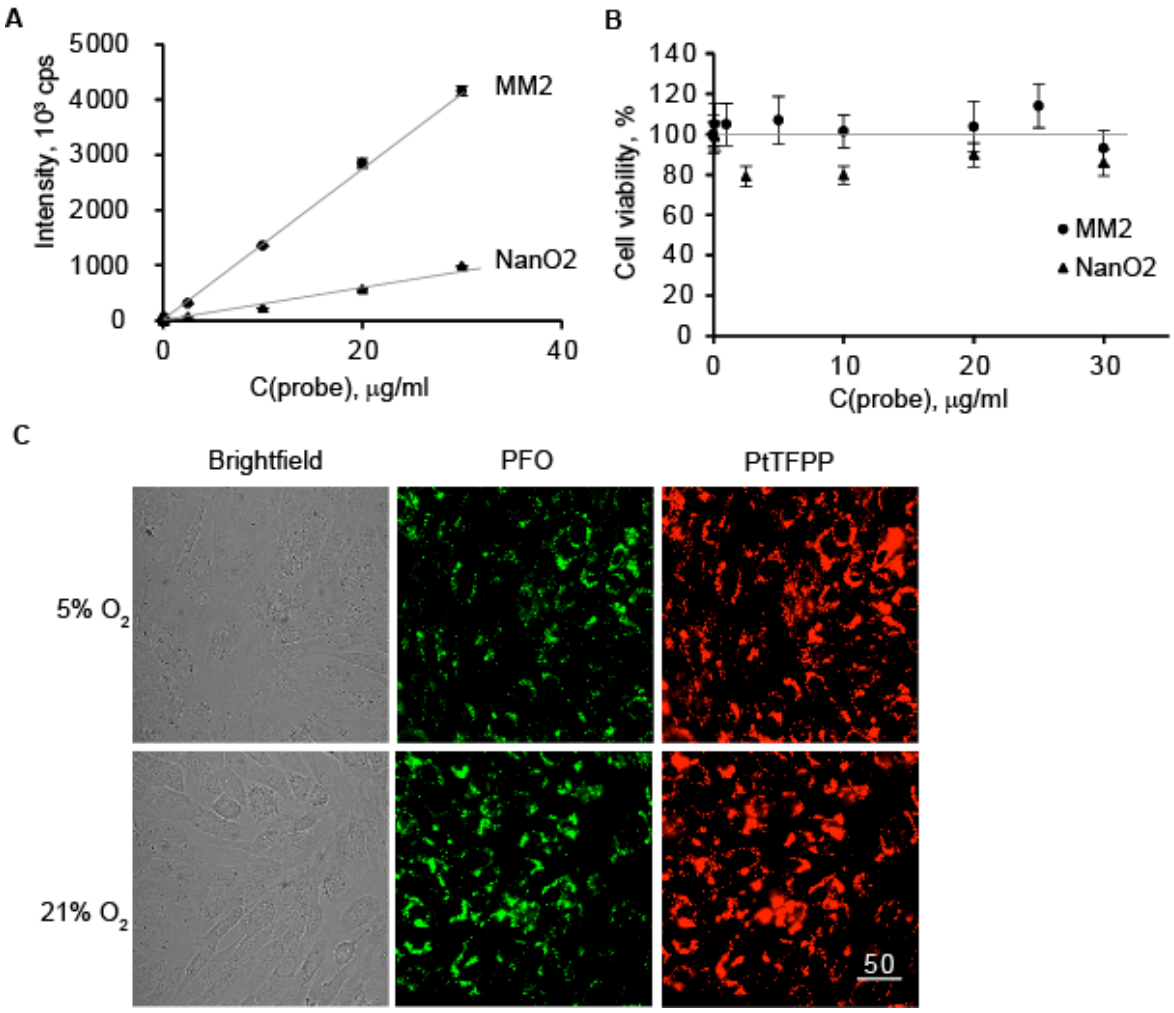

Figure 5.4 The effect of concentration of MM2 and NanO2 probes (0-30 μg ml^{-1}, 16 h) on (A) TR-F signals measured on the microplate reader and (B) on cell viability analyzed using a Cell Titer-Glo kit. C. Comparison of MM2 staining efficiency (10 μg ml^{-1}, 16 h) with MEF cells at 5% and 21% of atmospheric O_2. Scale bar in μm. Mean values are calculated from 6 replicates with standard deviation expressed in error bars.

Since low O_2 availability and hypoxia may influence probe uptake [181], we compared staining efficiency of MEF cells with 10 μg ml^{-1} concentration of MM2 at 5% and 21% of atmospheric O_2. No significant difference in luminescence signals was observed with wide-field microscopy (Figure 5.4 C). Intracellular distribution of MM2 probe in MEF cells was similar to NanO2 probe: perinuclear localization resembling endoplasmic reticulum and lysosomes, and no significant co-localization with the mitochondria. Taken

together, MM2 probe accumulates efficiently in mammalian cells, such as MEF cells, and retains its photophysical and O_2 sensing properties.

5.4 Lifetime calibration of the probe for O_2 measurements

Detection on a TR-F plate reader using rapid lifetime determination (RLD) method [163] and microsecond FLIM microscopy are the most promising platforms for the optical O_2 sensing [182]. The first allows simple, high throughput analysis of cell populations, while the second – analysis of individual cells with high spatial resolution and possibility to reconstruct detailed O_2 maps for complex biological samples. Until recently, O_2 FLIM was mainly realized on the wide-field microscopes, however laser scanning confocal and multiphoton systems with 3D imaging capabilities are now rapidly emerging [183]. To calculate icO_2 concentration lifetime values should be translated according to the calibration function of the probe in the biological environment. We calibrated MM2 probe with MEF cells on TR-F plate reader and wide-field microsecond FLIM system, and compared the results.

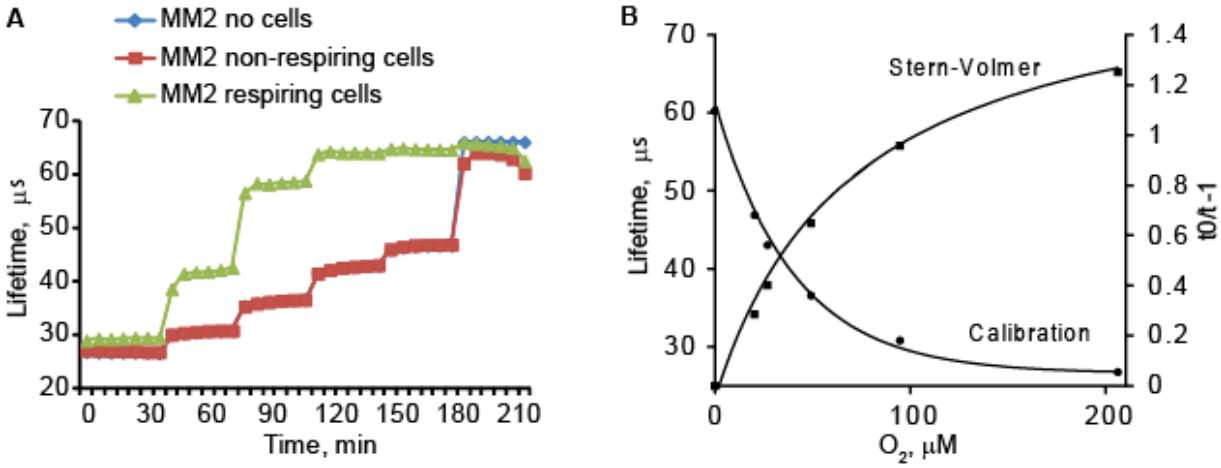

Figure 5.5 Calibration of MM2 probe with MEF cells (10 µg ml^{-1}, 16 h loading) on Victor2 TR-F plate reader. A. Phosphorescence lifetime signals of MM2 probe at 0, 2, 3, 5, 10 and 21% O_2 with resting, non-respiring cells and without cells. B. Lifetime calibration and Stern-Volmer plots.

O_2 calibration measurements on Victor2 reader (PerkinElmer) are shown on the Figure 5.5 A. MEF cells were seeded to 96-WP at concentration 30000 cell well^{-1}, cultured till confluent monolayer and loaded with 10 μg ml^{-1} of the MM2 probe for 16 hours. Victor2 reader was placed in hypoxia chamber with gas mixer (0-21% O_2). Recording of phosphorescence intensities and lifetime values followed after temperature and gas equilibration (delay time of 20 minutes was used before each set of measurements) in the plate compartment. To eliminate the effect of the local gradients and set exact O_2 concentration, cell respiration was blocked by the addition of 10 μM AntA 15 minutes prior to the measurement. Lifetime values for respiring cells showed similar values to the calibration measurements only at high O_2 concentrations and significantly higher at low O_2 due to the self-deoxygenation of cells. Control calibration of the probe in PBS buffer without cells revealed no influence of biological environment on the readings, when compared to the AntA treated cells. The range of lifetime changes for MM2 (28–61 μs) was comparable with that for NanO2 [106], Stern-Volmer plot also showed slightly curved shape (Figure 5.5 B). Measured lifetime values were very reproducible (≈ 0.2 μs) and accurate, therefore one time calibration was deemed sufficient. From the corresponding fit we determined calibration function:

$$[O_2] = 18861*\exp(-\tau/ 5.79) + 9.62, \quad \text{(Eq.1.8)}$$

and Stern-Volmer equation:

$$\tau_0/\tau - 1 = 0.67*(1 - 0.04*[O_2]). \quad \text{(Eq.1.9)}$$

Regarding the differences in the detection systems, calibration of the new probe was performed as well on the wide-field FLIM microscope, equipped with gated CCD camera and gas mixing chamber for O_2 concentration adjustment. We obtained phosphorescence lifetime images of cell culture loaded with standard concentration of MM2 probe at different levels of atmospheric O_2 (Figure 5.6 A).

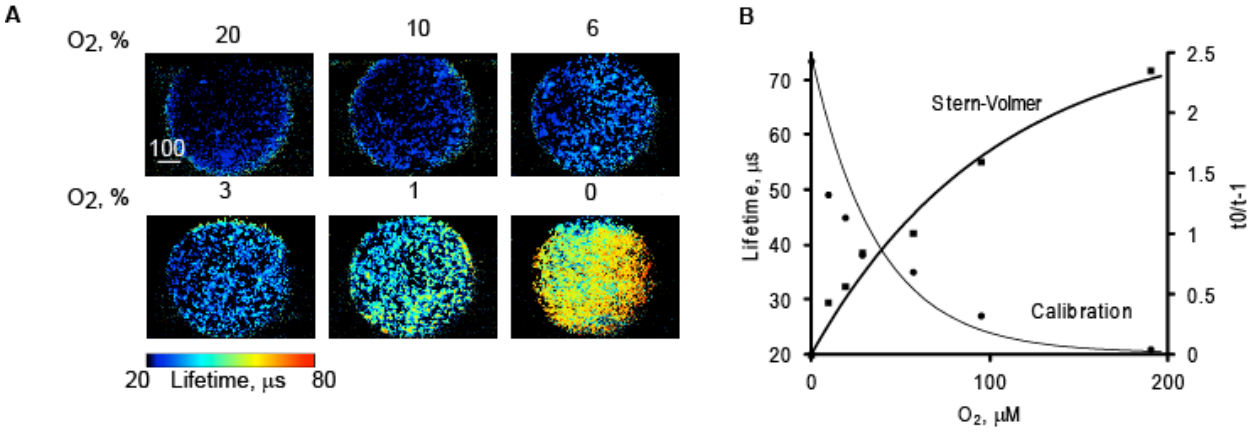

Figure 5.6 Calibration of MM2 probe with MEF cells (10 μg ml^{-1}, 16 h loading) on the wide-field FLIM microscope. A. Phosphorescent lifetime images of MEF cell culture loaded with MM2 probe at 0-20% of atmospheric O_2. B. Calibration and Stern-Volmer plots. Scale bar in μm.

Similarly to the TR-F calibration, average lifetimes calculated for 6 characteristic intracellular regions were plotted versus O_2 concentrations (Figure 5.6 B). Calibration function and Stern-Volmer equation were determined from the best fit:

$$[O_2] = 1546*\exp(-\tau/ 9.98) + 0.06, \quad \text{(Eq.1.10)}$$

$$\tau_0/\tau - 1 = 2.69*(1 - 0.99*[O_2]). \quad \text{(Eq.1.11)}$$

Due to the complicated data processing and subjective choosing of characteristic regions, lifetime values are less reproducible and calibration equation was obtained from 3 separate experiments to increase accuracy. In the future experiments these calibration functions obtained with TR-F plate reader and wide-field FLIM microscope were used.

5.5 Performance of the probe in ratiometric mode

The presence of O_2 - insensitive PFO fluorophore in the nanosensors allows measurement of icO_2 in ratiometric intensity mode. A steady-state luminescent spectroscopy of mammalian cell suspension in quartz cuvettes was chosen as a convenient platform for ratiometric measurements. MEF cells were loaded by standard procedure in culture flask

with 25 μg ml^{-1} MM2 probe and prepared as $1*10^6$ cell ml^{-1} suspension. MM2 probe produces approximately two-fold increase in the emission of the O_2 sensitive dye (650 nm) when changing from air-saturated (21 % O_2) to deoxygenated (0 % O_2) condition, while PFO fluorescence (410–450 nm) remained steady (Figure 5.7 A).

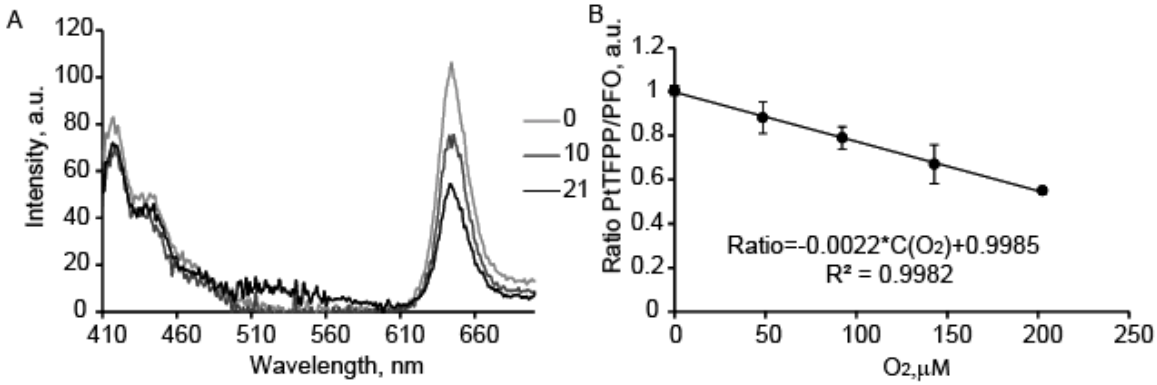

Figure 5.7 Performance of MM2 probe (25 μg ml^{-1}, 16 h loading) in ratiometric intensity-based mode. (A) Emission spectra and (B) O_2 calibration measured in $1*10^6$ cell ml^{-1} suspension of MEF cells stained with MM2 probe. Mean values are calculated from 4 repeats with standard deviation expressed in error bars.

Calibration function for ratiometric mode was obtained by spectra measuring, calculation of [PtTFPP]/[PFO] ratio and plotting these values versus the ambient O_2 concentration. For that, cells were treated with 10 μg ml^{-1} AntA to block respiration, placed in the cuvettes and incubated in hypoxia chamber about 20 minutes for the temperature (37°C) and gas equilibration (1-21 % O_2). Then the cuvette was tightly sealed with a cap and proceeded to the preheated at 37°C measurement unit to maintain dissolved O_2 concentration. To achieve 0 % O_2 chemical deoxygenation was used (see Materials and Methods section). The changes in the intensity ratio were in agreement with lifetime changes (Figure 5.7 B):

$$[PtTFPP]/[PFO] = - 0.0022*[O_2] + 0.9985 \quad \text{(Eq.1.12)}$$

As an example of using MM2 probe in ratiometric mode we performed drug treatments of MEF cells in suspensions and measured their metabolic responses on luminescence

spectrophotometer. 10 μM AntA was used to block cell respiration, 1 μM FCCP – to stimulate respiration and 2.5 mg ml^{-1} EGTA to increased energy requirements and cause rapid spike of cell respiration [121, 157]. Metabolic responses are causing little changes in cell oxygenation, especially if the measured volume is significant (1 ml in our case) and require sensitive platform to be detected. The difference between stimulated and resting cells is barely noticeable and often mistaken in the intensity mode by spectral heights at 650 nm (Figure 5.8 A).

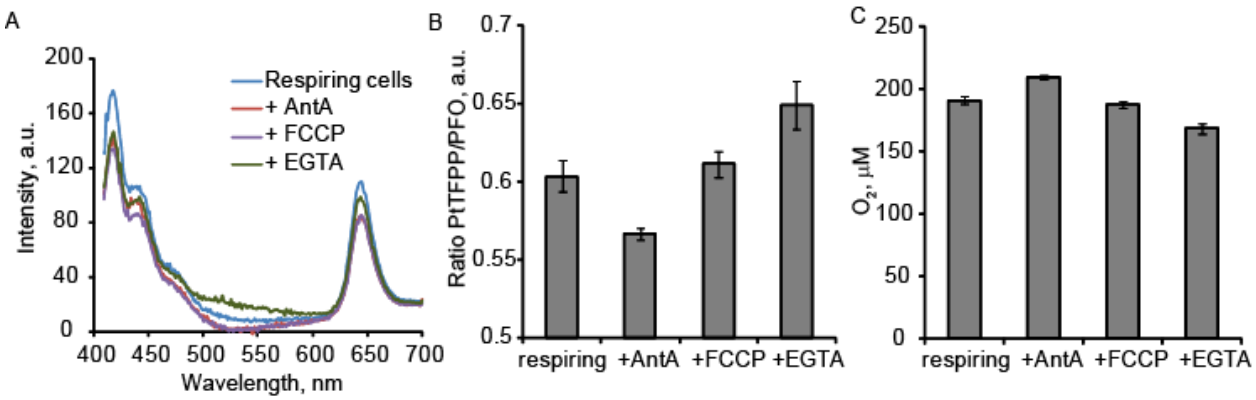

Figure 5.8 Monitoring of cell responses to metabolic stimulations (10 μM AntA, 1 μM FCCP, 2.5 mg ml^{-1} EGTA) in (A) intensity mode by emission spectra, (B) ratiometric mode in ratio signal scale and (C) ratiometric mode in O_2 scale, calculated from ratiometric signals according to calibration (Fig. 5.7 B). Mean values are calculated from 4 repeats with standard deviation expressed in error bars.

The dilution of cell suspension with stimulant upon addition causes additional errors (even in case of high concentrated stock solutions). Ratiometric responses for all stimulations were calculated as described above and recalculated to O_2 concentration with the use of the ratiometric MM2 calibration (Figure 5.8 B, C). We obtained expected effects of treatments on cell respiration in the narrow physiological O_2 range with complete reoxygenation of cells after treatment with AntA (200 μM O_2) (Figure 5.8 C). Similarly, MM2 probe can be used in ratiometric mode with two-photon excitation (optimal at 760 nm) [184].

5.6 Applications of the multi-modal probe MM2

5.6.1 Monitoring of cell responses to metabolic stimulations

Monitoring of local oxygenation of the cell layer at rest and upon stimulation with FCCP and AntA drugs was also performed in lifetime modality. MEF cells were seeded to 96-WP, loaded by standard procedure with 10 μg ml^{-1} MM2, washed three times and analyzed by TR-F measurements on plate reader Victor2. Ambient O_2 concentration influences cell respiration activity, O_2 diffusion to cell layer and its steady-state oxygenation consequently. Detection at 10% of atmospheric O_2 significantly reduces resting icO_2 levels compared to 20 % O_2 conditions, and amplifies responses to stimulants (Figure 5.9 A). Measurements at low ambient O_2 can be used to enhance sensitivity of the readings and confirm differences between responses to stimulants with similar action. Upon monitoring at 10% O_2 profiles are shifted to higher lifetime and lower O_2 values, as can be expected (Figure 5.9 A, B).

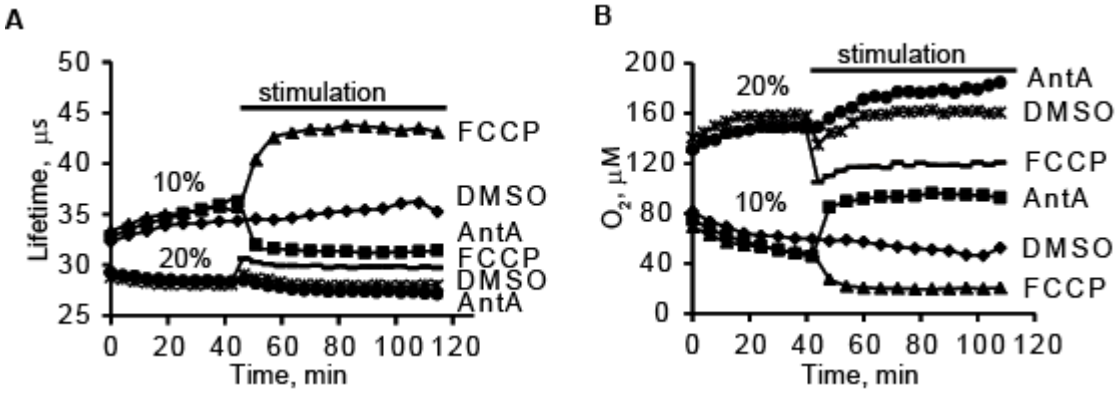

Figure 5.9 Profiles of phosphorescence lifetime (A) and icO_2 (B) in adherent MEF cells stained with MM2 probe (10 μg ml^{-1}, 16 h), measured at 10% and 20% of atmospheric O_2 in microplates. Stimulations with 1 μM FCCP and 10 μM AntA are indicated with bars.

Measurement of cell oxygenation in lifetime mode with plate reader provides the possibility for monitoring of cell responses over time, studying the re-establishment of O_2 gradients and development of response in case of complex kinetic process. At the same time, control samples of non-treated cells are always included in experiments to monitor resting cell oxygenation and viability in parallel. Profiles of phosphorescence lifetime and

icO_2 concentration (calculated using MM2 calibration function for TR-F plate reader system) showed the anticipated effects of drug treatments, good reproducibility and smoothness (Figure 5.9 A, B).

5.6.2 Monitoring of neurosphere oxygenation

Another application of multimodal probe is O_2 imaging in large and complex biological objects. Cell aggregates become popular 3D model, healing the gap between 2D cell cultures and live tissues. Intracellular localization of the probe in such objects allows for the accurate mapping of O_2, avoiding measurement artifacts. Such artifacts can be caused by the probe aggregation on the cell surface or heterogeneous distribution across cell aggregates due to the limited diffusion in depth. We tested MM2 probe for 2D mapping of O_2 in neurosphere, formed by dissected from (E)18 rat embryos neuronal stem cells (courtesy of Dr. R. Dmitriev). Neurospheres were grow *in situ* for 7 days with additions of 20 μg ml^{-1} MM2 probe on 2, 4 and 6 days to obtain equal intracellular staining. Imaging with wide-field FLIM system at 21 % of atmospheric O_2 revealed that the neurosphere interior has largely reduced O_2 levels, i.e. below 30 μM, probably due to the intensive cell respiration and reduced gas diffusion (Figure 5.10 A, B). The area surrounding the neurosphere also had reduced O_2 (below 21 %), thus indicating that the whole structure respires actively and acts as O_2 sink.

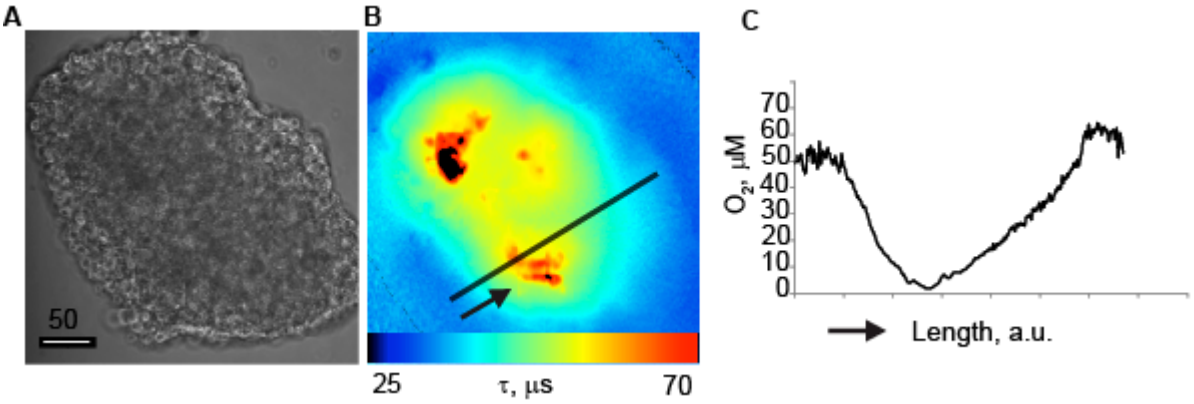

Figure 5.10 Brightfield image (A), lifetime image (B), and profile of O_2 concentration across the neurosphere (C) measured on the wide-field FLIM microscope.

Oxygenation profile was plotted for the neurosphere in the indicated direction, showing exact O_2 concentration in intracellular space at different depth of 3D object (Figure 5.10 C). Remarkably, the core of the neurosphere structure was found to be almost anoxic (below 5 μM O_2), what can lead to the future O_2 deprivation of cells, their death and forming of necrotic core. Similar experiments with neurosphere oxygenation monitoring upon resting and metabolic treatments employing MM2 probe were also performed on confocal and multi-photon microscopes [184].

5.7 Near-IR probe

In vivo applications favour the use of near-infrared (near-IR) O_2 sensitive dyes. We produced NanO2-IR probe as an analogue of the NanO2 probe [94] in which PtTFPP is substituted with a longwave platinum(II)-*meso*-tetra(4-fluorophenyl)tetrabenzoporphyrin (PtTPTBPF) [185] (Fig. 5.11 A).

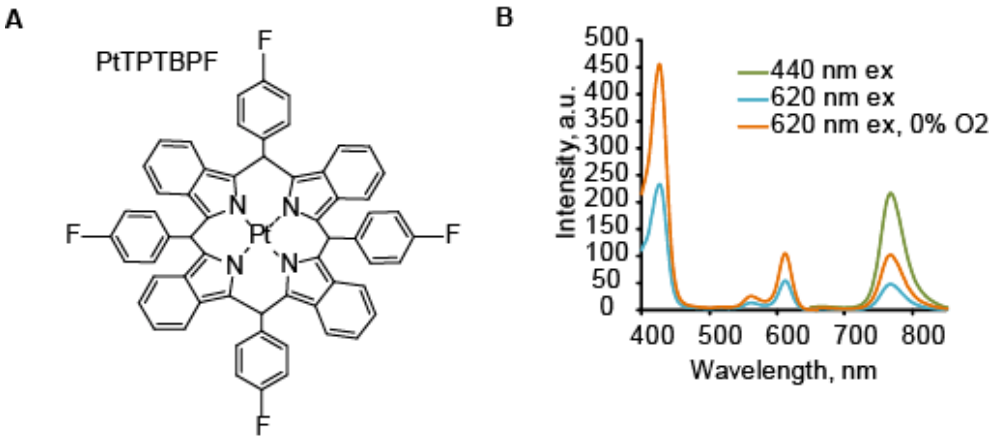

Figure 5.11 A. Chemical structure of the reporter near-IR PtTPTBPF dye. B. Excitation and emission spectra of NanO2-IR probe at 0 and 21% O_2.

Excitation optimum for this probe is 620 nm and emission - 765 nm (Figure 5.11 B). Probe can be excited at Soret band as well (440 nm) which is about four times more intense. In absence of O_2 emission intensity signal is increased two-fold, providing optimal response over the physiological O_2 range (0–21 kPa). Such spectral characteristics are well suited for *in vivo* imaging, provide deep light penetration into

tissue and compatibility with commercial light sources and detectors of animal imagers [183].

Cell penetrating properties of NanO2-IR probe were evaluated with MEF cells after 16 hours staining with 1 μg ml^{-1}. Localisation of the probe is similar to those of NanO2 [94] due to the particle-forming polymer material (RL-100), similar size (35 nm) and charge (+58 mV). Phosphorescence intensity images of cell population were collected at 1, 5 and 21% of ambient O_2 and at 620 and 390 nm excitations (Fig. 5.12 A). One can see clear increase in phosphorescence signals upon deoxygenation of cell culture with both types of excitation.

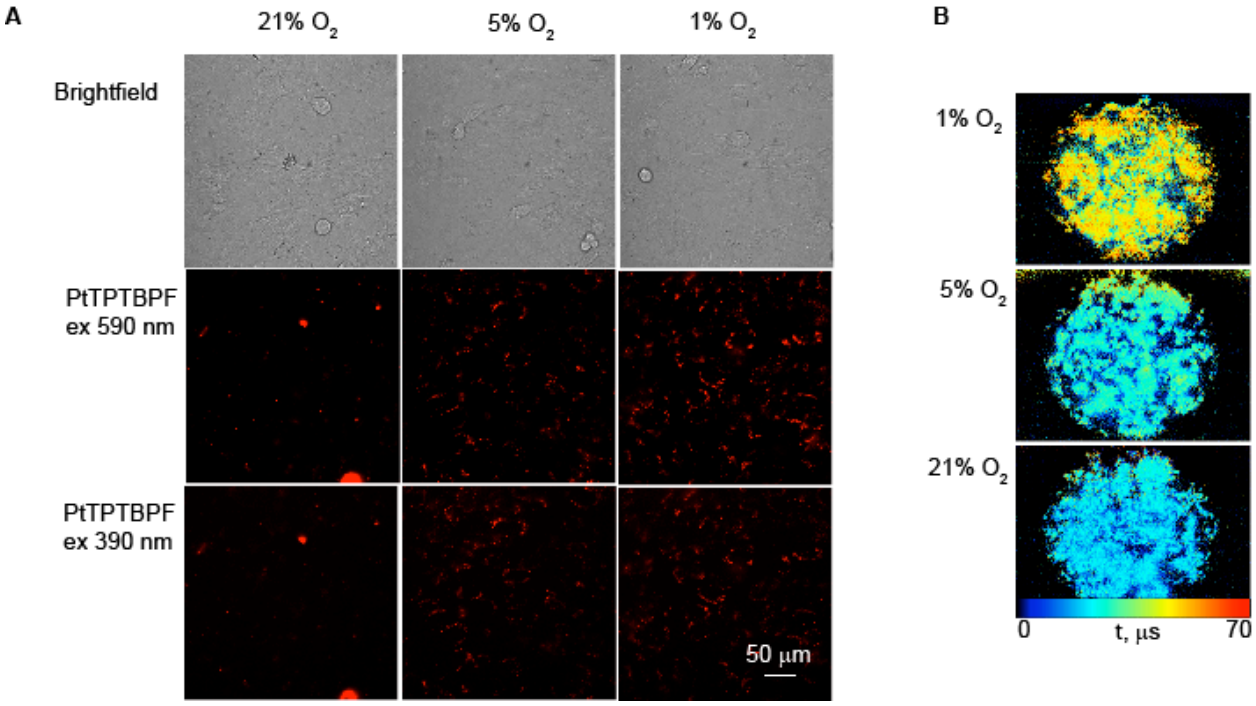

Figure 5.12 Staining properties of NanO2-IR probe (1 μg ml^{-1}, 16 h) with MEF cells. A. PtTPTBPF phosphorescent signal at 1, 5 and 21% of ambient O_2 at 590 and 390 nm excitation. B. Phosphorescent lifetime images of MEF cell culture stained with NanO2-IR (10 μg ml^{-1}, 16 h) probe at 1-21% of atmospheric O_2.

Evaluation of the probe was carried out with loaded MEF cells (10 μg ml^{-1}, 16 h) at 1, 5 and 21% of O_2 (Fig. 5.12 B). FLIM images under 590 nm LED excitation demonstrate bright signals and accurate determination of O_2 concentration by phosphorescence

lifetime of the NanO2-IR probe (colour scale). The new near-IR probe shows similar staining behaviour with the NanO2, improved spectral characteristics, and the possibility of use with animal models [183].

5.8 Conclusions

The multimodal nanoparticle probe MM2, based on the biocompatible polymer RL-100, PtTFPP reporter and PFO antennae dyes, was designed and optimized for sensing of icO_2 in respiring samples, and then evaluated with several common biological models and detection platforms. Compared to the existing probes, MM2 possesses advantageous features including simple synthesis and use, convenient photophysical properties, high brightness and photostability, efficient cell staining, low toxicity and side effects, general flexibility and optimal sensitivity to O_2. The probe is compatible with different detection platforms, ranging from simple fluorescent spectrometers and TR-F readers to sophisticated live cell imaging and FLIM systems. It can provide readout of O_2 concentration in luminescence intensity, ratiometric and lifetime based modalities, under one- and two-photon excitation. Lifetime based O_2 sensing and FLIM are regarded as preferred modalities, they provide superior analytical performance and reliable and accurate quantification of cellular O_2. MM2 shows potential for a broad range of measurement tasks and physiological experiments, such as studies of mitochondrial and cellular function, cell metabolism, bioenergetics and adaptation to hypoxia. Near-IR nanoparticle probe NanO2-IR with similar construction was developed and evaluated for oxygen monitoring in 3D cell models with mild longwave irradiation. This nanosensor approach can be explored further to develop probes with other features, for example for low O_2 concentrations, *in vivo* applications, extracellular use or with subcellular targeting capabilities.

Chapter 6.

Extended range of icO$_2$ probes

The existing probes satisfy many requirements of O_2 sensing but still have limitations. Efforts to develop improved probes for specific cell lines, multicellular spheroids and tissue samples, customized detection platforms and assays are made by many research groups. The main challenges are to improve cell permeability, brightness and photostability, to minimize non-specific adsorption and toxicity, tune excitation to longer wavelength (to avoid sample damage), facilitate multiplexing with other luminescent probes and monitoring in different detection modalities. In this chapter several new materials and delivery vectors were tested to produce probes with improved O_2 sensing properties.

6.1 Anionic intracellular NP-based probes for neural cell models

6.1.1 Design and characterization of multi-modal anionic intracellular NP-based probes

Cell-permeable phosphorescent probes are mostly represented by cationic small molecule and nanoparticle structures, however certain cell types and particularly neural cells are still difficult to stain [186]. Positively charged probes NanO2, NanO2-IR and MM2 demonstrate poor 'patchy' intracellular staining of neuron-like PC12, SH-SY5Y cell lines and neurospheres from primary cells. As it was discussed before, cell permeability of NP probe mostly depends on the used polymeric material and particle size, and less or independent on the nature of encapsulated material [177]. Therefore, alternative polymers allowing easy fabrication of O_2 sensors by water precipitation technique are required [92]. Poly(methyl methacrylate-co-methacrylic acid) (PMMA-MA) forms stable NPs in aqueous solution, however bears carboxylic groups and has moderate gas permeability, so was not widely used for development of intracellular or O_2 probes (Fig. 6.1 A) [187]. Two NP structures were prepared from this polymer: PA1, containing O_2 sensitive phosphorescent dye PtTFPP, and PA2 with PtTFPP and PFO, which is analogue of

cationic multi-modal MM2 probe (Courtesy of Prof. S. Borisov, Graz University of Technology).

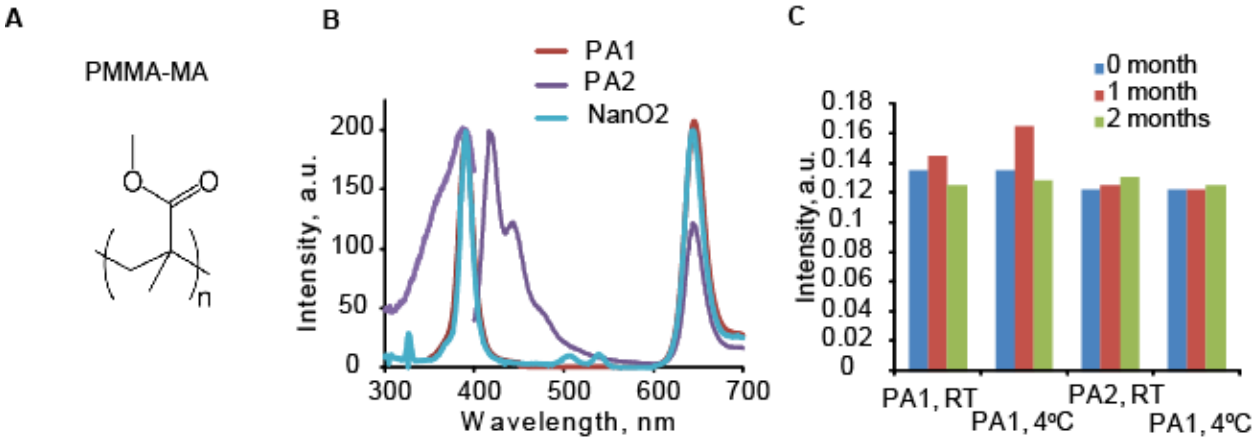

Figure 6.1 A. Chemical structure of PMMA-MA polymer. B. Excitation and emission spectra of NanO2, PA1 and PA2 probes at 21 kPa O_2. C. Storage stability of PA1 and PA2 probes by phosphorescence intensity signals in 1 mg ml^{-1} stock solutions over 2 months at room temperature (preserved with 0.02% NaN_3) and at 4°C.

The PA1 NPs have size of 72 nm, when PA2 NPs have increased size of 95 nm, what is characteristic for two-dye probes (35nm for NanO2 probe against 70 nm for MM2). Zeta potentials are -35 mV and -18 mV for PA1 and PA2 particles respectively. Spectral characteristics of these probes and their cationic analogues NanO2 and MM2 are similar (Fig. 6.1 B) [94, 184]. PA2 probe shows efficient FRET according to the shape of the excitation spectrum. Antenna and a reference dye in the structure (PFO) provides O_2 monitoring and imaging in ratiometric mode under one- and two-photon excitation, similar to MM2 probe. Phosphorescence lifetimes were estimated as 39 and 68 μs for PA1 and 31 and 70 μs for PA2 probes at 21 and 0 kPa O_2, respectively (PBS, 37°C), well suited for O_2 sensing in the physiological range (0-200 μM). Stability of the probes was monitored in 1 mg ml^{-1} stock solutions upon storage at room temperature (preserved with 0.02% NaN_3) and at 4°C (Fig. 6.1 C). Both PA1 and PA2 probes demonstrated good stability over 2 months even at low stock concentration in chosen conditions. Exposure to the low pH is expected upon internalisation of NP probes to mammalian cells (e.g. in lysosomes). Stability of the probes at pH 4, 5 (citric-phosphate buffer) and pH 7.5 (PBS)

was tested (37°C, 24 h), however only marginal increase of absorbance intensity was detected at lower pH values. Altogether, newly prepared NP probes PA1 and PA2 have promising sensing characteristics and stability for measurement of cellular O_2.

6.1.1.1 Cell staining behavior

First of all, PA1 and PA2 were evaluated with neuron-like PC12 cells to assess possible advantages in cell penetrating over the cationic probes (NanO2, MM2), where no internalisation was observed.

We performed time-course loading of PC12 cells with 5 μg ml^{-1} of PA1 and PA2 probes in parallel, visualising staining efficiency after 1, 5 and 22 hours with wide-field microscope (Fig. 6.2 A). As one can see from the image, bright staining with PA1 probe was achieved already after 1 hour of incubation, whereas PA2 probe requires 6-16 hours to provide efficient staining, probably due to the bigger NPs size. Both probes have lysosomal pattern of localisation, when brightfield images show no significant influence of probes on cell morphology.

Brightness and toxicity of new anionic probes were studied on the PC12 and MEF cell lines with PA2. With PC12 cells linear concentration dependence of staining up to 25 μg ml^{-1} (3, 20 h) was shown, while with MEF cells saturation was observed at 2.5 and 10 μg ml^{-1} concentration after 3 hours (Fig. 6.2 B, C). This observation together with greater intensity signals in PC12 cells point at different mechanisms of PA probes internalisation in different cell types. Nonetheless, PA2 probe with all tested cells produced sufficient phosphorescent signals for O_2 monitoring experiments (exceeded 30,000 cps threshold on the TR-F reader [94]). Total ATP assay revealed no toxicity of PA2 probe in PC12 (~94% viability) and MEF cells (~97% viability) at concentrations 0-25 μg ml^{-1} and staining times 3 and 20 hours (Fig. 6.2 D). This is in agreement with low toxicity of PMMA-MA polymer nanoparticles, reported before [188].

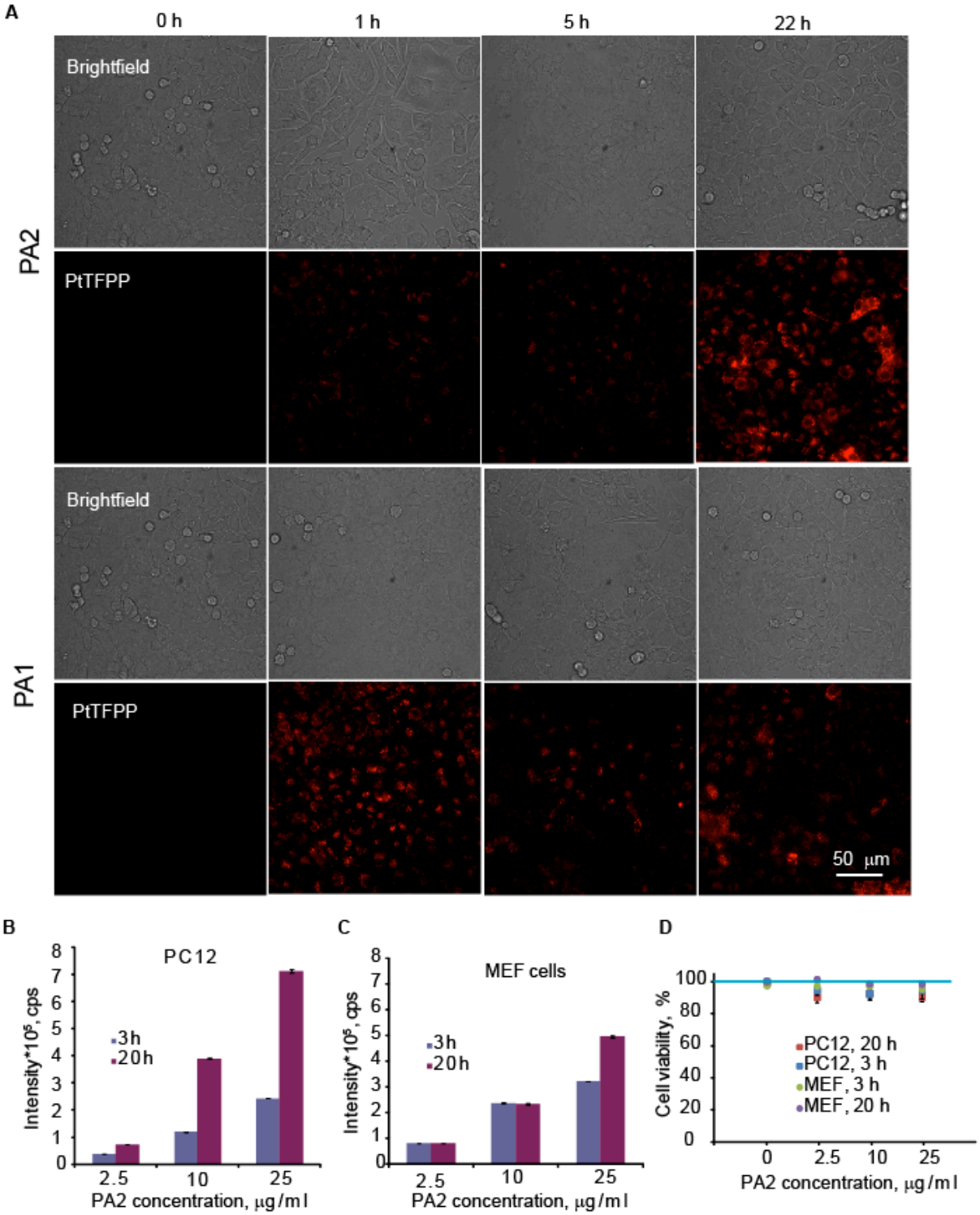

Figure 6.2 A. Staining kinetics of PA1 and PA2 probes (5 μg ml^{-1}) with PC12 cells shown in PtTFPP phosphorescence signals. The effect of PA2 probe concentration (0-25 μg ml^{-1}, 3 or 20 h) on TR-F signals measured on the microplate reader with PC12 (B),

and MEF (C) cells, and on cell viability, analyzed with a Cell Titer-Glo kit (D). Mean values are calculated from 6 replicates with standard deviation expressed in error bars.

6.1.1.2 Study of cell penetration mechanism of PA2 probe

Differences in the staining kinetics of PA1 and PA2 suggested influence of probe size on the cell penetration mechanism. First of all, we tested size dependence of PA2 probe in aqueous solutions: MQ water, PBS (pH 7.5), DMEM with 10% FBS and acetic buffer (AB, pH 4.6). Size of the probe tends to increase, especially in cell growth medium (DMEM with 10% FBS) to compare with standard measurement conditions (PBS). This can be caused by electrostatic interactions on the surface of anionic particle, however size distribution stays in a narrow range (Fig. 6.3 A). Formation of NPs by the water precipitation technique allows preparation of probes with different sizes, depending on the speeds of mixing and water addition [92]. Using modified synthesis procedure, we produced PA2 probe with increased size, titled PA2 L (135 nm, -25 mV), and observed size dependence of probe internalisation with MEF cells after staining with 10 μg ml^{-1} over 16 hours (Fig. 6.3 B). NPs with size >100 nm showed probe aggregation outside cells and low internalisation rate, while at standard size of 95 nm they located mostly inside cells (shown by PtTFPP and PFO signals).

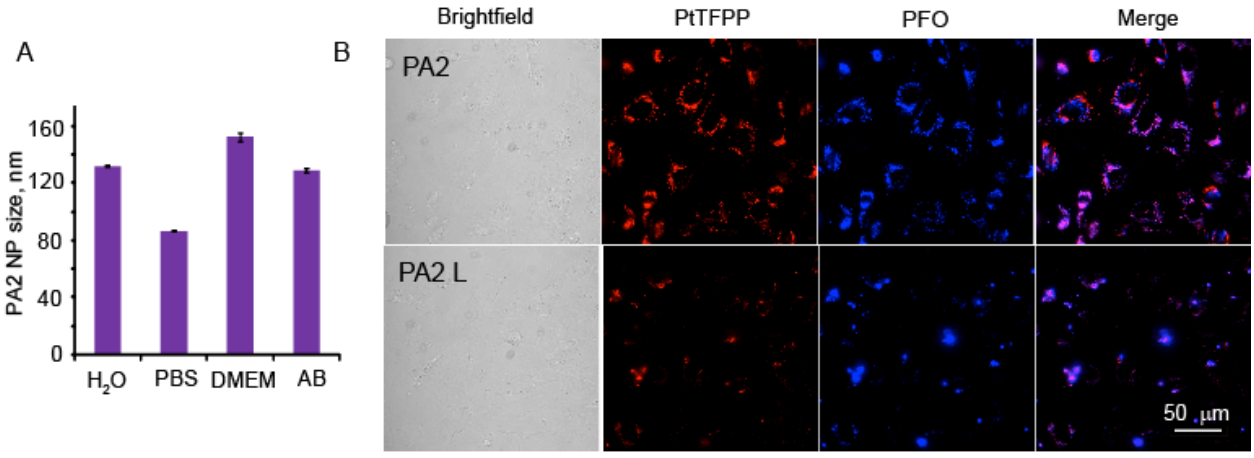

Figure 6.3 A. Average sizes of PA2 NPs in different aqueous solutions (MQ water, PBS (pH 7.5), DMEM with 10% FBS and acetic buffer (pH 4.6). B. Staining efficiency of MEF cells with PA2 (95 nm) and PA2 L (135 nm) probes (10 μg ml^{-1}, 16h). Mean values are calculated from 3 repeats with standard deviation expressed in error bars.

Cell staining efficiency depends on many factors, revealing mechanism of cell membrane penetration. To study this mechanism we stained mixed population of primary neurons and astrocytes (Courtesy of Dr. Ujval Anilkumar, University College Cork) with PA2 probe (5 μg ml^{-1}, 2 h) at standard conditions (37°C) and at low temperature (4°C). As expected, decrease of temperature led to slowing down metabolic processes in cells, including probe internalisation, however did not inhibit it completely (Fig. 6.4 A, left panels). Under ATP depletion conditions (pre-incubation in glucose free (Glc-) medium over 2 hours) we observed a significant decrease of PA2 uptake by neural cells (10 μg ml^{-1}, 2 h) to compare with normal Glc+ conditions (Fig. 6.4 A, right panels).

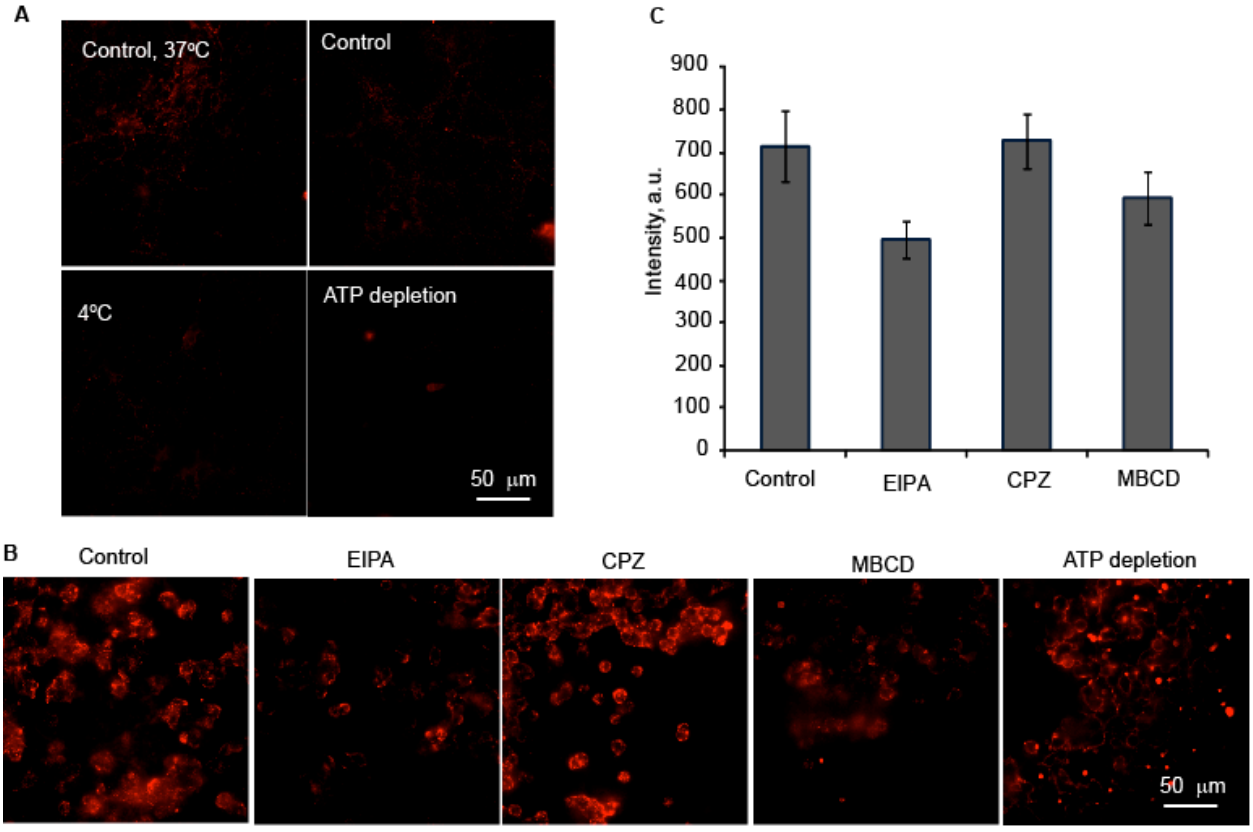

Figure 6.4 Study of the cell penetration mechanism of PA2 probe. A. Effects of temperature (37°C/4°C) and ATP depletion (Glc+/Glc- medium) on PA2 internalisation to primary neurons. Effects of endocytosis inhibitors on cellular uptake of PA2 (10 μg ml^{-1}, 3 h). Microscopy images (B) and bar charts (C) are shown for PC12 cells treated for 2 h with CPZ (50 μM), EIPA (50 μM) or MβCD (5 mM). Intensity values are averaged

from 10 randomly selected ROI and normalized to background signals. Error bars show standard deviations.

Detailed study of PA2 internalization mechanism was performed with PC12 cells, using treatments with inhibitors of endocytic pathways: CPZ for clathrin-mediated, EIPA for macropinocytosis and MβCD for lipid-raft/caveolae-dependent [189]. Significant decrease in cell penetration was observed with EIPA and MβCD treatments, when CPZ did not cause any remarkable changes (Fig. 6.4 B, C). Interestingly, ATP depletion of PC12s caused probe aggregation and staining of cell surface (Fig. 6.4 C). With primary neuronal culture the biggest inhibition of internalization was observed for CPZ, what once more proves specificity of penetration mechanism for each cell line [190]. Altogether, PA2 utilises mixed endocytic energy- and temperature - dependent mechanisms of cell entry, similarly to the cationic RL100-based probes [94].

6.1.1.3 Lifetime-based sensing of cellular O_2 on TR-F reader

Efficient cell penetration of PA1 and PA2 allows measurement of intracellular O_2 in neuron-like cells on a TR-F plate reader (high throughput analysis of cell populations) and by FLIM systems (single cell, O_2 gradients analysi). Using the TR-F reader, we calibrated PA1 and PA2 probes at 37°C with non-respiring MEF cells, exposed to the different levels of atmospheric O_2 (Fig. 6.5 A).

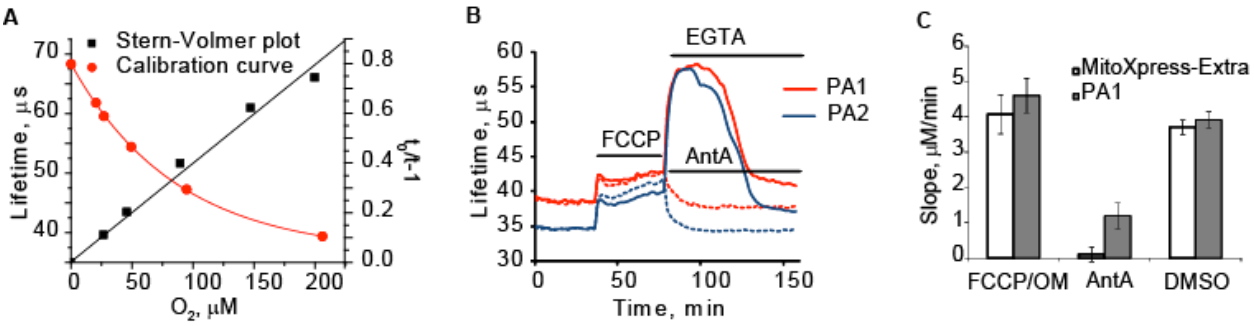

Figure 6.5 A. Calibration curve and Stern-Volmer plot of PA1 probe with MEF cells on the TR-F plate reader (37°C). B. Profiles of phosphorescence lifetime in PC12 cells stained with PA1 and PA2 probes (10 µg ml^{-1}, 16 h); stimulations with 1 µM FCCP, 5 mM EGTA and 10 µM AntA are indicated with bars. C. Performance of PA1 probe in µ-

slide OCR platform with metabolic stimulations (1 μM FCCP/10 μM OM, 10 μM AntA) in comparison with MitoXpress-Extra. Mean values are calculated from 6 replicates with standard deviations expressed in error bars.

Probes displayed slightly curved down Stern-Volmer plot, which reflects heterogeneous environment within the NP interior [68]. However, the calibrations did not display drift of the lifetime signal in stained cells (in comparison with calibration in PBS), what would indicate leakage of the dye(s) or degradation of NPs by cells (e.g. within lysosomes). Calibration equation, obtained by fitting of experimental data for PA1 probe, is:

$$[O_2] = 11231.5*\exp(-\tau/9.866), \quad \text{(Eq.1.13)}$$

And for PA2 probe is:

$$[O_2] = 87270.1*\exp(-\tau/5.07006). \quad \text{(Eq.1.14)}$$

For demonstration of probes performance in lifetime mode, we stained a confluent monolayer of PC12 cells with PA1 and PA2 by standard procedure (10 μg ml^{-1}, 16 h) and monitored oxygenation level on Victor2 plate reader (Fig. 6.5 B). Changes in cell respiration rates were trigged by treatments with 1 μM FCCP and 5 mM EGTA or 10 μM AntA (shown with horizontal bars). As expected, FCCP caused increase of probe phosphorescence lifetime due to the activation of respiration, and AntA inhibited respiration, causing deoxygenation drop in the lifetime scale. Addition of EGTA led to Ca^{2+} chelating, membrane depolarisation and spike in deoxygenation, followed by decrease and approaching of O_2 level of resting cells. Different lifetime values for basic cell respiration levels with PA1 and PA2 probes can be seen on the graph (correlate with the calibration functions), which can be caused by the different encapsulation of dyes inside NPs.

PA1 probe was also tested for OCR sensing in Ibidi μ-slide platform (see Chapter 3) in comparison with extracellular MitoXpress-Extra probe (Fig. 6.5 C). For this MEF cells were stained with PA1 probe in the flask, seeded to the μ-slide, allowed to adhere for 1 hour and monitored on the plate reader upon resting and treatments with metabolic stimulants: 1 μM FCCP/10 μM OM for maximal respiration upon mitochondrial

uncoupling, 10 μM AntA for respiration inhibition and DMSO – resting control. All treatments show anticipated results, similar to EC probe performing. This data demonstrates that O_2 and OCR in neuron-like cells can be reliably measured with PA-type probes in lifetime modality.

6.1.2 Green shifted O_2 probes

The multimodal nanoparticle probes MM2 and PA2 possess many useful features, however, their excitation at 390-405 nm can be damaging for some sensitive cell lines and 3D cell models upon long monitoring. Fluorescent dyes excitable in the green spectral range provide milder irradiation and can potentially be used as a pair (reference dye and FRET antenna) for O_2 sensitive dye. Coumarin dye excitable at convenient 450–490 nm and emitting fluorescence at 510–540 nm, would be an appropriate pair for PtTFPP. However, leaking of C545T from the NPs upon loading to MEF cells makes this probe unsuitable for quantitative sensing of icO_2 (see Chapter 5). This led us looking for other possible constructions of longwaver excitable probes.

6.1.2.1 Probe design and characterization

Two main approaches were considered: i) synthesis of coumarin derivatives with long aliphatic chains, which can hold them inside the polymeric NPs and ii) use of other polymers for better dye encapsulation in NPs. Second approach provides wide area of optimization by applying of different commercial and custom-made polymers. Such, anionic PMMA-MA polymer, which proved efficient NP formation by water precipitation and intracellular internalization, can be employed. So, the probe containing 1% w/w of PtTFPP and 1.33% w/w of coumarine C545T was prepared in PMMA-MA NPs (analogue of MM1 probe) and termed MM1x.

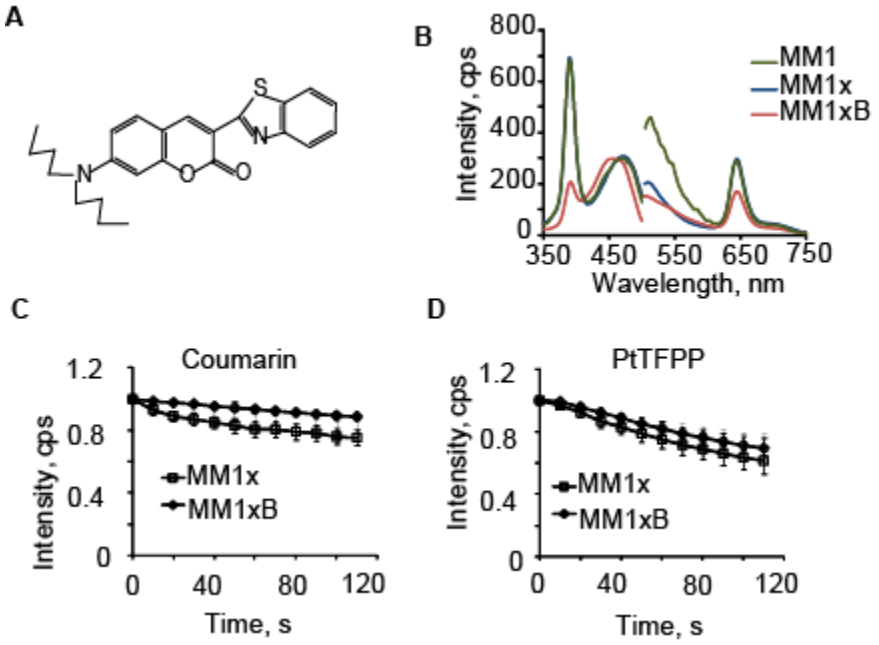

Figure 6.6 A. Chemical structures of the coumarin with enlarged aliphatic chains B. Excitation and emission spectra of MM1, MM1x and MM1xB probes at 21 kPa O_2. Photostability of coumarin (C) and PtTFPP (D) dyes in MM1x and MM1xB probes. Error bars show standard deviations.

The probe has increased size of 75 nm, what is expected for PMMA-MA polymer, and charge -15.9 mV. Another similar probe, containing coumarine molecule with enlarged aliphatic groups instead of cyclic structure of C545T (Fig. 6.6 A), was also prepared and termed MM1xB (0.5% w/w PtTFPP, 3% w/w coumarin, 75 nm size).

Spectral characterization of the probes was performed on luminescence spectrophotometer, in comparison with MM1 probe, containing 1% w/w PtTFPP dye and 1.33% w/w of coumarin C545T in RL-100 NPs (Figure 6.6 B). Both probes show efficient FRET (by the shape of excitation spectra) and allow using longer wavelength (420-470 nm) for simultaneous excitation of both dyes. The non-cycled coumarin derivative (Figure 6.6 A) shifts excitation maximum to 460 nm against 470 nm for C545T. Phosphorescence lifetime ranges are 43 - 66 μs for MM1x and 41 - 73 μs for MM1xB at 21 - 0 kPa O_2 (PBS, 37°C), what allows O_2 sensing in the physiological range (0-200 μM). Photostability of PtTFPP and coumarin dyes in MM1xB probe is similar to those in MM2 and PA2 and slightly decreased in MM1x probe (Figure 6.6 C, D).

6.1.2.2 Cell staining behavior and loading stability

Efficient cell penetration and stability inside cells (due to the PMMA-MA material of NPs) are desirable features of newly developed probes, which were expected to advance existing methods of sensing. Stability was evaluated by imaging of MEF cells stained with probes (10 μg ml^{-1}, 16 h) on wide-field microscope (Fig. 6.7). As can be seen from the image, efficient staining with MM1x and MM1xB probes was achieved with lysosomal pattern of localisation similar to the PA2 probe. Merge images demonstrate co-localisation of PtTFPP dye with coumarin in yellow colour. In contrast to RL-100 polymer, which was used for MM1 particle formation (see Chapter 5), PMMA-MA provides efficient encapsulation for both unmodified C545T and modified coumarins. Exposure to the medium and cell interior upon staining (e.g. acidic lysosomal environment) did not destroy the structure of the probe.

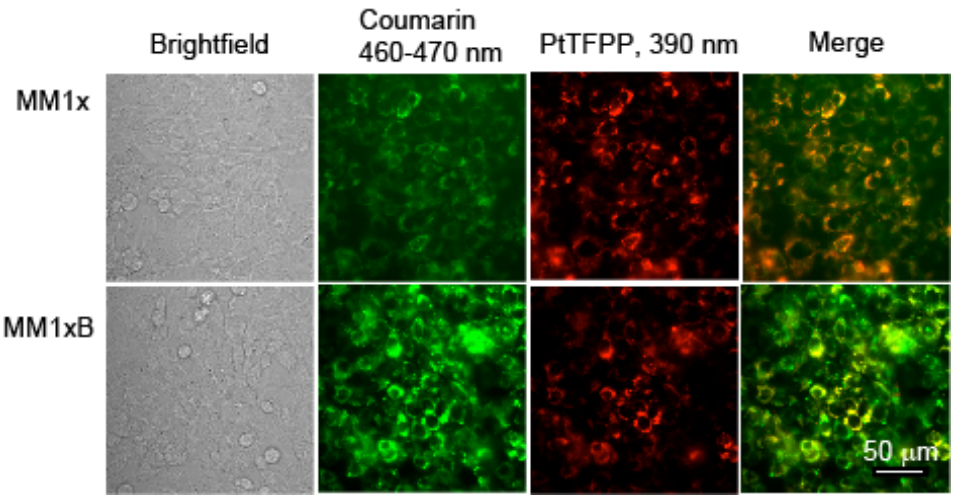

Figure 6.7 Staining of MEF cells with MM1x and MM1xB probes (10 μg ml^{-1}, 16 h).

Altogether, PMMA-MA polymer provides efficient encapsulation of longwave reference dyes and staining of different cell types including primary neurons.

6.1.3 Design and characterization of ratiometric IR probe

Advantages of multi-modal probes, described previously, cause interest in the futher improvement of probe characteristics and development of IR analogue of MM probes.

NPs containing PtTPTBPF as O_2 sensor and azaBodipy as a reference dye were prepared in PMMA-MA (MM-IRx) and RL-100 (MM-IR) polymers (Fig. 6.8 A). AzaBodipy has a wide excitation band at 570-670 nm (optimum at 645 nm) and emission at 650-700 nm (optimum at 675 nm). The overlap of luminescence spectra of PtTPTBPF and azaBodipy allows exciting of both dyes at 620 nm and collecting of their intensity signals simultaneously (Fig. 6.8 B). Such, MM-IRx shows optimal excitation at 620 nm with emission bands at 660 nm (reference) and 770 nm (reporter).

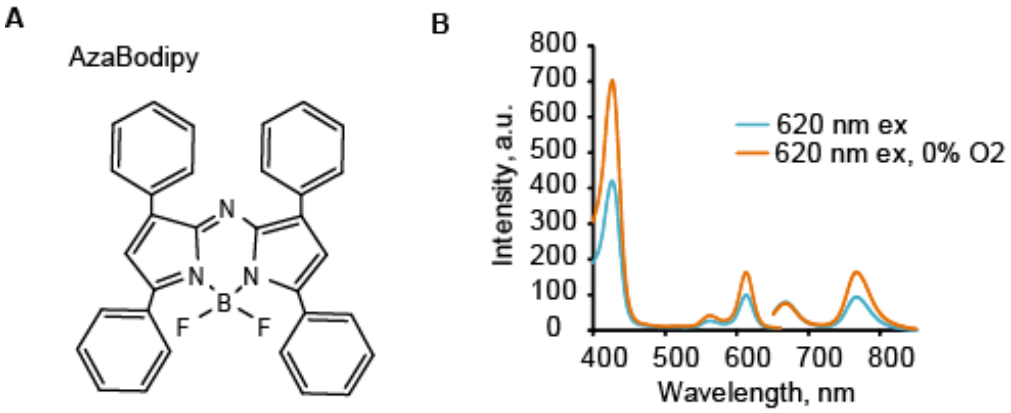

Figure 6.8 A. Chemical structure of the reference azaBodipy dye. B. Excitation and emission spectra of MM-IR probe at 0 and 21 kPa O_2.

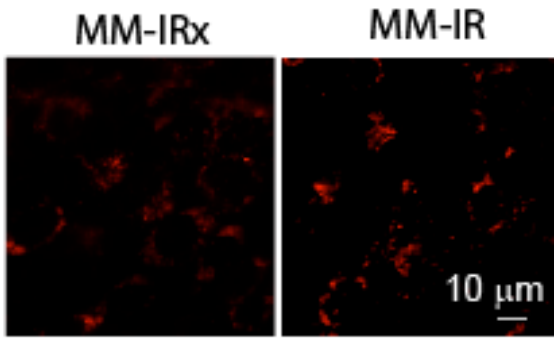

Figure 6.9 Staining properties of MM-IR and MM-IRx probes with MEF cells (10 μg ml^{-1}, 16h).

New IR probes were imaged on the luminescence microscope with MEF cells (10 μg ml^{-1}, 16h). Characteristic localization of RL-100 by "patches" is demonstrated with MM-IR

probe, when staining with MM-IRx probe is more efficient and diffused around the cytosol (Fig. 6.9). Cell penetration mechanism, toxicity, performing in different modalities and other properties of the probes are expected to be identical to MM2 and PA2 (See Chapters 5 and 6.1.1).

6.2 Cell-penetrating PtTFPP conjugates

NP-based phosphorescence probes represent a valuable tool for monitoring of cell oxygenation, respiration and O_2 imaging. However, they often do not provide the desirable bio-distribution, bio-compatibility and analytical performance. Therefore, we worked on development of cell-penetrating conjugates of phosphorescent PtTFPP dye, produced by simple click-modification [153].

Conjugates of PtCP and IrOEP with short peptides and especially with histidine-containing ligands for intracellular delivery were designed and studied before [66, 104]. Showing satisfactory cell-permeability, intracellular distribution and brightness, these probes are susceptible to rapid photodegradation, which limited their applicability. Therefore, we decided to bind cell-penetrating peptide and saccharide vectors to highly stable PtTFPP dye. Tetra-substituted conjugates were expected to be more promising and ease to purify, so, PtTFPP dye was functionalised with four arginine and four glucose (Glc) or galactose (Gal) residues (Fig. 6.10 A) [191]. Peptide conjugates were prepared by introducing of a 3-mercaptopropionic acid linker and then coupling it with peptide free amino groups by carbodiimide method [192]. The Pt-Glc and Pt-Gal conjugates were produced in one-step using thio-hexoses. Hydrophobicity of newly synthesized probes was analysed by HPLC and compared with PtTFPP (100% hydrophobic). Significant reduction of hydrophobicity was shown for all three conjugates: 64.5% for Pt-Arg, 64,2% for Pt-Glc and Pt-Gal. Peptide conjugate Pt-Arg showed largely reduced phosphorescence lifetimes (23.1 and 37.3 μs for air saturated and fully deoxygenased solutions respectively), whereas saccharide conjugates were similar to unmodified PtTFPP (20.3 – 57.0 μs). Therefore, our future research was focused on Pt-Glc(Gal)

conjugates, which possessed small molecular size, simple synthesis procedure, convenient photophysical characteristics and sensing in physiological O_2 range.

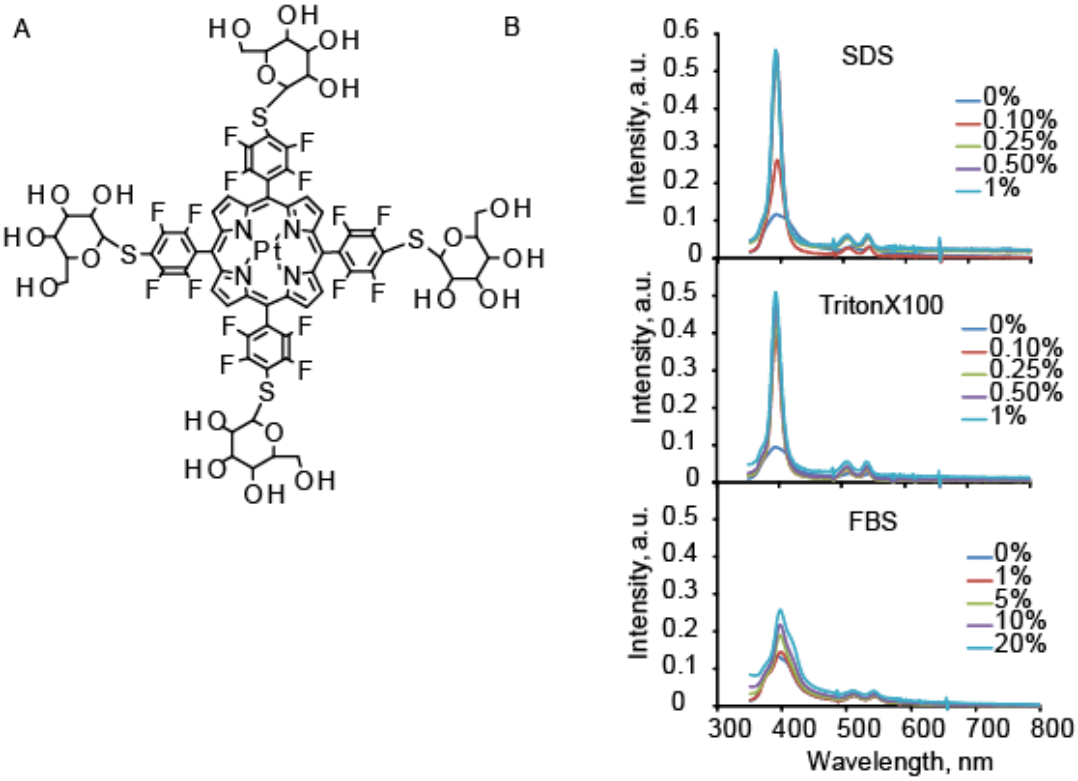

Figure 6.10 A. Chemical structure of Pt-Glc(Gal) probe. B. Absorption spectra of Pt-Glc probe upon additions of 0-1% of SDS, 0-1% of Triton-X100 and 0-20% of FBS.

For small molecule probes such as Pt-Glc(Gal) aggregation in aqueous solution due to the stacking of porphyrin rings can be a serious issue. We studied aggregation of Pt-Glc probe (Pt-Gal is expected to show similar behaviour) by analysing of their absorption spectra in PBS and upon additions of SDS, Triton-X100 and FBS. Both anionic (SDS) and nonionic (Triton-X100) surfactants led to narrowing and increase of spectral bands, which are indications of aggregation destroing (Fig. 6.10 B). Serum-containing media, used with cells and tissue samples, shows decrease in aggregation as well (Fig. 6.10 B, lower chart).

6.2.1 Cellular uptake and toxicity of Pt-Glc and Pt-Gal conjugates

Having carbohydrates as intracellular vectors, Pt-Glc and Pt-Gal probes are expected to use glucose transport pathways and therefore show cell-specificity [Samaroo, Vinodu 2007]. First of all, we analysed cell-permeability and brightness of probes by loading of MEF cells (were used for evaluation of other NP- and small molecule-based O_2 probes) with different concentrations over 16 hours, followed by monitoring of intensity signal on Victor2 plate reader (Fig. 6.11 A).

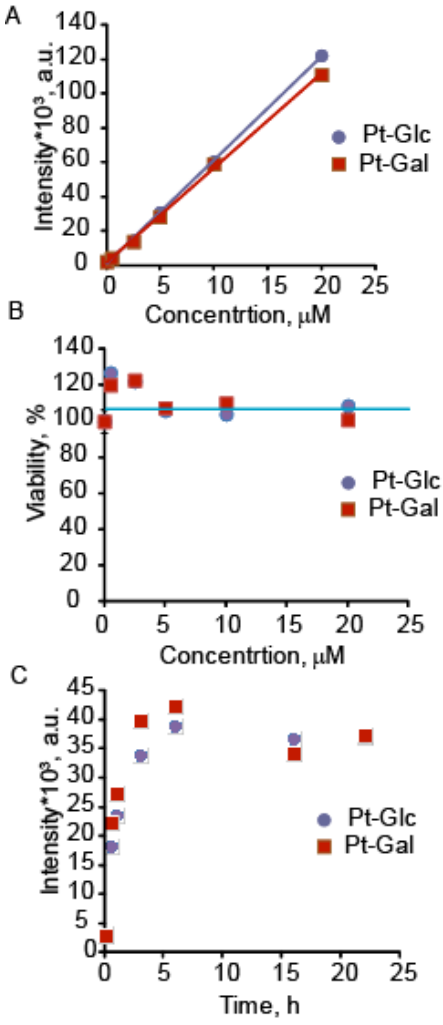

Figure 6.11 The effect of concentration of Pt-Glc and Pt-Gal probes (0-20 μM, 16 h) on (A) TR-F signals measured on the microplate reader and (B) on cell viability analyzed using a Cell Titer-Glo kit. C. Staining kinetics of Pt-Glc and Pt-Gal probes (5 μM, 0-22 h) shown in TR-F signals measured on the microplate reader.

Concentrations up to 20 μM of both conjugates show linear dependence without saturation of intensity signals. Close intensity values for Pt-Glc and Pt-Gal is an evidence of similar loading mechanisms for MEF cells.

Using of glucose transporting pathways can cause significant cell toxic effects of new carbohydrate-based probes. Total ATP assay demonstrated no toxicity for MEF cells after exposure to 0-20 μM of probes concentrations (Fig. 6.11 B). However, cell specificity of these probes requires assessment of toxic effects for each cell model separately in the range of working concentrations.

Loading kinetic was studied with the same cell line upon exposure to 5 μM concentration of Pt-Glc or Pt-Gal for up to 22 hours (Fig. 6.11 C). Both conjugates showed similar kinetics of intracellular staining, achieving maximal loading at 4–6 hours, what is 3–4 times faster than that for the NP probes, such as NanO2 [94].

6.2.2 Imaging of Pt-Glc and Pt-Gal probes with different cell lines

After initial evaluation of cell permeability, brightness and toxicity on the plate reader we moved to imaging experiments with new probes. We started from loading of MEF cells with 5 μM of Pt-Glc and Pt-Gal probes for 6 hours, followed by counter-staining of cell interior with TMRM and imaging on wide-field microscope (Fig. 6.12). As was expected by the initial plate reader evaluation, probes demonstrated similar loading efficiency and perinuclear distribution resembling endoplasmic reticulum. Probes displayed sufficient brightness and photostability for high-resolution imaging.

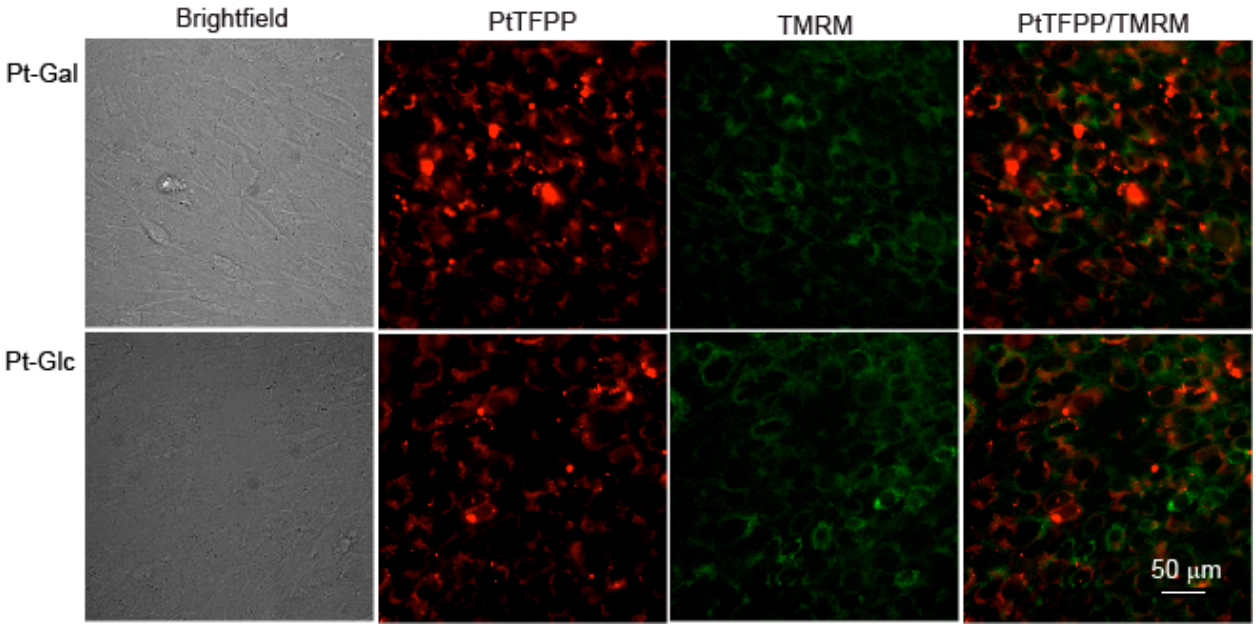

Figure 6.12 Staining properties of Pt-Glc and Pt-Gal probes with MEF cells (5 µM, 6 h), counter-stained with TMRM.

Development of new small-molecule conjugates aimed to advance O_2 sensing by loading of the probe to different cell lines with high efficiency, what is often not possible with NP-based probes. Therefore, conjugates were tested with extended panel of cell lines: PC12, COS-7, SH-SY5Y, HepG2, HCT116, Caco-2 and primary neurons (Courtesy of Dr. Ruslan Dmitriev, University College Cork). Intracellular accumulation was demonstrated with all tested cell lines, however some of them show preference to one or another probe. Such in MEF, HepG2 and SH-SY5Y cells internalisation rate was identical, when in PC12s loading efficiency with Pt-Glc was significantly higher than with Pt-Gal and vice versa in Caco-2 cells. Such differences can be explained by different cell glycolitic activity [191].

Altogether, newly developed saccharide-based probes Pt-Glc and Pt-Gal demonstrate minimal aggregation, photodegradation and cellular toxicity. They possess bright intracellular staining of different cell types, multi-cellular aggregates and tissues [191] at low working concentrations (5 µM). By many of these characteristics new probes overcome previously developed small molecule and NP-based probes. Spectral

compatibility with common light sources and detection systems makes them suitable for imaging and FLIM measurements with variety of 2D and 3D cell and tissue models.

6.3 Conclusions

Newly developed optical probes help overcoming existing limitations in O_2 sensing. First of all, cell-specific loading of the probes was solved by employing of PMMA-MA polymer for NPs formation. The analogue of MM2 probe in this polymer, titled PA2, demonstrates improved permeability with a number of cell lines, including primary neurons, and high sensitive performance. Similarly to the cationic RL-100-based probe MM2, PA2 utilises mixed endocytic energy- and temperature-dependent mechanisms of cell entry.

Secondly, the problem of light penetration to thick 3D cell models and damage of live cell sample upon long O_2 monitoring was solved by development of longwaver probes. Excitable in the green spectral range (450–490 nm), coumarin derivative was used as a reference dye and FRET antenna for construction of MM1x and MM1xB multimodal probes. They require the use of PMMA-MA polymer, which was found to provide reliable encapsulation of both sensitive and reference dyes. Another approach employed near-IR O_2 sensitive dye PtTPTBPF and azaBodipy as a reference dye in PMMA-MA NPs. This probe MM-IRx provides live cell O_2 sensing and imaging in different detection modalities with optimal excitation at 620 nm.

Finally, small molecule approach was employed to improve cell penetration properties of O_2 probes. Newly developed PtTFPP conjugates with saccharides possess bright intracellular staining of different cell types, multi-cellular aggregates and tissues. Their spectral characteristics allow monitoring with common light sources, detection systems and laboratory equipment. Minimal aggregation, cytotoxicity and low working concentrations provide flexibility in the choice of 2D and 3D cell and tissue models. Altogether, the extended range of newly developed O_2 probes overcomes existing limitations and can be used for bioanalytical applications as well as for the further development of the O_2 probes with improved properties.

Overall conclusion

Intracellular O_2 sensing was advanced by a number of novel measurement techniques, calculation approaches and new luminescent probes. An OCR platform, based on the commercial μ-slide device, phosphorescent probes and standard plate readers was developed. It was compared to standard 96-WP platform and demonstrated faster measurement, two-fold higher sensitivity, and more reliable results. The semi-closed design of the new platform allows performing additions and changing measurement conditions, what was not possible with previously used techniques [31]. This platform was applied for monitoring of cell responses to various metabolic stimulations with both IC and EC probes, comparison of cell respiration rates and study of "energy budget". The μ-slide platform can be further multiplexed with other luminescence assays and provide versatile tool for studies of cell metabolism and drug toxicity screenings.

Continuing the development of cellular O_2 sensing methodology, we compared and calibrated three optical platforms: hermetically sealed micro-cuvettes for measurement of absolute OCRs, the partially sealed by mineral oil 96-WP for relative OCRs and the open 96-WP for steady state cell oxygenations. High throughput 96-WP platforms are preferable for screening assays, however low sensitivity and relative results limit their use [121]. We calibrated them against absolute OCR platform and found correlations for substitution of cumbersome absolute measurements in quartz cuvettes. Using these correlations, we calculated absolute OCRs upon monitoring in partially sealed 96-WP and upon treatments in open 96-WP, what cannot be performed with sealed platforms.

Existing $ic O_2$ probes often are not optimized for physiological tasks and require further improvement of characteristics (Table 2) [46]. A new multimodal probe MM2 was developed, which can be used in different detection platforms. It is based on the PtTFPP reporter dye and PFO reference and two-photon antenna, which are embedded in cationic RL-100 NPs. Such structure possesses low toxicity, high brightness, photostability, cell-permeability and flexibility in the platforms and samples used. The probe is compatible with different detection systems, including spectrophotomers, TR-F plate readers and FLIM microscopes with one- or two-photon excitation. The MM2 probe was evaluated

for intracellular O_2sensing in 2D and 3D cell cultures upon resting and metabolic treatments. High performance was shown in luminescence intensity, ratiometric and lifetime based modalities in physiological experiments, where MM2 outperforms existing probes.

We studied several other approaches for development of IC probes, including improvement of cell-targeting, spectral characteristics and usability of the probes. Unexpectedly, we found that anionic NP probes PA1 and PA2 can provide efficient staining of different cell lines and primary neurons. The used polymer PMMA-MA also ensures efficient encapsulation of coumarin and prevents its leaking from NP probes MM1x and MM1xB. Such structures allow excitation of the probe at longer wavelengths in comparison to MM2 and protects live cell samples from excessive irradiation. The same result can be achieved by the near-IR imaging probes NanO2-IR, MM-IR and MM-IRx with excitation band of the PtTBTPPF dye at 570-670 nm. Additionally, improved photostability and intracellular distribution, fast and efficient staining were achieved with small molecule probes (Pt-Glc, Pt-Gal), based on the PtTFPP dye. The extended range of icO_2 probes overcomes existing limitations and can advance O_2 sensing and imaging.

Table 2. Comparison of old and new NP-based and small molecule icO_2 probes.

Probe type		Probes	Advantages	Disadvantages
NP-based	**Old**	RGB, NIR PEBLEs [108, 141]	Ratiometric, IR-excitation, non-toxic, possibilities for sub-cellular targeting	Cumbersome and long preparation, temperature dependant calibration, moderate sensitivity
		$[Ru(dpp)_3](TMSPS)_2$ in polystyrene [93]	Two-photon excitable, non-toxic	Large size (121 nm), long loading time
		NanO2 [94]	Efficient staining of MEFs, bright, photostable, non-toxic	Cell-specific staining, “patchy” localisation, short excitation wavelength, 6-16 h loading time

	New	MM2	Multi-modal, efficient staining of MEFs, bright, photostable, non-toxic	Cell-specific staining, "patchy" localisation, short excitation wavelength, 6-16 h loading time
		PA1, PA2	Efficient staining of different mammalian cells, bright, photostable, non-toxic	Short excitation wavelength, 6-16 h loading time
		MM-IR, MM-IRx	IR-excitation, multi-modal	6-16 h loading time
		MM1x, MM1xB	Green shifted excitation, efficient staining of different mammalian cells, bright, photostable, non-toxic, multi-modal	6-16 h loading time
Small-molecule	**Old**	Ir(III)-porfyrins conjugates[66]	Simple coupling with various delivery vectors, bright staining of some mammalian cells	Low photostability, moderate sensitivity
		PtCP-TAT conjugates [103]	Passive loading to various mammalian cells	Low photostability, moderate sensitivity, short lifetimes
	New	Pt-Glc (Pt-Gal)	Bright, photostable, non-toxic, efficient staining of wide range of mammalian cells, 1-6 h loading time, low working concentrations, in-depth tissue staining	Possible aggregation

In summary, the results presented here describe the optimisation of measurement techniques, probes and adaptation of new platforms for O_2 sensing, allowing increased sensitivity, general flexibility and improved performance with different detection systems.

Future work

Increased interest in non-invasive intracellular O_2 sensing approaches ensures the further development of new probes and techniques as well as applications for various metabolic studies. Physiological 3D cell and tissue models are becoming more popular, and require longwave shifted probes, with the option for multi-photon excitation and time-laps monitoring. Sufficient brightness, minimal toxicity, the possibility for multiplexing with other assays and general usability are important requirements for such probes. The prospective development of co-polymeric probes with up to 10 times greater brightness is now of high interest and can become a framework for the new generation of probes [99]. For small-molecule probes, improvements in photostability and sub-cellular targeting represent important challenges. In particular, the staining of different cell compartments with the use of specific delivery vectors will allow for the monitoring of O_2 gradients in detailed studies of cell metabolism [191]. With regards to O_2 sensing techniques, simplicity, usability and versatility of platforms and calculations will serve to the future advancement of bioanalytical studies [112].

Thesis outcome

Peer reviewed papers:

Kondrashina, A. V., Dmitriev, R. I., Borisov, S. M., Klimant, I., O'Brien, I., Nolan, Y. M., ... & Papkovsky, D. B. (2012). A phosphorescent nanoparticle-based probe for sensing and imaging of (intra) cellular oxygen in multiple detection modalities. *Advanced Functional Materials*, 22(23), 4931-4939.

Kondrashina, A. V., Papkovsky, D. B., & Dmitriev, R. I. (2013). Measurement of cell respiration and oxygenation in standard multichannel biochips using phosphorescent O_2-sensitive probes. *Analyst*, 138(17), 4915-4921.

Dmitriev, R. I., Kondrashina, A. V., Koren, K., Klimant, I., Zhdanov, A. V., Pakan, J. M., ... & Papkovsky, D. B. (2014). Small molecule phosphorescent probes for O 2 imaging in 3D tissue models. *Biomaterials Science*, 2(6), 853-866.

Dmitriev, R. I., Borisov, S. M., Kondrashina, A. V., Pakan, J. M., Anilkumar, U., Prehn, J. H., ... & Papkovsky, D. B. (2014). Imaging oxygen in neural cell and tissue models by means of anionic cell-permeable phosphorescent nanoparticles. *Cellular and Molecular Life Sciences*, 1-15.

Kondrashina, A. V., Ogurtsov, V. I., & Papkovsky, D. B. (2015). Comparison of the three optical platforms for measurement of cellular respiration. *Analytical biochemistry*, 468, 1-3.

Conference presentations (posters):

Koren, K., Dmitriev, R., Kondrashina, A., Borisov, S., Papkovsky, D., & Klimant, I. (2013). Molecular probes for intracellular oxygen based on Pt- and Pd pentafluorophenylporphyrins produced by click chemistry. *Gordon Research Conference*, Newport, RI, USA.

Kondrashina, A., Dmitriev, R., Borisov, S., Klimant, I., Zhdanov, A., & Papkovsky, D. (2013). Phosphorescent nanoparticle based probes for imaging and measurement of cellular oxygen. *The FASEB Journal*, 27, 576-2. Experimental Biology 2013, 20-24 April 2013, Boston, MA, USA.

Dmitriev, R., Borisov, S., Kondrashina, A., Pakan, J., & Papkovsky, D. (2014). Real-time monitoring of oxygenation in cultured organotypic brain slices (1180.20*). The FASEB Journal*, 28(1 Supplement), 1180-20. Experimental Biology 2014, 26-30 April 2014, San Diego, CA, USA.

Kondrashina, A., Dmitriev, R., & Papkovsky, D. (2014). Comparison of different techniques for monitoring of mammalian cell respiration (960.4). *The FASEB Journal*, 28(1 Supplement), 960-4. Experimental Biology 2014, 26-30 April 2014, San Diego, CA, USA.

Dmitriev, R., Kondrashina, A., Foley, T., & Papkovsky, D. (2014). Imaging of molecular oxygen at subcellular resolution in mammalian cell culture: from 2D to 3D models (764.1). *The FASEB Journal*, 28(1 Supplement), 764-1. Experimental Biology 2014, 26-30 April 2014, San Diego, CA, USA.

Research statement

NP-based probes were prepared, optimized and characterized by Prof. Sergey Borisov (Graz University of Technology, Graz, Austria).

Primary neurons and neurospheres were cultured by Dr. Ruslan Dmitriev and Dr. Ujval Anilkumar (University College Cork, Cork, Ireland).

7. Bibliography

[1] Plecitá-Hlavatá L, Lessard M, Šantorová J, Bewersdorf J, Ježek P. Mitochondrial oxidative phosphorylation and energetic status are reflected by morphology of mitochondrial network in INS-1E and HEP-G2 cells viewed by 4Pi microscopy. Biochimica et Biophysica Acta (BBA)-Bioenergetics. 2008;1777:834-46.
[2] Intaglietta M, Johnson PC, Winslow RM. Microvascular and tissue oxygen distribution. Cardiovascular research. 1996;32:632-43.
[3] Cadenas E. Biochemistry of oxygen toxicity. Annual review of biochemistry. 1989;58:79-110.
[4] Duranteau J, Chandel NS, Kulisz A, Shao Z, Schumacker PT. Intracellular signaling by reactive oxygen species during hypoxia in cardiomyocytes. Journal of biological chemistry. 1998;273:11619-24.
[5] Beeson CC, Beeson GC, Schnellmann RG. A high-throughput respirometric assay for mitochondrial biogenesis and toxicity. Analytical biochemistry. 2010;404:75-81.
[6] Wolin MS, Ahmad M, Gupte SA. Oxidant and redox signaling in vascular oxygen sensing mechanisms: basic concepts, current controversies, and potential importance of cytosolic NADPH. American Journal of Physiology-Lung Cellular and Molecular Physiology. 2005;289:L159-L73.
[7] Entz B, Bakonyi G, Mahunka S, Papp L, Báldi A, Csuzdi C, et al. The dissolved oxygen determination method is 120 years old in memoriam Lajos Winkler (1863–1939) and Rezső Maucha (1882–1964). Acta Zoologica Academiae Scientiarum Hungaricae. 2008;54:7-11.
[8] Carvalho Ad, Calado J, Moura Md. Spectrophotometric Determination of Dissolved Oxygen in Demineralized Water. Rev Port Quim. 1963;5:15.
[9] Swinnerton JW, Linnenbom VJ, Cheek CH. Determination of Dissolved Gases in Aqueous Solutions by Gas Chromatography. Analytical Chemistry. 1962;34:483-5.
[10] Clark LC, Wolf R, Granger D, Taylor Z. Continuous recording of blood oxygen tensions by polarography. Journal of applied physiology. 1953;6:189-93.
[11] Papandreou I, Cairns RA, Fontana L, Lim AL, Denko NC. HIF-1 mediates adaptation to hypoxia by actively downregulating mitochondrial oxygen consumption. Cell metabolism. 2006;3:187-97.
[12] Travis Jr R, Clark Jr L. Changes in evoked brain oxygen during sensory stimulation and conditioning. Electroencephalography and clinical neurophysiology. 1965;19:484-91.
[13] Ward WK, Van Albert S, Bodo M, Pearce F, Gray R, Harlson S, et al. Design and Assessment of a Miniaturized Amperometric Oxygen Sensor in Rats and Pigs. Sensors Journal, IEEE. 2010;10:1259-65.
[14] Rumsey W, Schlosser C, Nuutinen E, Robiolio M, Wilson D. Cellular energetics and the oxygen dependence of respiration in cardiac myocytes isolated from adult rat. Journal of Biological Chemistry. 1990;265:15392-402.
[15] Severinghaus JW, Astrup PB. History of blood gas analysis. VI. Oximetry. Journal of clinical monitoring. 1986;2:270-88.
[16] Severinghaus JW. The invention and development of blood gas analysis apparatus. Anesthesiology. 2002;97:253-6.
[17] Schlager O, Gschwandtner ME, Willfort-Ehringer A, Kurz M, Mueller M, Koppensteiner R, et al. Transcutaneous oxygen tension monitoring in critically ill patients receiving packed red blood cells. Journal of Critical Care. 2014.
[18] Hutton L, Newton ME, Unwin PR, Macpherson JV. Amperometric oxygen sensor based on a platinum nanoparticle-modified polycrystalline boron doped diamond disk electrode. Analytical chemistry. 2008;81:1023-32.

[19] Sarapuu A, Tammeveski K, Tenno TT, Sammelselg V, Kontturi K, Schiffrin DJ. Electrochemical reduction of oxygen on thin-film Au electrodes in acid solution. Electrochemistry communications. 2001;3:446-50.
[20] Holmström N, Nilsson P, Carlsten J, Bowald S. Long-term in vivo experience of an electrochemical sensor using the potential step technique for measurement of mixed venous oxygen pressure. Biosensors and Bioelectronics. 1998;13:1287-95.
[21] El-Deab MS, Okajima T, Ohsaka T. Electrochemical reduction of oxygen on gold nanoparticle-electrodeposited glassy carbon electrodes. Journal of the electrochemical society. 2003;150:A851-A7.
[22] Ward W, Wood M, Slobodzian E. Continuous amperometric monitoring of subcutaneous oxygen in rabbit by telemetry. Journal of medical engineering & technology. 2002;26:158-67.
[23] Voskerician G, Anderson J. Sensor Biocompatibility and Biofouling in Real-Time Monitoring. Wiley Encyclopedia of Biomedical Engineering. 2006.
[24] Lindgren I. Continuous measurement of arterial oxygen saturation in man. Cardiology. 1948;13:226-40.
[25] Millikan GA. The oximeter, an instrument for measuring continuously the oxygen saturation of arterial blood in man. Review of Scientific Instruments. 1942;13:434-44.
[26] Tremper KK. Pulse oximetry. CHEST Journal. 1989;95:713-5.
[27] Sinex JE. Pulse oximetry: principles and limitations. The American journal of emergency medicine. 1999;17:59-66.
[28] Aoyagi T. Pulse oximetry: its invention, theory, and future. Journal of anesthesia. 2003;17:259-66.
[29] Froncisz W, Lai CS, Hyde JS. Spin-label oximetry: kinetic study of cell respiration using a rapid-passage T1-sensitive electron spin resonance display. Proceedings of the National Academy of Sciences. 1985;82:411-5.
[30] Presley T, Kuppusamy P, Zweier JL, Ilangovan G. Electron paramagnetic resonance oximetry as a quantitative method to measure cellular respiration: a consideration of oxygen diffusion interference. Biophysical journal. 2006;91:4623-31.
[31] Diepart C, Verrax J, Calderon PB, Feron O, Jordan BF, Gallez B. Comparison of methods for measuring oxygen consumption in tumor cells in vitro. Analytical biochemistry. 2010;396:250-6.
[32] Krishna MC, Matsumoto S, Yasui H, Saito K, Devasahayam N, Subramanian S, et al. Electron paramagnetic resonance imaging of tumor pO2. Radiation research. 2012;177:376-86.
[33] Zepeda A, Arias C, Sengpiel F. Optical imaging of intrinsic signals: recent developments in the methodology and its applications. Journal of neuroscience methods. 2004;136:1-21.
[34] Sette G, Baron J, Mazoyer B, Levasseur M, Pappata S, Crouzel C. LOCAL BRAIN HAEMODYNAMICS AND OXYGEN METABOLISM IN CEREBROVASCULAR DISEASE POSITRON EMISSION TOMOGRAPHY. Brain. 1989;112:931-51.
[35] Robinson SP, Howe FA, Rodrigues LM, Stubbs M, Griffiths JR. Magnetic resonance imaging techniques for monitoring changes in tumor oxygenation and blood flow. Seminars in Radiation Oncology: Elsevier; 1998. p. 197-207.
[36] Frostig RD, Lieke EE, Ts'o DY, Grinvald A. Cortical functional architecture and local coupling between neuronal activity and the microcirculation revealed by in vivo high-resolution optical imaging of intrinsic signals. Proceedings of the National Academy of Sciences. 1990;87:6082-6.
[37] Fox MD, Raichle ME. Spontaneous fluctuations in brain activity observed with functional magnetic resonance imaging. Nature Reviews Neuroscience. 2007;8:700-11.
[38] Villringer A, Planck J, Hock C, Schleinkofer L, Dirnagl U. Near infrared spectroscopy (NIRS): a new tool to study hemodynamic changes during activation of brain function in human adults. Neuroscience letters. 1993;154:101-4.

[39] Zhang X. Instrumentation in Diffuse Optical Imaging. Optics. 2014;1:9-32.
[40] Mayevsky A, Barbiro-Michaely E. Shedding light on mitochondrial function by real time monitoring of NADH fluorescence: I. Basic methodology and animal studies. Journal of clinical monitoring and computing. 2013;27:1-34.
[41] Dmitriev RI, Papkovsky DB. Optical probes and techniques for O2 measurement in live cells and tissue. Cellular and Molecular Life Sciences. 2012;69:2025-39.
[42] Lakowicz JR, Weber G. Quenching of fluorescence by oxygen. Probe for structural fluctuations in macromolecules. Biochemistry. 1973;12:4161-70.
[43] Lakowicz J. Quenching of Fluorescence. In: Lakowicz J, editor. Principles of Fluorescence Spectroscopy: Springer US; 2006. p. 277-330.
[44] Björkman O, Demmig B. Photon yield of O2 evolution and chlorophyll fluorescence characteristics at 77 K among vascular plants of diverse origins. Planta. 1987;170:489-504.
[45] Dmitriev RI, Papkovsky DB. O2-Sensitive Probes Based on Phosphorescent Metalloporphyrins. Phosphorescent Oxygen-Sensitive Probes: Springer; 2012. p. 1-28.
[46] Papkovsky DB, Dmitriev RI. Biological detection by optical oxygen sensing. Chemical Society Reviews. 2013;42:8700-32.
[47] Stich MI, Fischer LH, Wolfbeis OS. Multiple fluorescent chemical sensing and imaging. Chemical Society Reviews. 2010;39:3102-14.
[48] Ballew RM, Demas J. An error analysis of the rapid lifetime determination method for the evaluation of single exponential decays. Analytical Chemistry. 1989;61:30-3.
[49] Kautsky H. Quenching of luminescence by oxygen. Transactions of the Faraday Society. 1939;35:216-9.
[50] Quaranta M, Borisov SM, Klimant I. Indicators for optical oxygen sensors. Bioanalytical reviews. 2012;4:115-57.
[51] Basu BJ, Anandan C, Rajam K. Study of the mechanism of degradation of pyrene-based pressure sensitive paints. Sensors and Actuators B: Chemical. 2003;94:257-66.
[52] Peterson JI, Fitzgerald RV, Buckhold DK. Fiber-optic probe for in vivo measurement of oxygen partial pressure. Analytical chemistry. 1984;56:62-7.
[53] Knopp JA, Longmuir IS. Intracellular measurement of oxygen by quenching of fluorescence of pyrenebutyric acid. Biochimica et Biophysica Acta (BBA)-General Subjects. 1972;279:393-7.
[54] Kober EM, Caspar JV, Lumpkin RS, Meyer TJ. Application of the energy gap law to excited-state decay of osmium (II)-polypyridine complexes: calculation of relative nonradiative decay rates from emission spectral profiles. The Journal of Physical Chemistry. 1986;90:3722-34.
[55] Sacksteder L, Demas J, DeGraff B. Design of oxygen sensors based on quenching of luminescent metal complexes: effect of ligand size on heterogeneity. Analytical Chemistry. 1993;65:3480-3.
[56] Lamansky S, Djurovich P, Murphy D, Abdel-Razzaq F, Lee H-E, Adachi C, et al. Highly phosphorescent bis-cyclometalated iridium complexes: synthesis, photophysical characterization, and use in organic light emitting diodes. Journal of the American Chemical Society. 2001;123:4304-12.
[57] Liu Y, Guo H, Zhao J. Ratiometric luminescent molecular oxygen sensors based on uni-luminophores of C [caret] N Pt (II)(acac) complexes that show intense visible-light absorption and balanced fluorescence/phosphorescence dual emission. Chemical Communications. 2011;47:11471-3.
[58] Amao Y, Okura I. An oxygen sensing system based on the phosphorescence quenching of metalloporphyrin thin film on alumina plates. Analyst. 2000;125:1601-4.
[59] Douglas P, Eaton K. Response characteristics of thin film oxygen sensors, Pt and Pd octaethylporphyrins in polymer films. Sensors and Actuators B: Chemical. 2002;82:200-8.

[60] Papkovsky DB. New oxygen sensors and their application to biosensing. Sensors and Actuators B: Chemical. 1995;29:213-8.
[61] Puklin E, Carlson B, Gouin S, Costin C, Green E, Ponomarev S, et al. Ideality of pressure-sensitive paint. I. Platinum tetra (pentafluorophenyl) porphine in fluoroacrylic polymer. Journal of Applied Polymer Science. 2000;77:2795-804.
[62] Dmitriev RI, Ropiak HM, Ponomarev GV, Yashunsky DV, Papkovsky DB. Cell-penetrating conjugates of coproporphyrins with oligoarginine peptides: rational design and application for sensing intracellular O2. Bioconjugate chemistry. 2011;22:2507-18.
[63] Rogers JE, Nguyen KA, Hufnagle DC, McLean DG, Su W, Gossett KM, et al. Observation and Interpretation of Annulated Porphyrins: Studies on the Photophysical Properties of m eso-Tetraphenylmetalloporphyrins. The Journal of Physical Chemistry A. 2003;107:11331-9.
[64] Napp J, Behnke T, Fischer L, Würth C, Wottawa M, Katschinski DrM, et al. Targeted luminescent near-infrared polymer-nanoprobes for in vivo imaging of tumor hypoxia. Analytical chemistry. 2011;83:9039-46.
[65] Koren K, Borisov SM, Saf R, Klimant I. Strongly phosphorescent iridium (III)–porphyrins–new oxygen indicators with tuneable photophysical properties and functionalities. European journal of inorganic chemistry. 2011;2011:1531-4.
[66] Koren K, Dmitriev RI, Borisov SM, Papkovsky DB, Klimant I. Complexes of IrIII-Octaethylporphyrin with Peptides as Probes for Sensing Cellular O2. ChemBioChem. 2012;13:1184-90.
[67] McDonagh C, Burke CS, MacCraith BD. Optical chemical sensors. Chemical reviews. 2008;108:400-22.
[68] Carraway E, Demas J, DeGraff B, Bacon J. Photophysics and photochemistry of oxygen sensors based on luminescent transition-metal complexes. Analytical chemistry. 1991;63:337-42.
[69] Wang X-d, Chen H-x, Zhao Y, Chen X, Wang X-r, Chen X. Optical oxygen sensors move towards colorimetric determination. TrAC Trends in Analytical Chemistry. 2010;29:319-38.
[70] Amao Y, Asai K, Miyashita T, Okura I. Novel optical oxygen sensing material: platinum porphyrin-fluoropolymer film. Polymers for Advanced Technologies. 2000;11:705-9.
[71] Amao Y. Probes and polymers for optical sensing of oxygen. Microchimica Acta. 2003;143:1-12.
[72] Mills A, Lepre A. Controlling the response characteristics of luminescent porphyrin plastic film sensors for oxygen. Analytical Chemistry. 1997;69:4653-9.
[73] Lee S-K, Okura I. Optical Sensor for Oxygen Using a Porphyrin-doped Sol–GelGlass. Analyst. 1997;122:81-4.
[74] Chang G, Morigaki K, Tatsu Y, Hikawa T, Goto T, Imaishi H. Vertically integrated human P450 and oxygen sensing film for the assays of P450 metabolic activities. Analytical chemistry. 2011;83:2956-63.
[75] Bukowski RM, Ciriminna R, Pagliaro M, Bright FV. High-performance quenchometric oxygen sensors based on fluorinated xerogels doped with [Ru (dpp) 3] 2+. Analytical chemistry. 2005;77:2670-2.
[76] Orellana G, Moreno-Bondi MC. Frontiers in chemical sensors: novel principles and techniques: Springer; 2006.
[77] Molter TW, McQuaide SC, Suchorolski MT, Strovas TJ, Burgess LW, Meldrum DR, et al. A microwell array device capable of measuring single-cell oxygen consumption rates. Sensors and Actuators B: Chemical. 2009;135:678-86.
[78] Grist SM, Chrostowski L, Cheung KC. Optical oxygen sensors for applications in microfluidic cell culture. Sensors. 2010;10:9286-316.

[79] Klimant I, Kühl M, Glud R, Holst G. Optical measurement of oxygen and temperature in microscale: strategies and biological applications. Sensors and Actuators B: Chemical. 1997;38:29-37.
[80] Rosenzweig Z, Kopelman R. Development of a submicrometer optical fiber oxygen sensor. Analytical chemistry. 1995;67:2650-4.
[81] Chen GY, Ding M, Newson TP, Brambilla G. A review of microfiber and nanofiber based optical sensors. The Open Opt J. 2013;7:21-57.
[82] Wu M, Neilson A, Swift AL, Moran R, Tamagnine J, Parslow D, et al. Multiparameter metabolic analysis reveals a close link between attenuated mitochondrial bioenergetic function and enhanced glycolysis dependency in human tumor cells. American Journal of Physiology-Cell Physiology. 2007;292:C125-C36.
[83] John GT, Klimant I, Wittmann C, Heinzle E. Integrated optical sensing of dissolved oxygen in microtiter plates: a novel tool for microbial cultivation. Biotechnology and bioengineering. 2003;81:829-36.
[84] Zhao Q, Huang C, Li F. Phosphorescent heavy-metal complexes for bioimaging. Chemical Society Reviews. 2011;40:2508-24.
[85] Hynes J, Floyd S, Soini AE, O'Connor R, Papkovsky DB. Fluorescence-based cell viability screening assays using water-soluble oxygen probes. Journal of biomolecular screening. 2003;8:264-72.
[86] Dunphy I, Vinogradov SA, Wilson DF. Oxyphor R2 and G2: phosphors for measuring oxygen by oxygen-dependent quenching of phosphorescence. Analytical biochemistry. 2002;310:191-8.
[87] Astruc D, Boisselier E, Ornelas C. Dendrimers designed for functions: from physical, photophysical, and supramolecular properties to applications in sensing, catalysis, molecular electronics, photonics, and nanomedicine. Chemical Reviews. 2010;110:1857-959.
[88] Lebedev AY, Cheprakov AV, Sakadzic S, Boas DA, Wilson DF, Vinogradov SA. Dendritic phosphorescent probes for oxygen imaging in biological systems. ACS applied materials & interfaces. 2009;1:1292-304.
[89] Esipova TV, Karagodov A, Miller J, Wilson DF, Busch TM, Vinogradov SA. Two new "protected" oxyphors for biological oximetry: properties and application in tumor imaging. Analytical chemistry. 2011;83:8756-65.
[90] Dowd A, Pissuwan D, Cortie MB. Optical readout of the intracellular environment using nanoparticle transducers. Trends in Biotechnology. 2014.
[91] Zamborini FP, Bao L, Dasari R. Nanoparticles in measurement science. Analytical chemistry. 2011;84:541-76.
[92] Borisov SM, Mayr T, Mistlberger G, Waich K, Koren K, Chojnacki P, et al. Precipitation as a simple and versatile method for preparation of optical nanochemosensors. Talanta. 2009;79:1322-30.
[93] Wang X-d, Achatz DE, Hupf C, Sperber M, Wegener J, Bange S, et al. Imaging of cellular oxygen via two-photon excitation of fluorescent sensor nanoparticles. Sensors and Actuators B: Chemical. 2013;188:257-62.
[94] Fercher A, Borisov SM, Zhdanov AV, Klimant I, Papkovsky DB. Intracellular O2 sensing probe based on cell-penetrating phosphorescent nanoparticles. Acs Nano. 2011;5:5499-508.
[95] Clark HA, Barker SL, Brasuel M, Miller MT, Monson E, Parus S, et al. Subcellular optochemical nanobiosensors: probes encapsulated by biologically localised embedding (PEBBLEs). Sensors and Actuators B: Chemical. 1998;51:12-6.
[96] Lee Y, Kopelman R. Nanoparticle PEBBLE sensors in live cells. Methods Enzymol. 2012;504:419-70.

[97] Clark HA, Hoyer M, Philbert MA, Kopelman R. Optical nanosensors for chemical analysis inside single living cells. 1. Fabrication, characterization, and methods for intracellular delivery of PEBBLE sensors. Analytical Chemistry. 1999;71:4831-6.
[98] Xu H, Aylott JW, Kopelman R, Miller TJ, Philbert MA. A real-time ratiometric method for the determination of molecular oxygen inside living cells using sol-gel-based spherical optical nanosensors with applications to rat C6 glioma. Analytical chemistry. 2001;73:4124-33.
[99] Xiang H, Zhou L, Feng Y, Cheng J, Wu D, Zhou X. Tunable fluorescent/phosphorescent platinum (II) porphyrin–fluorene copolymers for ratiometric dual emissive oxygen sensing. Inorganic chemistry. 2012;51:5208-12.
[100] Zhdanov AV, Waters AH, Golubeva AV, Dmitriev RI, Papkovsky DB. Availability of the key metabolic substrates dictates the respiratory response of cancer cells to the mitochondrial uncoupling. Biochimica et Biophysica Acta (BBA)-Bioenergetics. 2014;1837:51-62.
[101] Wang X-d, Stolwijk JA, Lang T, Sperber M, Meier RJ, Wegener J, et al. Ultra-small, highly stable, and sensitive dual nanosensors for imaging intracellular oxygen and pH in cytosol. Journal of the American Chemical Society. 2012;134:17011-4.
[102] Zhao M, Weissleder R. Intracellular cargo delivery using tat peptide and derivatives. Medicinal research reviews. 2004;24:1-12.
[103] Dmitriev RI, Zhdanov AV, Ponomarev GV, Yashunski DV, Papkovsky DB. Intracellular oxygen-sensitive phosphorescent probes based on cell-penetrating peptides. Analytical biochemistry. 2010;398:24-33.
[104] Dmitriev RI, Ropiak HM, Yashunsky DV, Ponomarev GV, Zhdanov AV, Papkovsky DB. Bactenecin 7 peptide fragment as a tool for intracellular delivery of a phosphorescent oxygen sensor. FEBS journal. 2010;277:4651-61.
[105] Dickinson BC, Srikun D, Chang CJ. Mitochondrial-targeted fluorescent probes for reactive oxygen species. Current opinion in chemical biology. 2010;14:50-6.
[106] Dmitriev RI, Zhdanov AV, Jasionek G, Papkovsky DB. Assessment of cellular oxygen gradients with a panel of phosphorescent oxygen-sensitive probes. Analytical chemistry. 2012;84:2930-8.
[107] Guice KB, Caldorera ME, McShane MJ. Nanoscale internally referenced oxygen sensors produced from self-assembled nanofilms on fluorescent nanoparticles. Journal of biomedical optics. 2005;10:064031--10.
[108] Wang X-d, Gorris HH, Stolwijk JA, Meier RJ, Groegel DB, Wegener J, et al. Self-referenced RGB colour imaging of intracellular oxygen. Chemical Science. 2011;2:901-6.
[109] Brand M, Nicholls D. Assessing mitochondrial dysfunction in cells. Biochem J. 2011;435:297-312.
[110] Hynes J, Swiss RL, Will Y. High-throughput analysis of mitochondrial oxygen consumption. Mitochondrial Bioenergetics: Springer; 2012. p. 59-72.
[111] Hynes J, Natoli E, Will Y. Fluorescent pH and oxygen probes of the assessment of mitochondrial toxicity in isolated mitochondria and whole cells. Current Protocols in Toxicology. 2009:2.16. 1-2.. 22.
[112] Zhdanov A, Favre C, O'Flaherty L, Adam J, O'Connor R, Pollard P, et al. Comparative bioenergetic assessment of transformed cells using a cell energy budget platform. Integrative Biology. 2011;3:1135-42.
[113] Guarino RD, Dike LE, Haq TA, Rowley JA, Pitner JB, Timmins MR. Method for determining oxygen consumption rates of static cultures from microplate measurements of pericellular dissolved oxygen concentration. Biotechnology and bioengineering. 2004;86:775-87.

[114] Foster KA, Galeffi F, Gerich FJ, Turner DA, Müller M. Optical and pharmacological tools to investigate the role of mitochondria during oxidative stress and neurodegeneration. Progress in neurobiology. 2006;79:136-71.
[115] Wilson DF, Harrison DK, Vinogradov SA. Oxygen, pH, and mitochondrial oxidative phosphorylation. Journal of Applied Physiology. 2012;113:1838-45.
[116] Will Y, Hynes J, Ogurtsov VI, Papkovsky DB. Analysis of mitochondrial function using phosphorescent oxygen-sensitive probes. Nature protocols. 2007;1:2563-72.
[117] Rogers GW, Brand MD, Petrosyan S, Ashok D, Elorza AA, Ferrick DA, et al. High throughput microplate respiratory measurements using minimal quantities of isolated mitochondria. PloS one. 2011;6:e21746.
[118] Ferrick DA, Neilson A, Beeson C. Advances in measuring cellular bioenergetics using extracellular flux. Drug discovery today. 2008;13:268-74.
[119] Gerencser AA, Neilson A, Choi SW, Edman U, Yadava N, Oh RJ, et al. Quantitative microplate-based respirometry with correction for oxygen diffusion. Analytical chemistry. 2009;81:6868-78.
[120] Dragavon J, Molter T, Young C, Strovas T, McQuaide S, Holl M, et al. A cellular isolation system for real-time single-cell oxygen consumption monitoring. Journal of The Royal Society Interface. 2008;5:S151-S9.
[121] Zhdanov AV, Ogurtsov VI, Taylor CT, Papkovsky DB. Monitoring of cell oxygenation and responses to metabolic stimulation by intracellular oxygen sensing technique. Integrative Biology. 2010;2:443-51.
[122] Powers DE, Millman JR, Bonner-Weir S, Rappel MJ, Colton CK. Accurate control of oxygen level in cells during culture on silicone rubber membranes with application to stem cell differentiation. Biotechnology progress. 2010;26:805-18.
[123] Zhdanov AV, Hynes J, Dmitriev RI, Papkovsky DB. O2 Analysis on a Fluorescence Spectrometer or Plate Reader. Phosphorescent Oxygen-Sensitive Probes: Springer; 2012. p. 29-69.
[124] Chen Y-A, King AD, Shih H-C, Peng C-C, Wu C-Y, Liao W-H, et al. Generation of oxygen gradients in microfluidic devices for cell culture using spatially confined chemical reactions. Lab on a Chip. 2011;11:3626-33.
[125] Lo JF, Sinkala E, Eddington DT. Oxygen gradients for open well cellular cultures via microfluidic substrates. Lab on a Chip. 2010;10:2394-401.
[126] UCHIDA H, SATO A, MIYAYAMA A, TSUKADA K. Generation of an Oxygen Gradient in a Microfluidic Device and Cellular Analysis in Hypoxia. Advanced Biomedical Engineering. 2013;2:143-9.
[127] Takahashi E, Sato M. Intracellular Diffusion of Oxygen and Hypoxic Sensing: Role of Mitochondrial Respiration. New Frontiers in Respiratory Control: Springer; 2010. p. 213-7.
[128] Mik EG, Stap J, Sinaasappel M, Beek JF, Aten JA, van Leeuwen TG, et al. Mitochondrial PO2 measured by delayed fluorescence of endogenous protoporphyrin IX. Nature methods. 2006;3:939-45.
[129] Huh D, Hamilton GA, Ingber DE. From 3D cell culture to organs-on-chips. Trends in cell biology. 2011;21:745-54.
[130] Hynes J, Nadanaciva S, Swiss R, Carey C, Kirwan S, Will Y. A high-throughput dual parameter assay for assessing drug-induced mitochondrial dysfunction provides additional predictivity over two established mitochondrial toxicity assays. Toxicology in Vitro. 2013;27:560-9.

[131] Nadanaciva S, Rana P, Beeson GC, Chen D, Ferrick DA, Beeson CC, et al. Assessment of drug-induced mitochondrial dysfunction via altered cellular respiration and acidification measured in a 96-well platform. Journal of bioenergetics and biomembranes. 2012;44:421-37.
[132] Zhdanov AV, Dmitriev RI, Papkovsky DB. Bafilomycin A1 activates respiration of neuronal cells via uncoupling associated with flickering depolarization of mitochondria. Cellular and Molecular Life Sciences. 2011;68:903-17.
[133] Dmitriev RI, Zhdanov AV, Nolan YM, Papkovsky DB. Imaging of neurosphere oxygenation with phosphorescent probes. Biomaterials. 2013;34:9307-17.
[134] Sharifi S, Behzadi S, Laurent S, Forrest ML, Stroeve P, Mahmoudi M. Toxicity of nanomaterials. Chemical Society Reviews. 2012;41:2323-43.
[135] Fercher A, Ponomarev GV, Yashunski D, Papkovsky D. Evaluation of the derivates of phosphorescent Pt-coproporphyrin as intracellular oxygen-sensitive probes. Analytical and bioanalytical chemistry. 2010;396:1793-803.
[136] Schmälzlin E, van Dongen JT, Klimant I, Marmodée B, Steup M, Fisahn J, et al. An optical multifrequency phase-modulation method using microbeads for measuring intracellular oxygen concentrations in plants. Biophysical journal. 2005;89:1339-45.
[137] O'Riordan TC, Fitzgerald K, Ponomarev GV, Mackrill J, Hynes J, Taylor C, et al. Sensing intracellular oxygen using near-infrared phosphorescent probes and live-cell fluorescence imaging. American Journal of Physiology-Regulatory, Integrative and Comparative Physiology. 2007;292:R1613-R20.
[138] Ji J, Rosenzweig N, Rosenzweig Z, Jones I. Novel fluorescent oxygen indicator for intracellular oxygen measurements. Journal of biomedical optics. 2002;7:404-9.
[139] Feng Y, Cheng J, Zhou L, Zhou X, Xiang H. Ratiometric optical oxygen sensing: a review in respect of material design. Analyst. 2012;137:4885-901.
[140] Yoshihara T, Yamaguchi Y, Hosaka M, Takeuchi T, Tobita S. Ratiometric molecular sensor for monitoring oxygen levels in living cells. Angewandte Chemie. 2012;124:4224-7.
[141] Koo Lee Y-E, Ulbrich EE, Kim G, Hah H, Strollo C, Fan W, et al. Near infrared luminescent oxygen nanosensors with nanoparticle matrix tailored sensitivity. Analytical chemistry. 2010;82:8446-55.
[142] Wang XH, Peng HS, Yang L, You FT, Teng F, Hou LL, et al. Targetable Phosphorescent Oxygen Nanosensors for the Assessment of Tumor Mitochondrial Dysfunction By Monitoring the Respiratory Activity. Angewandte Chemie. 2014.
[143] Becker W. Fluorescence lifetime imaging–techniques and applications. Journal of microscopy. 2012;247:119-36.
[144] Liebsch G, Klimant I, Frank B, Holst G, Wolfbeis OS. Luminescence lifetime imaging of oxygen, pH, and carbon dioxide distribution using optical sensors. Applied Spectroscopy. 2000;54:548-59.
[145] Baggaley E, Botchway SW, Haycock JW, Morris H, Sazanovich IV, Williams JG, et al. Long-lived metal complexes open up microsecond lifetime imaging microscopy under multiphoton excitation: from FLIM to PLIM and beyond. Chemical Science. 2014;5:879-86.
[146] Hogan MC. Phosphorescence quenching method for measurement of intracellular in isolated skeletal muscle fibers. Journal of Applied Physiology. 1999;86:720-4.
[147] Schmälzlin E, Walz B, Klimant I, Schewe B, Löhmannsröben H-G. Monitoring hormone-induced oxygen consumption in the salivary glands of the blowfly,< i> Calliphora vicina</i>, by use of luminescent microbeads. Sensors and Actuators B: Chemical. 2006;119:251-4.
[148] Pampaloni F, Reynaud EG, Stelzer EH. The third dimension bridges the gap between cell culture and live tissue. Nature reviews Molecular cell biology. 2007;8:839-45.

[149] Nichols AJ, Roussakis E, Klein OJ, Evans CL. Click-Assembled, Oxygen-Sensing Nanoconjugates for Depth-Resolved, Near-Infrared Imaging in a 3 D Cancer Model. Angewandte Chemie International Edition. 2014;53:3671-4.
[150] Choi NW, Verbridge SS, Williams RM, Chen J, Kim J-Y, Schmehl R, et al. Phosphorescent nanoparticles for quantitative measurements of oxygen profiles< i> in vitro</i> and< i> in vivo</i>. Biomaterials. 2012;33:2710-22.
[151] Lambrechts D, Roeffaers M, Kerckhofs G, Roberts SJ, Hofkens J, Van de Putte T, et al. Fluorescent oxygen sensitive microbead incorporation for measuring oxygen tension in cell aggregates. Biomaterials. 2013;34:922-9.
[152] Roussakis E, Spencer JA, Lin CP, Vinogradov SA. Two-Photon Antenna-Core Oxygen Probe with Enhanced Performance. Analytical chemistry. 2014.
[153] Koren K, Borisov SM, Klimant I. Stable optical oxygen sensing materials based on click-coupling of fluorinated platinum (II) and palladium (II) porphyrins—a convenient way to eliminate dye migration and leaching. Sensors and Actuators B: Chemical. 2012;169:173-81.
[154] Zhdanov AV, Dmitriev RI, Golubeva AV, Gavrilova SA, Papkovsky DB. Chronic hypoxia leads to a glycolytic phenotype and suppressed HIF-2 signaling in PC12 cells. Biochimica et Biophysica Acta (BBA)-General Subjects. 2013;1830:3553-69.
[155] Wallace DC. Mitochondria and cancer. Nature Reviews Cancer. 2012;12:685-98.
[156] Krohn KA, Link JM, Mason RP. Molecular imaging of hypoxia. Journal of Nuclear Medicine. 2008;49:129S-48S.
[157] Zhdanov AV, Ward MW, Prehn JH, Papkovsky DB. Dynamics of intracellular oxygen in PC12 cells upon stimulation of neurotransmission. Journal of Biological Chemistry. 2008;283:5650-61.
[158] Frezza C, Zheng L, Tennant DA, Papkovsky DB, Hedley BA, Kalna G, et al. Metabolic profiling of hypoxic cells revealed a catabolic signature required for cell survival. PloS one. 2011;6:e24411.
[159] Lo JF, Wang Y, Blake A, Yu G, Harvat TA, Jeon H, et al. Islet preconditioning via multimodal microfluidic modulation of intermittent hypoxia. Analytical chemistry. 2012;84:1987-93.
[160] Ungerböck B, Charwat V, Ertl P, Mayr T. Microfluidic oxygen imaging using integrated optical sensor layers and a color camera. Lab on a Chip. 2013;13:1593-601.
[161] Schneckenburger H, Weber P, Wagner M, Schickinger S, Richter V, Bruns T, et al. Light exposure and cell viability in fluorescence microscopy. Journal of microscopy. 2012;245:311-8.
[162] Thomas PC, Raghavan SR, Forry SP. Regulating oxygen levels in a microfluidic device. Analytical chemistry. 2011;83:8821-4.
[163] O'Riordan TC, Zhdanov AV, Ponomarev GV, Papkovsky DB. Analysis of intracellular oxygen and metabolic responses of mammalian cells by time-resolved fluorometry. Analytical chemistry. 2007;79:9414-9.
[164] Matsumoto T, Wang P-y, Ma W, Sung HJ, Matoba S, Hwang PM. Polo-like kinases mediate cell survival in mitochondrial dysfunction. Proceedings of the National Academy of Sciences. 2009;106:14542-6.
[165] Choi SW, Gerencser AA, Nicholls DG. Bioenergetic analysis of isolated cerebrocortical nerve terminals on a microgram scale: spare respiratory capacity and stochastic mitochondrial failure. Journal of neurochemistry. 2009;109:1179-91.
[166] Zhdanov AV, Ward MW, Taylor CT, Souslova EA, Chudakov DM, Prehn JH, et al. Extracellular calcium depletion transiently elevates oxygen consumption in neurosecretory PC12 cells through activation of mitochondrial Na< sup>+</sup>/Ca< sup> 2+</sup> exchange. Biochimica et Biophysica Acta (BBA)-Bioenergetics. 2010;1797:1627-37.
[167] Dietz KC, Casaccia P. HDAC inhibitors and neurodegeneration: at the edge between protection and damage. Pharmacological Research. 2010;62:11-7.

[168] Carew JS, Giles FJ, Nawrocki ST. Histone deacetylase inhibitors: mechanisms of cell death and promise in combination cancer therapy. Cancer letters. 2008;269:7-17.
[169] Semenza GL. Oxygen sensing, homeostasis, and disease. New England Journal of Medicine. 2011;365:537-47.
[170] Alderman J, Hynes J, Floyd SM, Krüger J, O'Connor R, Papkovsky DB. A low-volume platform for cell-respirometric screening based on quenched-luminescence oxygen sensing. Biosensors and Bioelectronics. 2004;19:1529-35.
[171] Ziemer LS, Lee WM, Vinogradov SA, Sehgal C, Wilson DF. Oxygen distribution in murine tumors: characterization using oxygen-dependent quenching of phosphorescence. Journal of Applied Physiology. 2005;98:1503-10.
[172] Kondrashina AV, Papkovsky DB, Dmitriev RI. Measurement of cell respiration and oxygenation in standard multichannel biochips using phosphorescent O 2-sensitive probes. Analyst. 2013;138:4915-21.
[173] Devor A, Sakadžić S, Srinivasan VJ, Yaseen MA, Nizar K, Saisan PA, et al. Frontiers in optical imaging of cerebral blood flow and metabolism. Journal of Cerebral Blood Flow & Metabolism. 2012;32:1259-76.
[174] Finikova OS, Lebedev AY, Aprelev A, Troxler T, Gao F, Garnacho C, et al. Oxygen microscopy by two-photon-excited phosphorescence. ChemPhysChem. 2008;9:1673-9.
[175] Golub AS, Pittman RN. PO2 measurements in the microcirculation using phosphorescence quenching microscopy at high magnification. American Journal of Physiology-Heart and Circulatory Physiology. 2008;294:H2905-H16.
[176] Neugebauer U, Pellegrin Y, Devocelle M, Forster RJ, Signac W, Moran N, et al. Ruthenium polypyridyl peptide conjugates: membrane permeable probes for cellular imaging. Chemical Communications. 2008:5307-9.
[177] Albanese A, Tang PS, Chan WC. The effect of nanoparticle size, shape, and surface chemistry on biological systems. Annual review of biomedical engineering. 2012;14:1-16.
[178] Bodmeier R, Chen H, Tyle P, Jarosz P. Spontaneous formation of drug-containing acrylic nanoparticles. Journal of microencapsulation. 1991;8:161-70.
[179] Wu C, Bull B, Christensen K, McNeill J. Ratiometric Single-Nanoparticle Oxygen Sensors for Biological Imaging. Angewandte Chemie International Edition. 2009;48:2741-5.
[180] Lee YEK, Kopelman R. Optical nanoparticle sensors for quantitative intracellular imaging. Wiley Interdisciplinary Reviews: Nanomedicine and Nanobiotechnology. 2009;1:98-110.
[181] Grigoriev I, Yu KL, Martinez-Sanchez E, Serra-Marques A, Smal I, Meijering E, et al. Rab6, Rab8, and MICAL3 cooperate in controlling docking and fusion of exocytotic carriers. Current Biology. 2011;21:967-74.
[182] Lecoq J, Parpaleix A, Roussakis E, Ducros M, Houssen YG, Vinogradov SA, et al. Simultaneous two-photon imaging of oxygen and blood flow in deep cerebral vessels. Nature medicine. 2011;17:893-8.
[183] Tsytsarev V, Arakawa H, Borisov S, Pumbo E, Erzurumlu RS, Papkovsky DB. < i> In vivo</i> imaging of brain metabolism activity using a phosphorescent oxygen-sensitive probe. Journal of neuroscience methods. 2013;216:146-51.
[184] Kondrashina AV, Dmitriev RI, Borisov SM, Klimant I, O'Brien I, Nolan YM, et al. A phosphorescent nanoparticle-based probe for sensing and imaging of (intra) cellular oxygen in multiple detection modalities. Advanced Functional Materials. 2012;22:4931-9.
[185] Niedermair F, Borisov SM, Zenkl G, Hofmann OT, Weber Hr, Saf R, et al. Tunable phosphorescent NIR oxygen indicators based on mixed benzo-and naphthoporphyrin complexes. Inorganic chemistry. 2010;49:9333-42.

[186] Canton I, Battaglia G. Endocytosis at the nanoscale. Chemical Society Reviews. 2012;41:2718-39.
[187] Yang W-H, Smolen VF, Peppas NA. Oxygen permeability coefficients of polymers for hard and soft contact lens applications. Journal of Membrane Science. 1981;9:53-67.
[188] Mendes AN, Hubber I, Siqueira M, Barbosa GM, de Lima Moreira D, Holandino C, et al. Preparation and Cytotoxicity of Poly (Methyl Methacrylate) Nanoparticles for Drug Encapsulation. Macromolecular Symposia: Wiley Online Library; 2012. p. 34-40.
[189] Ivanov AI. Pharmacological inhibition of endocytic pathways: is it specific enough to be useful? Exocytosis and Endocytosis: Springer; 2008. p. 15-33.
[190] Dmitriev RI, Borisov SM, Kondrashina AV, Pakan JM, Anilkumar U, Prehn JH, et al. Imaging oxygen in neural cell and tissue models by means of anionic cell-permeable phosphorescent nanoparticles. Cellular and Molecular Life Sciences. 2014:1-15.
[191] Dmitriev RI, Kondrashina AV, Koren K, Klimant I, Zhdanov AV, Pakan JM, et al. Small molecule phosphorescent probes for O 2 imaging in 3D tissue models. Biomaterials Science. 2014;2:853-66.
[192] Algar WR, Prasuhn DE, Stewart MH, Jennings TL, Blanco-Canosa JB, Dawson PE, et al. The controlled display of biomolecules on nanoparticles: a challenge suited to bioorthogonal chemistry. Bioconjugate chemistry. 2011;22:825-58.